Dissertation

Structural analysis of HCMV assembly and the associated cellular remodeling

The dissertation is submitted for the degree of Doctor rerum naturalium

at the Faculty for Mathematics, Informatics and Natural Sciences,

Department of Chemistry, University of Hamburg

by

Robert Gebauer

Hamburg, 2025

Members of the defence committee:

Prof. Dr. Kay Grünewald

Department of Chemistry

University of Hamburg

Role: supervisor, chair, reviewer

Prof. Dr. Wolfgang Maison

Department of Chemistry

University of Hamburg

Role: deputy chair

Dr. Gabrielle Vieyres

Leibniz Institute of Virology

Role: examiner

Prof. Dr. Meytal Landau

Centre for Structural Systems Biology

Role: reviewer

Thesis defense: 22.08.2025

The experimental work and preparation of this dissertation were performed at the Centre for Structural Systems Biology and the Leibniz Institute of Virology under the supervision of Prof. Dr. Kay Grünewald and co-supervision of Maya Topf between the 15th of June 2021 and the 29th of August 2025.

Publication

Hofstadter, W. A., Cook, K. C., Tsopurashvili, E., **Gebauer, R.**, Pražák, V., Machala, E. A., Park, J. W., Grünewald, K., Quemin, E. R. J., & Cristea, I. M. (2024). Infection-induced peripheral mitochondria fission drives ER encapsulations and inter-mitochondria contacts that rescue bioenergetics. Nature communications, 15(1), 7352.[95]

Abstract

Human cytomegalovirus (HCMV) is a highly prevalent member of the Herpesviridae family that establishes lifelong latent infections and can cause severe disease in newborns and immunocompromised individuals. HCMV induces profound and persistent changes in host cell architecture and metabolism to facilitate production and dissemination of viral progeny while evading immune detection. The aim of my doctoral research was to investigate HCMV assembly and the associated organelle remodeling in human fibroblast cells using in-situ electron cryo-tomography (cryo-ET). A major focus of this work was the structural characterization of peroxisomes and their remodeling during HCMV infection. To overcome the challenge of identifying peroxisomes in human fibroblasts, a novel correlative light and electron microscopy (cryo-CLEM) workflow was developed, combining cryo fluorescence microscopy (cryo-FM) and focused ion beam (FIB) milling with cryo-ET. This integrated approach enabled targeted identification and three-dimensional peroxisomes characterization in a near-native state. Using PTS1-mCherry as a specific peroxisomal marker, this revealed that mammalian peroxisomes human fibroblasts lack the distinctive crystalline bodies commonly observed in plants and fungi, appearing as inconspicuous spherical vesicles. In addition, this study provides detailed insight into the morphology and dynamics of membrane-bound structures within the viral assembly compartment (vAC) governing tegumentation and secondary envelopment of viral capsids during HCMV replication. Overview tomograms, acquired at low magnification to visualize the cellular ultrastructure within a section of a whole cell, were used as complementary tools to provide comprehensive spatial context for the organization and interactions of viral and cellular components within the vAC. This revealed capsids at various stages of secondary envelopment and the presence of multiviral bodies (MViBs). Overall, this thesis contributes to our understanding of viral replication and organelle remodeling in human fibroblast cells during HCMV infection, by providing new methodologies for the identification and characterization of intracellular structures in a near-native state.

Zusammenfassung

Das humane Cytomegalievirus (HCMV), auch humanes Betaherpesvirus 5 genannt, ist ein weltweit verbreitetes Mitglied der *Orthoherpesviridae* Familie, dass eine lebenslange Persistenz im Wirt etabliert und schwere Erkrankungen bei Neugeborenen und Personen mit einem geschwächten Immunsystem verursachen kann.HCMV manipuliert die Struktur und den Stoffwechsel der Wirtszelle, um seine Verbreitung sicherzustellen und gleichzeitig einer Immunreaktion zu entgehen. Das Ziel meiner Doktorarbeit war es, die Replikation von HCMV und die damit verbundenen strukturellen und funktionellen Veränderungen der Organellen in humanen Fibroblasten mittels *in-situ* Kryoelektronentomographie zu untersuchen. Ein Hauptfokus dieser Arbeit war die strukturelle Charakterisierung von Peroxisomen und welchen Einfluss eine HCMV Infektion auf diese Organellen hat. Um die Identifizierung von Peroxisomen in vitrifizierten Zellen zu ermöglichen, wurde ein neuartige korrelative Licht- und Elektronenmikroskopie Methode entwickelt, welche Kryofluoreszenzmikroskopie und Ionendünnung mit Kryo-ET verbindet. Dieser Ansatz ermöglicht die gezielte Identifizierung und dreidimensionale Charakterisierung von Peroxisomen, welche mit einem Fluorophor markiert wurden. Durch die Verwendung von PTS1-mCherry als spezifischer Peroxisome-marker, war meine Forschung in der Lage zu zeigen, dass, im Gegensatz zu Beobachtungen in Pflanzen und Hefen, Peroxisomen in vitrifizierten humanen Fibroblasten keine charakteristischen morphologischen Merkmale besitzen und demzufolge als unauffällige kugelförmige Vesikel auftreten. Darüber hinaus bietet diese Studie detaillierte Einblicke in die Morphologie und Dynamik membrangebundener Strukturen innerhalb des viralen Zusammenbaukompartiment, welches die Tegumentierung und sekundäre Behüllung viraler Kapside im Zuge der Replikation von HCMV ermöglicht und steuert. Übersichtstomogramme, welche bei geringer Vergrößerung aufgenommen wurden, um die zelluläre Ultrastruktur innerhalb einer gesamten Lamelle zu visualisieren, wurden als ergänzendes Werkzeug eingeführt, um einen umfassenden räumlichen Kontext für die Organisation und Wechselwirkungen viraler und zellulärer Komponenten innerhalb des viralen Zusammenbaukompartiment zu erlangen. Im Zuge dessen konnten Kapside in verschiedenen Stadien der sekundären Behüllung beobachtet und die Existenz von multiviral Körperchen gezeigt werden. Insgesamt trägt diese Dissertation zu unserem Verständnis der viralen Replikation und der damit verbundenen Umstrukturierung der Organellen in humanen Fibroblasten während einer HCMV-Infektion bei, indem sie neue Methoden für die Identifizierung und Charakterisierung intrazellulärer Strukturen in einem nahezu nativen Zustand bereitstellt.

Table of contents

Abbreviations

ACBD5	Acyl-CoA Binding Domain containing protein 5
CARD	Caspase Activation and Recruitment Domain
CLEM	Correlative light and electron microscopy
cryo	Cryogenic (under cryogenic conditions)
DE	Delayed early (genes)
DMSO	Dimethyl sulfoxide
DPA	Docosapentaenoic acid
DRP1	Dynamin-Related Protein 1
EM	Electron microscopy
EPA	Eicosapentaenoic acid
ER	Endoplasmic reticulum
ET	Electron tomography
EVA	Extracellular viral accumulations
FIB	Focused ion beam
FIS-1	Mitochondrial fission 1
FM	Fluorescence microscopy
GFP	Green fluorescent protein
GIS	Gas injection system
GSK3β	Glycogen Synthase Kinase 3 β
HCMV	Human cytomegalovirus
HFF	Human foreskin fibroblast
hpi	Hours post infection
HSV	Herpes simplex virus
IE	Immediate early (gene)
iFLM	Integrated fluorescence light microscope
IFN	Interferon
ILV	Intraluminal vesical
ISG	IFN-stimulated gene
L	Late (gene)
LINC	Linker of nucleoskeleton and cytoskeleton
MAVS	Mitochondrial antiviral signalling protein
MCP	Major capsid protein
MCS	Membrane contact site
MDA5	Melanoma Differentiation-Associated protein 5

MENC	Mitochondria-ER encapsulation
MFF	Mitochondrial fission factor
MFN2	MitoFusiN-2 (GTPase)
MICOS	Mitochondrial cristae-organizing system
MIEP	Major immediate early promoter
MIRO	Mitochondrial Rho GTPase
MOI	Multiplicity of infection
MRC-5	Medical research council 5 (human fibroblast cell line)
MT	Microtubule
MTOC	Microtubule organizing centre
MVB	Multivesicular body
MViB	Multiviral body
NA	Numerical aperture
OMM	Outer mitochondrial membrane
PAMP	Pathogen associated molecular patterns
PEX	Peroxin
PFA	Paraformaldehyde
PMP	Peroxisomal membrane protein
PRR	Pattern recognition receptors
PTPIP51	Protein tyrosine phosphatase-interacting protein 51
PTS	Peroxisomal targeting signal
RIG-1	Retinoic acid-inducible gene I
ROI	Region of interest
ROS	Reactive oxygen species
RT	Room temperature
SEM	Scanning electron microscopy
TEM	Transmission electron microscopy
TGN	Trans Golgi network
vAC	Viral assembly compartment
VAMP	Vesicle-associated membrane protein
VAPB	VAMP-associated protein B
vMIA	Viral Mitochondrion-localized inhibitor of apoptosis (pUL37x1)
vNEC	Viral nuclear egress complex
VPS13D	Vacuolar protein sorting 13 homolog D
vRC	Viral replication compartment
ZSD	Zellweger spectrum disorders

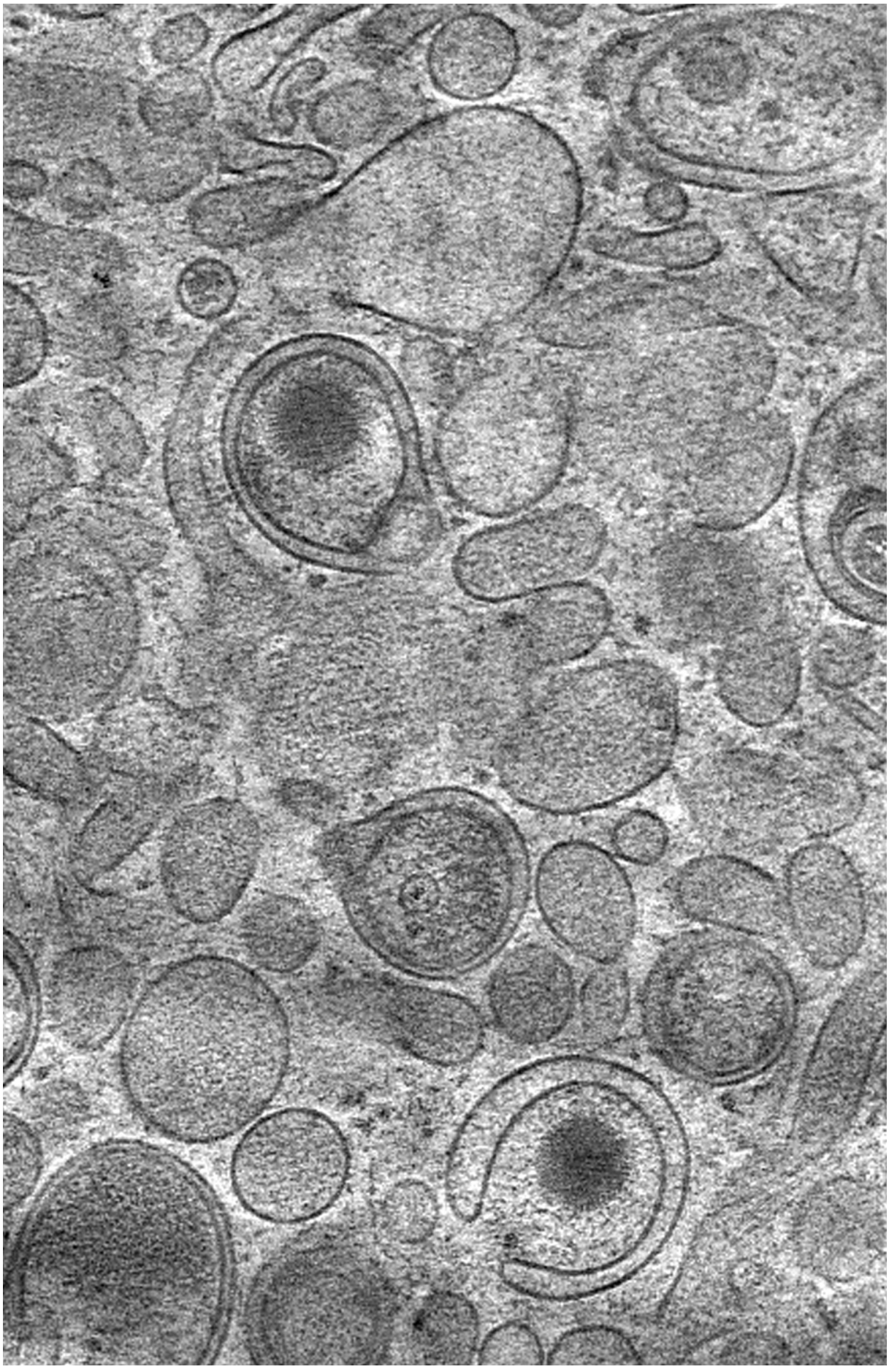

1 General introduction

1.1 The family Herpesviridae

Herpesviruses have become notorious for their ability to establish persistent infections in humans, which typically remain asymptomatic but can result in recurrent outbreaks of painful clinical manifestations such as cold sores and genital lesions. These diseases are caused by Herpes simplex virus 1 and 2 (HSV-1, HSV-2), both of which are members of the Herpesviridae family. However, the Herpesviridae family comprises over one hundred species of enveloped double-stranded DNA viruses that are divided into three subfamilies (Alpha-, Beta- and Gamma-herpesviridae) and are capable of causing severe and potentially fatal diseases in a wide range of hosts including mammals, birds, fish, reptiles and mollusks[1]. Three members of the Proboscivirus genus in the Betaherpesviridae subfamily can cause lethal haemorrhagic symptoms in young Asian elephants[2]. Meanwhile, a group of nine herpesvirus species comprising representatives from all three subfamilies are known to infect humans. The members of this group are referred to as human herpesviruses and include the four Beta-herpesviruses Human Cytomegalovirus (HCMV), Human Herpesvirus 6A, 6B and 7 (HHV-6A, HHV-6B, HHV-7), the three Alpha-herpesviruses HSV-1, HSV-2 and Varicella-Zoster Virus (VZV) as well as the two Gamma-herpesviruses Epstein-Barr Virus (EBV) and Kaposi Sarcoma-associated Herpesvirus (KHSV). Human herpesviruses establish life-long infections that can cause severe diseases such as myocarditis, encephalitis and certain types of cancer[3,2].

Despite the great diversity exhibited by human herpesviruses in their clinical manifestation and host cell tropism, the structure of their viral particles is conserved across the entire Herpesviridae family. The characteristic architecture of herpesvirus virions consists of four layers. The large linear double-stranded viral DNA is encased in an icosahedral nucleocapsid surrounded by an amorphous layer of proteins called the tegument. The viral envelope is the outermost layer of the virions, consisting of a lipid bilayer containing the viral glycoproteins[4].

Within the group of human herpesviruses, HCMV has the largest genome giving rise to an extensive repertoire of proteins, non-coding RNAs and other viral factors, which allows the virus to establish a complex network of interactions with the host cell to remodel extensively both metabolic and signalling pathways, as well as a vast array of immune evasion strategies[5].

1.2 Human Cytomegalovirus

The Human Cytomegalovirus (HCMV) owes its name to the significant enlargement of the host cell during infection. This characteristic of HCMV infection was first observed by histopathology in 1956[6]. At a much earlier point in time, about 6 Million years ago, herpesviruses were already infecting early human ancestors. Since then, they have been evolving together with mankind[7]. The seroprevalence of HCMV varies considerably across different geographical regions or demographic and socioeconomic backgrounds: ranging from 45% in developed countries to 100% in developing countries[8]. Multiple characteristic features of HCMV contribute to this remarkably high prevalence, one of which is the broad range of intricate immune evasion mechanisms encoded in its large genome[9,10,11]. Another essential strategy employed by HCMV and all other members of the Herpesviridae family to avoid detection by the host surveillance system, is based on their ability to establish both lytic and latent infections and to switch between these two fundamentally different types of infection.

During latent infection, human herpesviruses significantly limit the level of viral gene expression and abolish production of viral progeny, thereby avoiding detection by the host immune system. Hence, latency allows the pathogen to persist indefinitely within a healthy individual while maintaining the viral genome. Host cells that are lysogenized can serve as a viral reservoir enabling potential reactivation and passive dissemination of the virus. Reactivation of HCMV infection, *i.e.* the transition from latent to lytic phase, is linked in particular to the status of the host immune system or stress factors.

During latency, viral gene expression is primarily suppressed through chromatin-mediated silencing. However, inflammatory cytokines trigger remodeling of the corresponding histones, thereby enabling transcription of the viral genome[12,13,14]. Given that restored viral gene expression is indispensable for transitioning from latent to lytic cycle, such inflammatory cytokines play a crucial role in reactivation of HCMV infection[15]. The lytic phase of human herpesvirus infection is responsible for the manifestation of clinical symptoms and characterized by the production and dissemination of infectious virions. Whether an individual develops symptoms as a result of an HCMV infection largely depends on the presence of certain risk factors.

In most cases of primary HCMV infections in healthy humans, no pathology is observed, with only about one in ten developing acute mononucleosis[16]. Pregnancy represents a major risk factor for an HCMV infection leading to severe outcomes. Indeed, HCMV primary infection is considered as the leading cause of congenital viral infections in newborns in developed countries, capable of causing severe neurodevelopmental impairments some of which are incompatible with life[17]. However, the main risk group are in fact immunocompromised individuals, where HCMV can cause severe and potentially lethal symptoms. A compromised immune system can result from a large variety of causes including chronic diseases like cancer or autoimmune diseases. On top of that, the medications and procedures used to treat these conditions, such as radiation therapy, chemotherapy and immunosuppressive drugs, can lower the already compromised immune system even further[18,19].

In solid organ or stem cell transplant recipients, opportunistic HCMV infections are associated with a substantial increase in morbidity and mortality. The immunodeficiency caused by HIV/AIDS, particularly with the depletion of CD4+ T cells, is capable of significantly exacerbating the severity of HCMV symptoms. This is due to synergistic interactions between the two viruses facilitating viral replication and dissemination[20]. Given its high prevalence and clinical significance, HCMV remains a human pathogen of serious concern that demonstrates the remarkable ability to establish latency and many strategies to evade the host immune system.

1.2.1 Structure

HCMV is an enveloped double-stranded DNA virus. It possesses the largest genome among the human herpesviruses, which is densely packed inside a pseudo-icosahedral capsid of approximately 130 nm in diameter[21]. This capsid is constructed from 60 asymmetric units, each of which is assembled from sixteen copies of the major capsid protein (MCP) in various conformations, forming pentameric and hexameric capsomers. So-called triplex proteins encoded by UL85 and UL46 are essential components of capsid architecture, as they reinforce the interaction between MCPs[22]. During viral replication, a homododecamer of pUL104 serves as portal to facilitate the process of packaging the 235 kilobase pairs of HCMV genome into empty capsids[23,21]. Despite HCMV having a genome approximately 1.5 times larger than HSV-1, the capsids of these two herpesviruses remain similar in size, revealing the tremendous internal pressure found inside HCMV capsids[24].

The capsid is surrounded by an amorphous layer of viral and cellular proteins called tegument. Our current understanding is that the tegument consists of an inner and an outer layer. While inner tegument proteins are thought to form a semi-ordered mesh-like layer, proteins in the outer tegument layer exhibit a pleomorphic organization and asymmetric distribution. Inner tegument proteins are typically characterized by their strong association with structural components of the capsid[25,26,27]. The inner tegument protein pp150 is thought to form a filamentous protein structure around the capsid that acts as a supportive scaffold due to its ability to directly and tightly associate with capsid elements. This pp150 framework encasing the capsid is believed to serve as a foundational base facilitating further recruitment of tegument proteins[27]. The large tegument protein pUL48 represents another prominent component of the inner tegument layer. pUL48 has been shown to be integral to several processes during viral entry, including facilitating the release of the viral genome from the capsid[28].

The most abundant protein in the outer tegument layer is pp65, encoded by the HCMV gene UL83. Even though it is known to enhance viral genome replication while promoting the expression of IE genes, pp65 appears to be dispensable for viral replication[29]. Several outer tegument proteins are essential for successful secondary envelopment, including pp28. Encoded by the UL99 gene, pp28 plays a key role during HCMV replication. In particular, its absence or inability to interact with pp150 or pUL94 has been found to disrupt the secondary envelopment process[30].

The viral envelope is surrounding the tegument layer and represents the outermost layer of HCMV virions, which consists of a lipid bilayer derived from different host cell membranes[27,29]. The envelope is densely decorated with viral glycoproteins that protrude from the surface. These glycoproteins mediate interaction between the virus and host cell receptors, thereby facilitating viral entry. To enable viral entry into different host cell types, HCMV envelope glycoproteins, such as gH, gL and gO, can organize into several distinct complexes[31]. In total, HCMV virions are approximately 150 – 200 nm in diameter, which makes them roughly the same size as the flattened tips of gecko feet hair[32].

1.2.2 Viral infection cycle

HCMV, similar to other viruses, is an obligate intracellular parasite. Hence, viral genome replication and assembly of infectious viral progeny virions are only possible inside a susceptible host cell. In general, the infection or replication cycle of HCMV can be categorized into the following stages: entry, nuclear trafficking, early gene expression, genome replication, late gene expression, capsid assembly, genome packaging, nuclear egress, tegumentation, secondary envelopment, and egress.

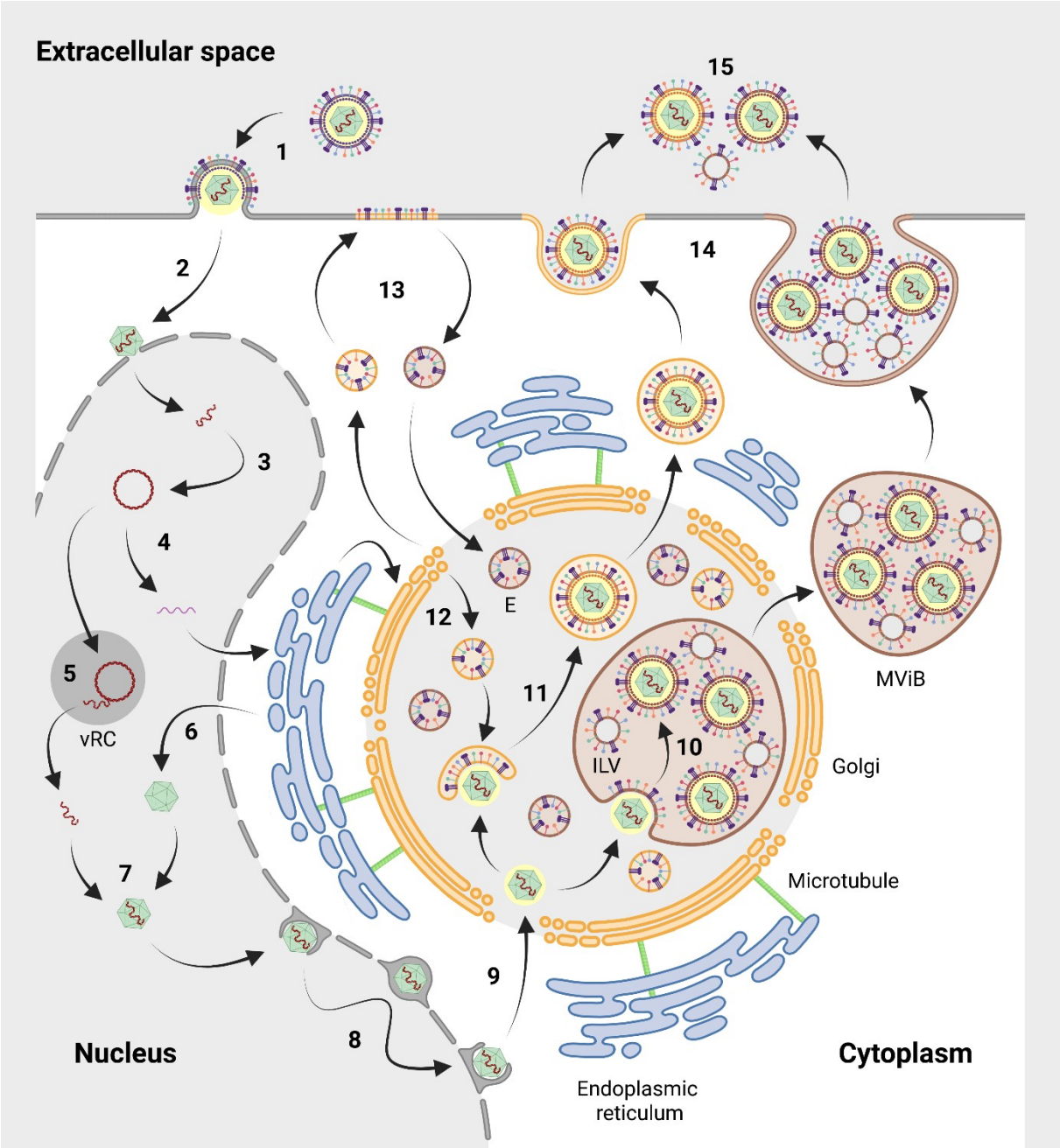

Figure 1.1 Schematic illustration of the HCMV infection cycle. After the virion fuses with the plasma membrane of the host cell (1), the capsid is trafficked to the nuclear envelope (2) where the viral genome is ejected from the capsid and injected into the nucleus. Following circularization of the viral genome (3), its replication (5) commences inside the viral replication compartment (vRC). Simultaneously, transcription (4) and subsequent expression of viral genes enables production of viral components required for capsid assembly. Translocation of these components from the endoplasmic reticulum to the nucleus (6) allows for capsid assembly and subsequent genome packaging (7). Following nuclear egress (8), the capsids are trafficked to the viral assembly compartment (vAC) where they undergo tegumentation (9). Here, secondary envelopment of the tegumented capsids is facilitated through budding into Golgi-derived cisternae (11) or vesicles derived from limiting endosomal (E) membrane (10). While inward budding of limiting endosomal membrane creates intraluminal vesicles (ILVs) within multivesicular bodies (MVBs), MVBs containing virions are referred to as multiviral bodies (MViBs). Following synthesis and subsequent accumulation in the Golgi apparatus (12), viral envelope glycoproteins may be trafficked into limiting endosomal membranes through a process involving them being shuttled to the plasma membrane and re-internalized through endocytosis (13). Through fusion of the vesicles with the plasma membrane (14), the infectious viral progeny as well as the intraluminal vesicles are released into the extracellular space (15). Figure was created using BioRender.

Entry and nuclear trafficking

The first step required to initiate the viral infection cycle of HCMV is the binding and subsequent entry of the infectious viral particles by fusion with the cellular membranes. This process is cell-type specific and facilitated by interaction between glycoproteins in the viral envelope and receptors in the plasma membrane of the host cell[33,34]. HCMV can establish lytic infection in a large variety of cell types including fibroblasts, monocytes, macrophages and epithelial cells. This broad cellular tropism stems from multiple glycoprotein complexes being present in the envelope of HCMV virions[35,36]. Two putative minimal entry complexes have been identified: the trimeric complex comprising the viral glycoproteins gH, gL and gO enables infection of fibroblasts. Here, the platelet-derived growth factor receptor alpha (PDGFRα) represents the predominant receptor for cell entry. The pentameric glycoprotein complex consisting of the five subunits gH, gL, UL128, UL130 and UL131A enables HCMV to infect additional cell types, particularly epithelial and myeloid cells[37,38,39]. The functional significance of the differences in composition between these two complexes has yet to be elucidated.

Following attachment, entry of HCMV into fibroblasts may commence via glycoprotein gB mediating direct fusion of the viral envelope with the host plasma membrane[40,41]. HCMV is also able to enter the host cell by triggering a dynamin II-dependent form of endocytosis called micropinocytosis and subsequently fusing with the endosomal membrane[42,43] (Figure 1.1 - 1) . Following membrane fusion, the majority of viral tegument proteins detach from the capsid and are released into the host cytoplasm. This complex ensemble of tegument proteins initiates the extensive remodeling and reprogramming of the host cell, particularly disrupting antiviral signalling to suppress corresponding immune responses[44,45]. The tegument proteins remaining associated with the capsid mediate delivery of the encapsulated viral genome to the nuclear envelope by exploiting the host cytoskeletal machinery to traffic the capsid along the microtubule network[46] (Figure 1.1 - 2).

Genome replication and gene expression

Once at the nuclear envelope, the viral genome escapes the viral capsid and enters in the nucleus via interaction with the nuclear pore complex[47]. There, transcription of the HCMV genome is initiated by the host RNA polymerase II (Figure 1.1 - 4). Simultaneously, its presence also activates a host intrinsic immune response aimed at suppressing viral gene expression. This antiviral response is triggered by DNA sensors such as the interferon-inducible protein IFI16 recognizing the presence of viral DNA in the nucleus. However, this process can be disrupted by the previously mentioned tegument proteins, particularly pUL83, which is released from the virion upon entry[45] (Figure 3.2).

The cascade of viral gene expression during lytic HCMV infection has been categorized into three distinct steps according to the time elapsed after infection: immediate early (IE), delayed early (DE) and late (L). Expression of IE genes acts as a driving force for progression of the viral replication cycle, inhibition of apoptosis, disruption of antiviral signalling as well as activation of DE genes[48]. Transcription of IE genes is tightly regulated by the major immediate early promoter (MIEP), with remodeling of the corresponding viral chromatin directly affecting MIEP activity. Consequently, the MIEP is integral to the regulation of HCMV latency and reactivation[49,50,15]. DE genes are essential for HCMV's ability to suppress immune and inflammatory signalling, manipulate the host cell cycle, and exploit cellular metabolism and trafficking pathways[48]. Proteins encoded in L genes predominantly form virion components required for assembly and production of infectious viral progeny[51,52].

The process of replicating HCMV virions during lytic infection continues with duplication of the viral genome. There, HCMV drives the formation of a structure occupying the majority of intranuclear space: the viral gene products UL112-113 undergo liquid-liquid phase separation and recruit viral proteins required for replication of the HCMV genome[53] (Figure 1.1 - 5). This virus-induced structure was termed the viral replication compartment (vRC).

Capsid assembly and genome packaging

Viral capsid assembly is initiated at the periphery of the vRC while viral genome replication proceeds in parallel inside the vRC. This stage of the viral infection cycle begins when major capsid proteins interact with scaffold fusion proteins to form a structural framework, which serves as a template to guide the assembly process[54] (Figure 1.1 - 6). The formation and maturation of the pseudo-icosahedral nucleocapsid represent the final steps of viral capsid assembly. This process yields nucleocapsids devoid of both scaffold and nucleic acids. Newly replicated copies of the HCMV genome are then cleaved and packed into mature capsids by a terminase complex, forming C-capsids[55,56] (Figure 1.1 - 7).

The molecular processes by which nucleocapsids then acquire tegument proteins and subsequently undergo secondary envelopment are confined to the cytoplasm of the host cell. Therefore, C-capsids have to cross the inner and outer membranes of the nuclear envelope before assembly of infectious HCMV particles can proceed. First, the capsids are trafficked from the periphery of the vRC to the rim of the nucleus. This active transport may be facilitated by F-actin but the exact mechanism has yet to be elucidated[57]. Capsids cross the nuclear envelope through a process involving envelopment and subsequent deenvelopment at the inner and outer nuclear membrane respectively, which is mediated by the viral nuclear egress complex (vNEC)[58,59] (Figure 1.1 - 8).

The viral assembly compartment

Following nuclear egress of the capsid, viral assembly proceeds within a cytoplasmic structure known as the viral Assembly Compartment (vAC). The vAC is a complex and dynamic structure orchestrating the final stages of the viral infection cycle, specifically tegumentation, secondary envelopment and egress[60]. The vAC forms in close proximity to the nuclear envelope as a non-classical organelle.

It emerges during the late stages of HCMV infection through extensive viral remodeling of the host cell endocytic and secretory pathways[61]. The term non-classical organelle refers to a cellular compartment that is not enclosed by a conventional lipid-bilayer membrane.

Instead, these membraneless organelles spatially organize based on other physical processes of confinement, such as liquid-liquid phase separation. The formation of the vAC involves accumulation of vesicles created after viral manipulation of these intracellular transport networks around concentric rings of fragmented Golgi stacks together with other Golgi- and ER-derived membranes. Even with the substantial remodeling of host cell organelles and vesicular trafficking pathways induced by HCMV, membranes appear to remain confined to discrete regions within the vAC reflective of their cellular origin[62,63]. As each of these vAC substructures appears to be dedicated to a specific step of viral assembly, this nested architecture is thought to facilitate precise spatial and temporal organization of tegumentation and secondary envelopment. This contributes to the crucial role of the vAC as platform orchestrating the process of sequential steps of assembly of the viral capsid[64,60,65].

In order to establish and maintain structural integrity and spatial organization of the vAC, HCMV relies on remodeling of the host cytoskeleton, particularly the microtubule network. HCMV increases microtubule nucleation and acetylation inside the vAC, thereby transforming it into a sort of Golgi-derived microtubule organizing centre (MTOC) while simultaneously suppressing centrosome function[66]. These MTOC-like capabilities enable the vAC to actively transport cargo along microtubule filaments. By exploiting this transport machinery, there is recruitment of viral and host proteins to the vAC, which is required for tegumentation, secondary envelopment and trafficking of viral components in there[63]. Another critical aspect of HCMV-induced restructuring of the microtubule network is the interaction between the vAC and the nucleus. HCMV exploits the nuclear membrane linker of nucleoskeleton and cytoskeleton (LINC in short) to establish a connection between the F-actin nucleoskeleton and the acetylated microtubules in the vAC[67]. This connection enables HCMV to exert control over nuclear morphology and facilitates an efficient transition from nuclear egress to tegumentation and secondary envelopment of capsids. With its strategic location in close proximity to the nucleus and nested organization of specialized substructures, each performing specific virion assembly functions, the vAC provides the means to efficiently orchestrate tegumentation and secondary envelopment.

Tegumentation

Following nuclear egress, the mature capsids are transported on microtubules to the vAC where they undergo tegumentation (Figure 1.1 - 9). The tegument is an amorphous layer of viral and cellular proteins as well as mRNAs, most of which are released into the host cell cytosol after fusion of HCMV with the plasma membrane. Tegument proteins play a crucial role in a multitude of processes essential for viral replication and immune evasion. However, conclusive evidence identifying and characterizing the specific molecular mechanisms by which mature capsids acquire their tegument layer has proven to be challenging. In practice, mature capsids accumulate in the centre of the vAC to undergo tegumentation. The central area of the vAC consists primarily of vesicles derived from various membrane-bound subcellular structures, especially the endocytic pathway and the Golgi apparatus. Here, tegumentation commences through pp150 interacting with the capsid and subsequently recruiting more inner tegument proteins[68]. These tegument proteins exhibit a dynamic behaviour, shifting from a nuclear localization in the early steps of HCMV infection to the cytoplasm during late stages of viral replication[69,70,71]. Therefore, a debate persists whether initial tegumentation takes place inside the nucleus or inside the cytoplasm, within the vAC per se. Beyond its main role for the transport and delivery of some of the viral factors, the tegument layer also acts as a scaffold that physically anchors the viral envelope to the capsid.

Secondary envelopment and cellular egress

Next, the process by which these tegumented capsids get enveloped is called secondary envelopment and like tegumentation, it takes place within the vAC. In general, secondary envelopment involves budding of the tegumented capsid into membrane-bound cellular structures enriched in viral envelope glycoproteins. This process is thought to primarily rely on two distinct pathways, distinguished by the origin of the membrane-bound compartment.

One host cell pathway HCMV exploits to facilitate secondary envelopment is the inward budding of limiting endosomal membrane, forming intraluminal vesicles (ILV) inside multivesicular bodies (MVBs)[72]. First, viral glycoproteins are shuttled from the TGN to the plasma membrane using the host cell secretory pathway. Subsequently, the viral glycoproteins are re-internalized through endocytosis. Through this process, HCMV produces limiting endosomal membrane enriched in viral glycoproteins for secondary envelopment (Figure 1.1 - 13). Virions are created inside MVBs when tegumented capsids bud into these limited endosomal membranes enriched in viral envelope glycoproteins, thereby creating multiviral bodies (MViBs)[73] (Figure 1.1 - 10). This viral remodeling of endosomal trafficking to enable secondary envelopment is a mechanism that appears to be conserved across all Beta-herpesviruses[74,75].

The second pathway involves budding of the tegumented viral capsids into small membrane cisternae derived from the trans-Golgi network (TGN) (Figure 1.1 - 11). In both cases, the glycoprotein content of the resulting viral envelope is believed to depend on the specific pathway. In both cases, HCMV glycoproteins exploit the host cell secretory pathway to be synthesized in the ER and subsequently modified in the Golgi apparatus, resulting in their accumulation within the TGN[72,76,77] (Figure 1.1 - 12). This allows tegumented capsids undergoing secondary envelopment via budding into TGN-derived membrane cisternae to directly acquire viral glycoproteins there. At the end of both secondary envelopment pathways, fusion of membrane-bound structures containing enveloped virions with the plasma membrane of the host cell (Figure 1.1 - 14) will result in the release of the viral progeny along with ILVs (Figure 1.1 - 15).

1.2.3 Organelle remodeling

A hallmark of HCMV infection is the profound remodeling of the host cell organelles induced to create a cellular environment that promotes viral replication. HCMV infection appears to drive convergent organelle remodeling across its broad cellular tropism despite the divergent organelle-associated proteome found in the different host cell types. Arguably, the most prominent change in cellular morphology is observed in the nucleus. However, the comprehensive organelle remodeling induced by HCMV typically affects all major subcellular compartments including mitochondria, peroxisomes and the endoplasmic reticulum (ER). The functional modulation of these organelles of the host cell leads to the establishment of a reorganized cellular environment that allows HCMV to effectively produce and disseminate the viral progeny[61,78,64].

Nucleus

HCMV orchestrates an extensive nuclear rearrangement that includes: (i) formation of phase-separated replication compartments that are essential for viral genome replication, (ii) disruption of the nuclear lamina and envelope facilitating nuclear egress of viral capsids, and (iii) restructuration of the nucleoskeleton to mediate trafficking of viral components[79,80]. Such substantial reorganization causes the nucleus of the host cell to adopt a morphology resembling the shape of a kidney bean or cashew nut.

Endoplasmic Reticulum

HCMV encodes the glycoprotein UL148, which specifically localizes to the ER and drives extensive structural reorganization of the organelle by activating its unfolded protein response. UL148 induces transformation of the characteristic tubular architecture of the ER network into a convoluted mesh-like network while promoting accumulation of ER-derived vesicles. The creation of these membrane structures has been found to play a crucial role in immune evasion and viral tropism.

In endothelial cells, HCMV has also been reported to form ER tunnelling nanotubes, enabling viral transmission from cell to cell. This direct cell spreading of the virus to neighbouring cells allows HCMV to evade extracellular immune detection[81,82,83].

Mitochondria

The HCMV-induced mitochondrial remodeling presents a bioenergetics contradiction. Given that the virus increases respiratory capacity of the organelle while paradoxically promoting mitochondrial fragmentation, this defies the established paradigm that mitochondrial fragmentation impairs energy production. The viral protein pUL37x1 promotes mitochondrial fragmentation by increasing recruitment of Dynamin-Related Protein 1 (DRP1) at the outer mitochondrial membrane (OMM), thereby driving peripheral mitochondrial fission. Simultaneously, pUL37x1, also known as viral mitochondrion-localized inhibitor of apoptosis (vMIA), is able to prevent the fragmented mitochondria from undergoing fusion by suppressing activity of the GTPase MitoFusiN-2 (MFN2)[84,85,86]. In order to compensate for the significant decrease in energy production commonly associated with mitochondrial fragmentation, HCMV employs multiple mechanisms to increase cellular respiration.

By upregulating mitochondrial biogenesis factors such as PGC1α, HCMV expands mitochondrial mass, which serves as a structural basis to establish a sustained increase in energy production. HCMV enhances mitochondrial respiratory capacity through the viral protein pUL13 interacting with the mitochondrial cristae-organizing system (MICOS) complex, which leads to substantial remodeling of cristae architecture. This change in mitochondrial cristae morphology induced by pUL13 drives oxidative phosphorylation by enabling increased electron transport chain throughput and citric acid cycle activity[87,84]. The effects of HCMV-induced organelle remodeling on mitochondria mirror those observed in peroxisomes with vMIA also emerging as principal orchestrator of peroxisome remodeling (see below and Chapter 3.1.2).

Peroxisomes

HCMV triggers a global upregulation of proteins involved in peroxisomal biogenesis through growth and fission (see Chapter 3.1.1) resulting in an increased cellular abundance of this organelle[78]. Intriguingly, the remodeling process appears to result in the emergence of two additional distinct peroxisome subpopulations in HCMV infected cells, with one being moderately smaller and the other substantially larger compared to peroxisomes not affected by the virus. Furthermore, peroxisomes were found to progressively transition from their characteristic spherical phenotype to an elongated and flattened morphology that seems to be particularly pronounced in the enlarged subpopulation. An increased surface-to-volume ratio in the peroxisomes exhibiting the elongated and flattened phenotype is suspected to proportionally increase metabolic throughput of processes involving peroxisomal membrane proteins[88]. Elevated lipid synthesis stemming for the enhanced peroxisomal metabolic capacity potentially reflects an evolutionary strategy designed to ensure adequate plasmalogens production, which is essential for the secondary envelopment stage during viral assembly[89,90]. In summary, the extensive impact of HCMV on peroxisomes appears to contribute significantly to sophisticated viral mechanisms that balance immune evasion with metabolic exploitation and support production of viral progeny.

Membrane contact sites

The comprehensive restructuring of membrane contact sites is another key aspect of HCMV-driven organelle remodeling in infected cells[93]. Membrane contact sites (MCSs) are regions where the membranes of two or more organelles approach within 30 nm proximity without undergoing fusion. These dynamic structures are typically formed through interaction of specialized membrane proteins in both organelles and enable rapid exchange of metabolites such as lipids independent of vesicular trafficking[91,92]. The ER-resident Vesicle-associated membrane protein (VAMP)-associated protein B (VAPB) can form a MCS with the Protein Tyrosine Phosphatase-Interacting Protein 51 (PTPIP51) in the outer mitochondrial membrane, while interaction of VAPB and the Acyl-CoA Binding Domain containing protein 5 (ACBD5) are involved in MCS between peroxisomes and the ER.

Through viral modulation of host gene expression, HCMV has been demonstrated to induce an almost global increase in synthesis of proteins involved in regulating the formation and activity of MCSs throughout the viral infection cycle[93]. HCMV is thought to increase metabolic cooperation between organelles at the level of MCSs and thereby promote production of viral components while simultaneously ensuring energy supply.

A notable instance of HCMV-induced manipulation of inter-organelle interaction involves the MCSs between mitochondria and the ER. As mentioned before, HCMV infection drives mitochondrial fragmentation and induces substantial remodeling of the ER. The newly produced pool of small mitochondria have been found to become encapsulated within the mesh-like topology of the restructured ER network[94]. These so-called Mitochondria-ER eNCapsulations (MENCs) rely on MCSs between ACBD5 and PTPIP51 forming a complex as well as a physical link between the two organelles. During HCMV infection, expression levels of both VAPB and PTPIP51 are significantly enhanced, which is thought to not only promote the formation of MENCs but also stabilize the corresponding interaction. The formation of MENCs is supposed to create a stable platform allowing HCMV to boost mitochondrial respiration to match the energy demands of viral replication[93,95].

By maintaining these intricate contacts between organelles in infected cells, HCMV likely inhibits recycling of the encapsulated mitochondria through mitophagy, simultaneously amplifying cellular energy production while suppressing mitochondria-mediated antiviral responses[93,96]. Furthermore, HCMV has been shown to introduce significant variations into the biogenesis and morphology of peroxisomes (see Chapter 3.1.2). Viral modulation of host gene expression associated with MCSs between peroxisomes and the ER such as VAPB, ACBD5 and GSK3β is suspected to play a crucial role in HCMV-induced peroxisome remodeling.

1.3 Electron cryo-microscopy

The maximal resolution that can be directly achieved with a light microscope is intrinsically limited by the diffraction of light, i.e. from photons, a fundamental principle described by Ernst Abbe in 1873[97]. According to Abbe's law, the minimum distance (d) between two points that can be resolved using light microscopy is defined by the following equation

$$d = \frac{\lambda}{2\,NA}$$

where λ is the wavelength of visible light and NA stands for the numerical aperture of the lens system. Since the NA in air can be approximated as 1 and the NA in vacuum actually being 1, then the wavelength becomes the limiting factor. The wavelength-limited maximum resolution is also referred to as the diffraction limit[98]. With the shortest wavelength visible to the human eye being approximately 380 nm (violet), the resolution of conventional light microscopy under ideal conditions is therefore diffraction-limited at roughly 190 nm.

It is possible to increase resolution beyond this limit by using imaging techniques based on particles that exhibit a wavelength significantly shorter than those of visible light photons. In 1923, Louis Victor Pierre Raymond, 7th Duc de Broglie theorized that particles, in particular electrons, not only present characteristics of particles but exhibit also wave-like properties including a given wavelength[99]. De Broglie determined that the wavelength of an electron is inversely proportional to its momentum. This discovery laid the foundation for the development of electron microscopy (EM). As an example, in an EM instrument with an acceleration voltage or high tension of 300 kV, electrons have a wavelength of approximately 0.002 nm, which is orders of magnitude smaller than the diameter of an atom or the length of an atomic bond. In this case, the resolution achievable by EM is instead limited by other factors, primarily those related to electron optics.

The most significant factor limiting EM resolution are indeed the unavoidable aberrations inherent to electron lenses. Unlike optical lenses focusing and dispersing light by refraction, electron lenses rely on electromagnetic fields to manipulate the trajectories of electrons[100]. Typically, electrons interact with matter so strongly that using them for imaging requires a high vacuum inside the microscope column to prevent any scattering prior to their interaction with the sample. While there are numerous different EM imaging modalities, we will focus here on the canonical implementations of transmission electron microscopy (TEM) and scanning electron microscopy (SEM).

In TEM, data acquisition relies on recording the electron beam after traversing the sample. The contrast in TEM images is created through differences in electron absorption, which originate from variations in the structure, composition and conductivity of the sample itself. A fundamental constraint in TEM is that the specimen must be thin enough to permit that sufficient electrons get transmitted through the sample for contrast formation[101,102]. To generate an image, SEM relies on collecting electrons scattered both elastically and inelastically as a result of the electron beam interacting with the sample[103]. Unlike elastic scattering, inelastic scattering of these accelerated incident electrons leads to a significant energy transfer to the irradiated sample. Following inelastic scattering, the transferred energy is released again based on three distinct processes, which differ in the energy lost by electrons in the process. The greatest energy loss occurs when inelastic scattering leads to the emission of secondary electrons. In comparison, the energy loss electrons experience during back-scattering is significantly lower. Back-scattering refers to scattering events that cause the primary electron to get deflected at an angle greater than 90 degrees, effectively reversing its trajectory. Lastly, the energy transferred during inelastic scattering can be released again by the emission of an X-ray photon[104,105].

The radiation damage resulting from these interactions between the electron beam and the sample represents another considerable constraint of EM. The impact of high energy electrons can displace atoms in the sample material, compromising its structural integrity. Dissipation of the energy transferred during scattering can cause molecular decomposition of the sample by breaking chemical bonds.

The extent of molecular and structural deterioration caused by such radiation damage is proportional to the acceleration voltage and dose rate of the electron beam[106]. This is particularly relevant for biological specimens, where it can result in radiolysis of water molecules and lead to the formation of hydrogen gas and multiple reactive oxygen species (ROS)[107]. The damage associated with these manifest as structural artefacts and fading of high-resolution information. Therefore, radiation damage typically limits the achievable resolution well before electron lens aberrations become the limiting factor, when working with biological specimens.

A well-established approach to mitigate beam-induced radiation damage of organic material involves vitrification of the sample prior to EM imaging. Vitrification refers to the process of cooling down the sample to liquid nitrogen temperature while preventing crystalline ice formation during the process. This is achieved by rapid freezing at a cooling rate exceeding 10^6 K/s, conditions under which water molecules can be immobilized in a glass-like amorphous state, called vitreous ice. Vitrification of reasonably thin biological specimens is typically done by quickly plunging the sample into a cryogenic solution consisting of ethane, propane or a mixture of both cooled to liquid nitrogen temperature[108]. Vitrification effectively limits energy dispersion and molecular dissociation in the sample thereby maintaining its structural integrity. Furthermore, vitrification abolished the need for additional steps. Methods commonly used to prepare samples for EM, such as chemical fixation and plastic embedding are widely recognized for causing substantial artefacts that can significantly distort cellular morphology, particularly affecting membranes[109,110]. Consequently, vitrification provides the means to preserve biological specimens in a near-native state instead. The method combining cryogenic fixation by vitrification and subsequent analysis by electron microscopy while maintaining the sample at liquid nitrogen temperature is referred to as electron cryo-microscopy (cryo-EM).

1.4 Focused ion beam milling

For cryo-TEM imaging to be effective, the examined sample must be electron-transparent. In a 300 kV instrument, this constraint restricts specimen thickness to approximately 300 nm, which is significantly smaller than the dimensions of a typical average mammalian cell. Therefore, cryo-TEM excels at visualizing inherently thin samples like purified proteins, macromolecular complexes in solution or isolated viral particles for example. The need for samples to be electron-transparent precludes the use of conventional cryo-TEM in studying intricate biological processes, such as viral replication or organelle remodeling, in their native cellular environment as a whole[111]. In recent years, the utilization of focused ion beam (FIB) milling for precise thinning of vitrified cellular specimens has been established as an effective strategy to overcome this limitation in sample thickness[112]. Initially developed for material science applications, the capability to manipulate material at nanometre resolution made this technique indispensable for the production of semiconductors in particular.

In the field of structural biology, FIB-milling can be used to prepare vitrified cellular specimens that are thin enough for cryo-TEM[113]. By carefully ablating material surrounding regions of interest, electron-transparent sections of the sample, called lamellae, are made. This process relies on the transfer of momentum from the ions to the targeted area of the sample causing the impacted atoms to be ejected through a process called sputtering. The majority of conventional FIB instruments employ liquid metal ion sources, with gallium being the most prevalent due to its favourable physical properties including a low melting point (29.8 °C). To create the ion beam, an electric field is applied to a tungsten needle wetted with liquid metal. Due to the resulting forces, the liquid metal is drawn into a distinctive cusp, known as a Taylor cone. The intense electric field at the tiny tip of this cusp causes ionization and field emission of the metal atoms[114].

More recently, there has been a growing interest in alternative ion sources, notably plasma-based ion beams utilizing noble gases such as argon and xenon. In theory, the use of plasma ion sources permits higher beam currents, facilitating efficient milling of large volumes and permitting high-throughput sample preparation. Furthermore, the ability to utilize multiple ion species is supposed to offer enhanced versatility, enabling tailored milling conditions for a wide range of materials and applications[115].

The emitted ions are then accelerated and focused into a beam, allowing for site-specific ablation of material at nanoscale precision. The electric current accelerating the ions can be precisely adjusted, enabling fine-tuning of beam characteristics in real-time for specific sample requirements throughout the milling process. High milling currents in the nanoampere regime maximize sputtering yield, enabling rapid bulk ablation of material. Low milling currents in the picoampere range restrict ion beam interaction, thereby achieving nanometre resolution for delicate thinning at the end of the milling process, commonly referred to as polishing[113,116].

However, exposing inherently sensitive biological samples like vitrified cells to a beam of high-energy ions also gives rise to the risk of radiation damage that can compromise the structural integrity of the specimen. Furthermore, the ion beam can induce charging effects in the sample, which is particularly crucial for non-conductive biological material. Accumulation of electrostatic charges within the sample compromises subsequent TEM imaging and deflects the ion beam during milling, causing erratic ablation of material[117]. To overcome these difficulties, a thin layer of conductive heavy metal, typically platinum, can be applied through condensation of organometallic precursors using gas injection systems (GIS) or physical vapour deposition of pure metal, commonly referred to as sputter coating[118]. This treatment also normalizes the surface morphology of the sample, creating a more uniform interaction with the ion beam. Since topographic variations of the sample surface lead to local differences in the sputter rate, platinum coating also mitigates the formation of corresponding artefacts referred to as curtaining effect. Ice contamination on the sample surface can severely compromise the adherence and homogeneity of the platinum layer.

Cryo-FIB instruments are often combined with scanning electron microscopes (SEM) in dual-beam systems. By integrating SEM modalities, these cryo-FIB-SEM instruments enable real-time monitoring and adjustment of the milling process, thereby providing precise control over the sample preparation workflow. Since both ion beam imaging and SEM are limited to visualizing the surface topology of the sample, they make it however difficult to distinguish the biological specimen from surrounding materials such as the support film, grids bars or ice. Consequently, identifying specific components of the sample based on biological characteristics is therefore virtually impossible. It follows that the platinum coating further exacerbates this problem. Accurately targeting the regions of interest in cells therefore represents one of the most significant challenges here, driving the need to integrate cryo-FIB-SEM with complementary labeling strategies within correlative approaches.

1.5 *In-situ* electron cryo-tomography

The specific advantage of cryo-EM lies in its capacity to visualize biological structures within their cellular context at unprecedented molecular resolution and under near-native conditions. By combining the principles of TEM with tomographic reconstruction, electron cryo-tomography (cryo-ET) is able to analyse a three-dimensional volume of a given object or region of interest inside cryogenically preserved samples[119]. The fundamental principle behind cryo-ET involves acquiring projection images or micrographs of the sample while it is physically tilted incrementally (i.e., every 3 degrees) around an axis perpendicular to the electron beam. Following data collection, the resulting set or stack of two-dimensional projection images of the specimen at multiple angles is commonly referred to as tilt series. During processing, tomogram reconstruction requires that the images in the tilt series are precisely aligned to correct for image distortion and movement of the sample during acquisition.

The alignment process typically relies on tracking distinctive features of known geometry present in all images like gold nanoparticles added to the sample before vitrification. In the absence of such fiducial markers, areas of the sample exhibiting pronounced structural characteristics may be identified through pattern recognition and tracked to align the tilt series. Through alignment, the three-dimensional coordinates of the tracked features in the sample are mapped to their respective two-dimensional positions in every image of the tilt series[120]. Tomogram reconstruction of the aligned tilt series then provides a three-dimensional representation of the original sample volume. Since most cellular specimens exceed the limitation of sample thickness imposed by cryo-ET, gaining a comprehensive insight into intracellular organization and macromolecular interactions there requires prior thinning of the sample at the region of interest. Consequently, the combination of cryo-FIB-SEM with cryo-ET applied to vitrified cells, commonly referred to as *in-situ* cryo-ET, enables three-dimensional structural analysis of nearly unperturbed intracellular environments[121,122].

1.6 Thesis outline

The aim of my PhD is to provide new insights into viral assembly and the associated organelle remodeling during HCMV infection directly in human fibroblast cells. The synergistic capabilities and recent advancements of electron cryo-tomography (cryo-ET) and cryo correlative light and electron microscopy (cryo-CLEM) approaches laid the foundation to reach this goal during the preparation of this thesis work.

Upon infection, HCMV orchestrates substantial alterations to cellular architecture and metabolic pathways of the infected host cell to facilitate production and dissemination of viral progeny. Recent studies leveraging super resolution fluorescence microscopy to investigate HCMV-induced organelle remodeling in live eukaryotic cells observed profound structural changes in mitochondria, peroxisomes and the ER[95,93]. Moreover, findings from such research revealed that viral manipulation of inter-organelle interactions through rearrangement of membrane contact sites connecting these organelles appears to be fundamentally important during HCMV infection.

However, the extent to which organelle remodeling and the associated restructuring of membrane contact sites contributes to viral replication during HCMV infection remains elusive. Along this line, the insufficient structural characterization of these complex mechanisms impedes our current ability to comprehend how HCMV-driven restructuring of cellular architecture promotes production and dissemination of viral progeny.

Therefore, the initial objective of my doctoral research project was the structural characterization of changes in organelle morphology occurring in the course of HCMV infection of human fibroblast cells in culture. For this purpose, we employed electron cryo-tomography (cryo-ET) in combination with focused ion beam (FIB) milling, enabling high-resolution, three-dimensional visualization of subcellular structures in their near-native state. At the beginning of my PhD, I focused on the HCMV-induced remodeling of mitochondria and ER. This involved investigating the viral restructuring of membrane contact sites between these organelles and the associated formation of mitochondria-ER encapsulations (MENCs)[95].

New findings from research conducted in the group of Ileana Cristea (Princeton University, NJ, USA) inspired me to subsequently shift the focus of my doctoral research towards peroxisomes in the framework of a collaboration with them. Peroxisomes were demonstrated to play a crucial role in efficient replication of enveloped viruses like HCMV and HSV-1. Moreover, during infection of both HCMV and HSV-1, there is significant increase in peroxisome biogenesis and induction of intriguing changes in peroxisome morphology during late stages of infection in particular[88].

Until now, research on peroxisomal morphology has predominantly focused on plant and fungal systems using conventional electron microscopy approaches, creating a fundamental gap of knowledge about the native morphology of peroxisomes in eukaryotic cells. To address this, identification and characterization of peroxisomes in human fibroblasts using cryo-ET was the goal pursued during the second part of my PhD.

The approach used to tackle this challenge involved establishment of a specific workflow integrating different imaging modalities such as cryo-FIB-SEM and cryo-ET with complementary cryo fluorescence microscopy, enabling the visualization of fluorescently labelled peroxisomes. The structure and composition of the vAC and the associated HCMV replication processes was also a topic investigated during my doctoral research. Rather than limiting our studies to high magnification tomograms of isolated elements within the vAC, we introduced the novel application of complementary overview tomograms recorded at lower magnification that allowed us to comprehensively analyse both individual components as well as their spatial organization and interactions by keeping a larger part of the cellular environment.

In summary, the work I conducted during my PhD takes advantage and highlights the value of complementary imaging modalities with newly developed approaches and workflows specifically applied. Throughout this thesis, the tailored pipelines were used to improve our understanding of HCMV interactions with the host cell, providing new perspectives in the intricate mechanisms underlying viral replication and associated organelle remodeling.

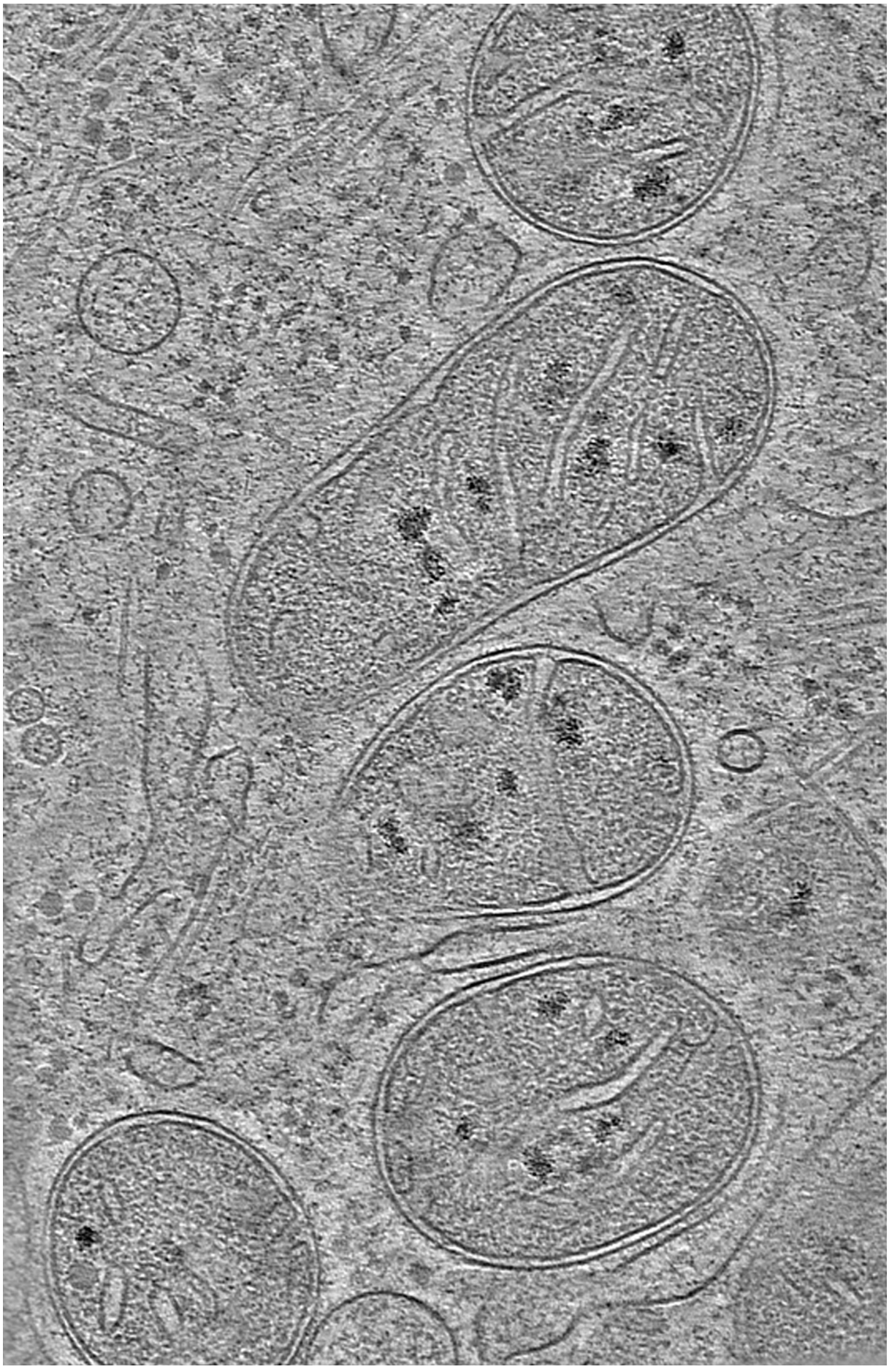

2 HCMV-induced remodeling of mitochondria

2.1 Introduction

HCMV infection represents a paradigm for understanding how viruses remodel host cell organelles to support the production of infectious progeny. Previous studies have established that HCMV infection induces profound mitochondrial fragmentation accompanied by enhanced respiration and inhibition of apoptosis[123,84]. In cells, mitochondria exist as dynamic networks that undergo continuous cycles of fission and fusion, processes that are fundamental to cellular energy homeostasis, stress responses and antiviral signaling[124,84]. During HCMV infection, the balance between these processes is disrupted through the expression of viral proteins, particularly pUL37x1, which localizes to mitochondria to promote fragmentation of the organelle[86]. Conventionally, mitochondrial fragmentation is associated with decreased bioenergetic output, oxidative stress, and targeting for autophagic degradation—conditions that would typically compromise viral replication[84,125]. The fact that HCMV drives both mitochondrial fragmentation and enhanced mitochondrial energy output therefore represents a striking paradox. The resolution of this paradox emerged through the discovery of mitochondria-ER encapsulations (MENCs), a novel type of membrane contact site (MCS) that forms preferentially around fragmented mitochondria during HCMV infection. In general, MCSs are specialized zones where two organelles maintain close proximity (typically 10-30 nm) without undergoing membrane fusion, facilitating the exchange of lipids, ions, and signalling molecules[126]. MENCs represent a previously uncharacterized form of ER-mitochondria interaction, distinct from classical mitochondria-ER contact sites (MERCs) in mammalian cells, typically involving dynamic interactions mediated by protein tethers such as PTPIP51 and VAPB[127,128,129]. These structures form stable, asymmetric encapsulations where ER tubules wrap around individual mitochondria in a cup-like manner. While classical MERCs have been extensively studied as dynamic platforms for cellular homeostasis, the stable encapsulation structures formed during viral infection represent a novel class of MCS with unique structural and functional properties[130,131].

The initial discovery of MENCs by the group of Ileana Cristea (Princeton University, NJ, USA) required integration of multiple complementary approaches, including live-cell super-resolution microscopy, mass spectrometry-based proteomics, and functional metabolic assays. To enable structural validation and characterization of these novel organelle interactions, complementary in-situ cryo-ET analysis was performed by me as part of a collaborative effort.

Based on:

Hofstadter, W. A., Cook, K. C., Tsopurashvili, E., **Gebauer, R.**, Pražák, V., Machala, E. A., Park, J. W., Grünewald, K., Quemin, E. R. J., & Cristea, I. M. (2024). Infection-induced peripheral mitochondria fission drives ER encapsulations and inter-mitochondria contacts that rescue bioenergetics. Nature communications, 15(1), 7352.[95]

2.2 Results and discussion

The primary objective of this study was to use in-situ cryo-ET to characterize the ultrastructural organization of MERCs in HCMV-infected human fibroblast cells, with particular focus on confirming the existence of MENCs and understanding their architecture in three-dimension. The cryo-ET analysis of human fibroblast cells infected by HCMV at 72 hours post infection (hpi) revealed the presence of MERC structures that matched the MENC morphology observed in previous live-cell fluorescence microscopy experiments.

Figure 2.1 a (corresponding to the left panel of Figure 3 C in the published work) shows a representative slice through a tomographic reconstruction containing such a MENC structure. The three-dimensional segmentation of this MENC is depicted in Figure 2.1 b (corresponding to the left panel of Figure 3 C in the published work). The ER membrane (shown in orange) forms a stable cup-like structure around the mitochondrion (shown in blue), with the ER membrane maintaining close proximity along extended regions of the mitochondrial surface.

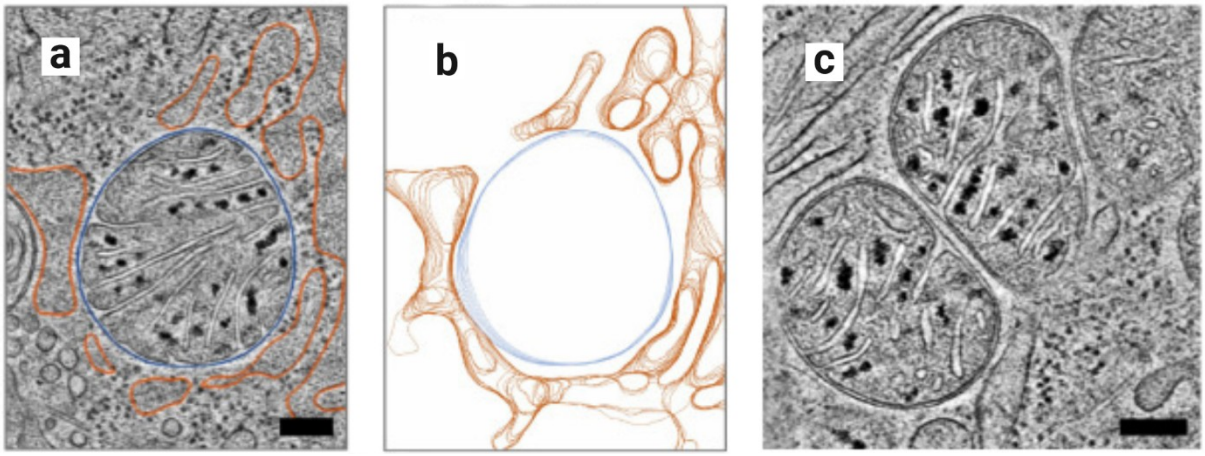

Figure 2.1 Mitochondria-ER encapsulation (MENC) and inter-mitochondria contact (IMCs). (a) Representative slice through tomogram reconstructed from cryo-TEM tilt-series of human fibroblast cell 72 hours post infection (hpi) with HCMV (scale bar 200 nm). (b) Three-dimensional segmentation of the MENC depicted in (a). The mitochondrial and ER membranes are outlined in blue and orange, respectively. (c) Representative slice through tomogram reconstructed from cryo-TEM tilt-series of human fibroblast cell 72 hours post infection (hpi) with HCMV showing IMCs (scale bar 200 nm).

These contacts were characterized by consistent intermembrane distances well within the established criteria for functional MCSs (10-30 nm), suggesting the presence of protein complexes mediating these interactions. This would be consistent with proteomic studies showing enrichment of PTPIP51 and VAP-B at MENC sites[125]. Unlike conventional MERCs, which typically involve small, localized interaction sites, MENCs encompass large portions of the mitochondrial surface. The asymmetric architecture of MENCs revealed by our cryo-ET analysis provides important insights into their potential functional roles during HCMV infection. The selective encapsulation of mitochondrial surfaces suggests that MENCs may create specialized microenvironments that regulate specific aspects of mitochondrial function while preserving others.

The extensive ER encapsulation observed in MENCs likely shields mitochondria from cellular stress signals that would trigger their autophagosomal degradation, which would be consistent with the observed suppression of mitophagy in HCMV-infected cells. The large contact interface may contribute to a more efficient exchange of metabolites, calcium ions and lipids between the two organelles, thereby facilitating the previously described increase in mitochondrial respiration and energy output during HCMV infection[132].

The results obtained through in-situ cryo-ET provide structural evidence for how HCMV-induced organelle remodeling creates specialized microenvironments that support viral replication.

In addition to MENCs, the cryo-ET analysis indicated the existence of inter-mitochondrial contact sites (IMCs) where mitochondria come into close proximity without undergoing fusion. These structures were consistent with the IMCs observed by live-cell fluorescence imaging studies. Figure 2.1 c (corresponding to Figure 5F in the published work) shows a representative example of an IMC observed in human fibroblast cells infected by HCMV at 72 hpi. The close proximity of the two outer mitochondrial membranes (OMMs) suggests the presence of protein tethers mediating the contact. IMCs are suspected to facilitate electrochemical coordination between fragmented mitochondria, thereby providing a structural basis for their enhanced respiratory capacity during HCMV infection. The results of the in-situ cryo-ET experiments presented here provide high-resolution ultrastructural insight into the viral remodeling of host cell organelles and associated MCSs by which HCMV increases cellular energy production to enable and maintain production of infectious viral progeny.

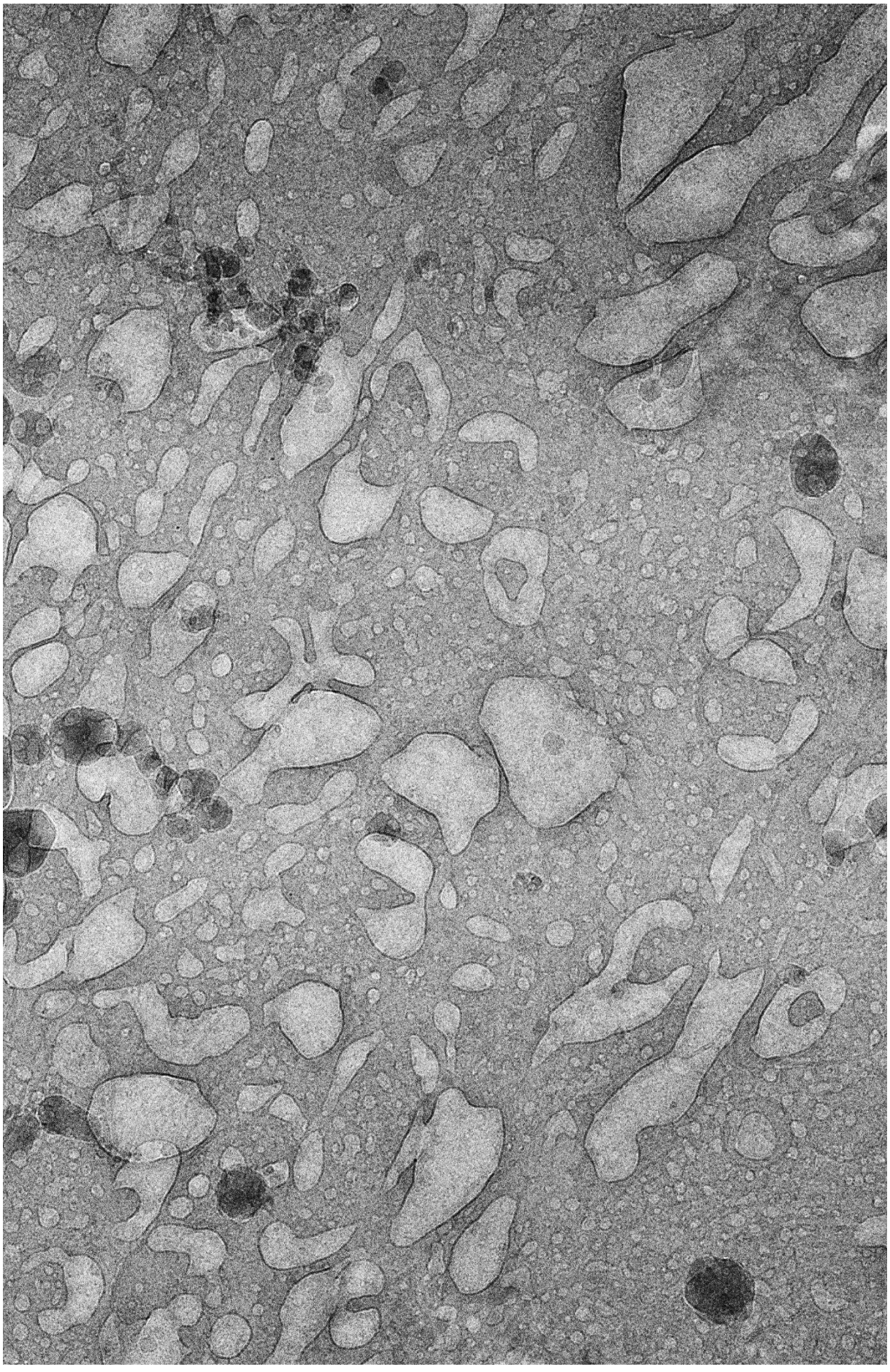

3 Identifying and characterizing organelles in cryo-ET

3.1 Introduction

3.1.1 Peroxisomes

Peroxisomes are found in almost every eukaryotic organism but exhibit great morphological and functional diversity[133,134,135]. These single-membrane-bound organelles compartmentalize enzymes, which catalyse numerous essential metabolic processes such as beta-oxidation of fatty acids, detoxification of reactive oxygen species (ROS) such as hydrogen peroxide, and synthesis of ether phospholipids like plasmalogens[136,137]. Recently, peroxisomes have been found to serve as signalling node for host pathogen interactions and to play a crucial role in non-metabolic functions like cellular stress, innate immune responses, and anti-viral or anti-inflammatory signaling[138,139,140].

The diverse functionality of peroxisomes partially stem from their collaborative relationship with other subcellular compartments, such as mitochondria, lysosomes, lipid droplets, and the ER. Peroxisomes dynamically engage in close physical interaction with other organelles through membrane contact sites. Thereby, peroxisomes form a network to facilitate metabolic cooperation and functional integration with other organelles[141,92,142]. Furthermore, peroxisomes possess the remarkable ability to rapidly and effectively modulate a vast number of cellular pathways in response to environmental or metabolic requirements. The balance between peroxisome biogenesis and pexophagy, the recycling of peroxisomes through autophagy, is a principal element of this. Peroxisomes also dynamically alter their cellular abundance and distribution by altering the ratio of these two processes . In fact, proteins encoded by the PEX gene family are responsible for orchestrating not only peroxisome biogenesis but also peroxisomal membrane and matrix protein trafficking. These proteins are referred to as peroxins and are conserved across eukaryotic organisms employing peroxisomes[143].

Dysregulation of the peroxisomal biogenesis and pexophagy pathways have been associated with a range of clinical disorders in humans. Mutations in any of the 14 PEX genes found in the human genome result in a clinically heterogeneous group of conditions collectively known as Zellweger spectrum disorders (ZSD). The severity of the individual clinical manifestation directly correlates with the degree of residual peroxisome activity. Complete disruption of peroxisome formation or functions cause the most severe phenotypes[144,145]. Thus, understanding the molecular mechanism underlying peroxisome biogenesis has the potential to elucidate novel therapeutic approaches for ZSDs.

Under normal physiological conditions, peroxisome biogenesis is driven by two distinct pathways, which are both regulated by peroxins. Formation of peroxisomes de novo involves fusion of precursor structures derived from other organelles and called pre-peroxisomal vesicles. In parallel, proliferation of peroxisomes can also result from an intricate multi-step mechanism that regulates the growth and division of mature peroxisomes[146,147].

De novo biogenesis of peroxisomes

New peroxisomes can be created through a process of *de novo* formation that begins with budding of pre-peroxisomal vesicles from the mitochondria or the ER. Maturation of those pre-peroxisomal vesicles requires interaction of the two membrane-bound early peroxins PEX3 and PEX16. In this context, maturation refers to the process of a pre-peroxisomal vesicle acquiring the peroxisomal matrix and membrane proteins necessary to transform it into a fully functional peroxisome. This protein complex comprising PEX3 and PEX16, and together with the cytosolic chaperone protein PEX19, is responsible for the targeting and subsequent insertion of peroxisomal membrane proteins (PMPs). The components of this PMP import machinery are divided between the two distinct types of pre-peroxisomal vesicles depending on whether they are derived from mitochondria or ER.

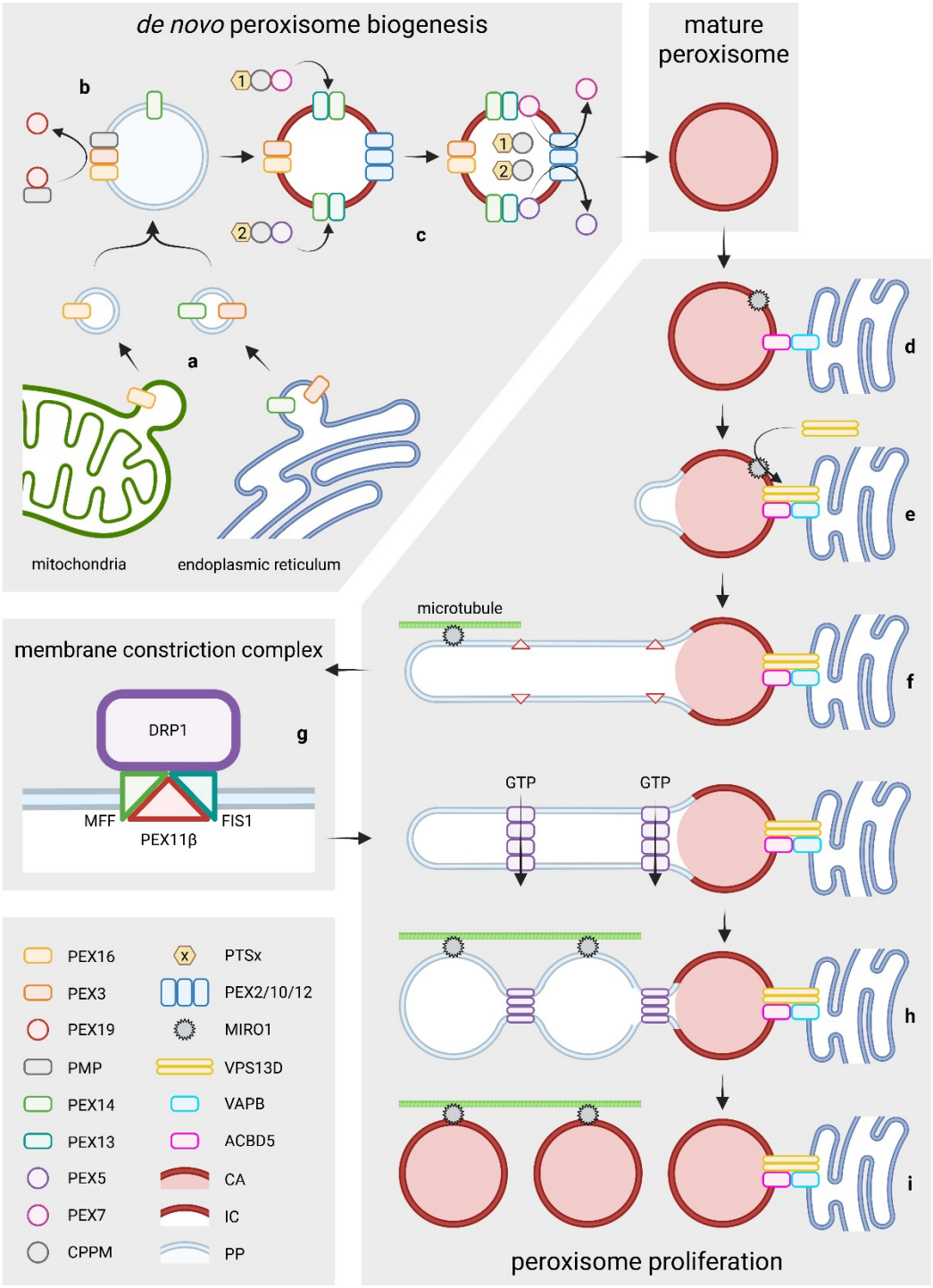

Figure 3.1 Schematic illustration of peroxisome biogenesis. De novo formation of peroxisomes is initiated by (a) formation and release of pre-peroxisomal (PP) vesicles derived from mitochondria and the ER. (b) Fusion of these vesicles enables peroxisomal membrane protein (PMP) insertion mediated by PEX3, PEX16 and PEX19. (c) Next, incorporation of the PMPs PEX2, PEX10, PEX12 and PEX13 forms the matrix protein import machinery, facilitating the recruitment and translocation of cytosolic peroxisomal matrix proteins (CPPM) trough interaction with PEX5 and PEX7, transforming the vesicle into an import competent (IC) organelle. Maturation is completed by accumulation of catalytically active (CA) CPPMs. (d) Peroxisome proliferation begins at membrane contact sites formed by interaction between peroxisomal ACBD5 and ER-resident VAPB. Following (e) recruitment of VPS13D by MIRO1, transfer of lipids initiates peroxisomal growth. (f) MIRO1 and PEX11β drive further membrane remodeling leading to the formation of a tubular protrusion. (g) Next, PEX11β recruits MFF and FIS1 to anchor DRP1, which oligomerises and constricts the tubular protrusion through GTP hydrolysis, forming a beads-on-a-string morphology. (h) Successful fission additionally requires interactions with the cytoskeleton mediated by membrane adapter proteins like MIRO1. (i) Newly formed peroxisomes must undergo maturation to become metabolically competent organelles. Figure was created using BioRender.

Maintaining these early peroxins in separate pre-peroxisomal vesicles plays a crucial role in adjusting the rate of de novo peroxisome formation in response to the abundance of mature peroxisomes. In practice, during the initial stage of de novo peroxisome formation, tubular membrane protrusions emerge from the OMM and actively accumulate PEX3 and PEX14. These OMM evaginations facilitate the formation and subsequent release of mitochondria derived pre-peroxisomal vesicles, which carry early peroxins indispensable for peroxisome biogenesis[148].

ER-derived pre-peroxisomal vesicles are created through budding at peroxisome specific membrane domains in the ER. These domains are enriched in certain PMPs, PEX16 in particular. Therefore, ER-derived pre-peroxisomal vesicles are enriched in PEX16 and required for the assembly of the peroxisomal membrane import machinery[149,150,151] (Figure 3.1 a). These ER-derived pre-peroxisomal vesicles also represent the primary source of lipids for de novo peroxisome biogenesis. As a result, the peroxisomal membrane exhibits a lipid composition similar to the ER characterized by phosphatidylcholine (PC) being the main phospholipid present[152].

The fusion of a mitochondria-derived pre-peroxisomal vesicle and an ER-derived one leads to the creation of a premature peroxisome. In the membrane of this peroxisome precursor, PEX3 and PEX16 are able to form a complex. This membrane protein complex is capable of leveraging cytosolic PEX19 to recruit and subsequently insert PMPs into the membrane of the nascent peroxisome (Figure 3.1 b).

Premature peroxisomes use this PMP import machinery to acquire the membrane-bound components of the peroxisomal matrix protein import machinery, namely PEX2, PEX10 and PEX12 and PEX13. Proteins containing one of two peroxisomal targeting sequences PTS1 or PTS2 are recruited to the PMP complex comprising PEX2, PEX10 and PEX12 and PEX13 by cytosolic receptor peroxins, PEX5 or PEX7 respectively. This is followed by import of these cargo-receptor complexes across the membrane and into the peroxisomal matrix through interaction with the PMP PEX14.

The peroxisomal matrix protein import machinery defies classical protein translocation paradigms because of its ability to accommodate natively folded proteins and even macromolecular complexes[153,154,155,156]. Following cargo delivery, the receptor peroxins undergo ubiquitination by a PMP complex comprising PEX2, PEX10 and PEX12. The ubiquitination triggers their membrane extraction and subsequent cytosolic recycling by recruiting the cytosolic peroxins PEX1 and PEX6[157,158] (Figure 3.1 c).

Once the import machinery for both membrane and matrix protein have been assembled, full metabolic competence of the premature peroxisomes can be established. This is achieved by populating the organelle interior with peroxisomal matrix proteins such as acyl-CoA oxidases mediating peroxisomal β-oxidation. Completion of this process concludes peroxisome maturation. Mature peroxisomes can further increase their cellular abundance through a mechanism of growth and division, enabling ongoing organelle proliferation after an initial pool of peroxisomes is established by *de novo* biogenesis as described hereinabove.

Peroxisome proliferation

Plants and fungi appear to continuously engage both generative (i.e., *de novo*) and proliferative peroxisome biogenesis mechanisms simultaneously. However, mammalian cells have been reported to primarily expand existing populations by division of mature peroxisomes and initiate de novo formation almost exclusively upon peroxisomal depletion[134,159].

Peroxisome proliferation involves several sequential stages of extensive membrane remodeling in mature spherical peroxisomes, such as elongation, constriction and final fission. This process is initiated at membrane contact sites formed by the interaction of the peroxisomal membrane protein Acyl-CoA Binding Domain containing protein 5 (ACBD5) and ER-resident Vesicle-associated membrane protein (VAMP)-associated protein B (VAPB). The interaction of ACBD5 and VAPB is a prerequisite for the remodeling of the peroxisomal membrane[160,127] (Figure 3.1 d).

At newly formed membrane contact sites between peroxisomes and the ER, Vacuolar Protein Sorting 13 homolog D (VPS13D) is recruited by Mitochondrial Rho GTPase 1 (MIRO1) to establish a hydrophobic channel. VPS13D facilitates lipid transfer between the two tethered organelles thereby enabling peroxisomes to acquire phospholipids capable of introducing membrane curvature from the ER, particularly phosphatidylethanolamine (PE) and phosphatidylinositol 4,5-bisphosphate (PI(4,5)P2)[161] (Figure 3.1 e). Members of the MIRO family of proteins primarily function as molecular adaptors linking membrane-bound organelles to microtubule-associated motor proteins. They are not only key for short-range mobility of peroxisomes but have also been proposed to have a major contribution in membrane elongation and fission during peroxisome proliferation[162]. The Glycogen Synthase Kinase 3 beta (GSK3β) plays a crucial role in regulating the interaction of ACBD5 and VAPB at these membrane contact sites. By directly phosphorylating ACBD5, GSK3β is able to inhibit formation of such membrane contact sites between peroxisomes and the ER as ACBD5 in the phosphorylated state is unable to bind VAPB[127].

Following initial membrane remodeling mediated by the aforementioned phospholipids, a tubular membrane protrusion emerges from the peroxisome. Here, MIRO1 and PMPs belonging to the PEX11 family directly link the membrane protrusion of peroxisomes to motor proteins and the cytoskeleton. This process is thought to drive further membrane deformation by generating additional membrane tension[163] (Figure 3.1 f). In this so-called elongated state, peroxisomes exhibit remarkable preferential and asymmetric localization of peroxins[164]. The spherical mature part of the elongated peroxisome appears to retain most matrix and membrane proteins associated with its catalytic activity until the division process is completed. PEX14, along with other early peroxins crucial for peroxisomal matrix and membrane protein import, have a strong affinity for cholesterol-enriched lipid rafts. In elongated peroxisomes, these lipid rafts are also found primarily in the tubular membrane extension (Figure 3.1 f).

The next stage in peroxisome proliferation involves the constriction of the membrane protrusion. The peroxin PEX11β is pivotal in initiating this. Beyond its membrane remodeling activity, PEX11β is indeed indispensable for membrane constriction and subsequent division[165,166]. The underlying mechanism involves the selective recruitment of the membrane adaptor proteins mitochondrial fission factor (MFF) and mitochondrial fission 1 protein (FIS1) by PEX11β. Thereby, a scaffold is formed, which represents an integral component of the molecular machinery that drives membrane fission[167]. MFF and FIS1 serve as membrane anchors for the GTPase Dynamin-Related Protein 1 (DRP1), which oligomerises into helical filaments and forms rings around the tubular membrane protrusion[168] (Figure 3.1 g). PEX11β then triggers the GTPase activity of DRP1, which causes the circularized filamentous structures to constrict. The resulting local contraction of the nascent peroxisomal membrane gives rise to an intermediate morphology resembling beads on a string[168] (Figure 3.1 h). However, DRP1-dependent constriction of membrane protrusion is necessary but not sufficient to complete peroxisomal division. Successful membrane scission likely requires simultaneous interaction between the premature peroxisomes and the cytoskeleton. Following fission, the newly formed premature peroxisomes are indeed separated from the mature organelle by microtubule-associated motor proteins[169,167] (Figure 3.1 k). The membrane fission machinery facilitating organelle proliferation through division exhibits striking similarity between peroxisomes and mitochondria. In particular, both organelles rely on a conserved set of proteins including MFF, FIS1, DRP1 and MIRO1, while PEX11β emerges as the only component of the machinery specific to peroxisomes.

Throughout the entire process of peroxisomal growth and division, the protrusion of the peroxisome exhibits no significant metabolic activity, while the majority of corresponding membrane and matrix proteins remain confined to the mature spherical parent structure. Therefore, the newly formed peroxisomes will need to complete maturation using a process similar to *de novo* biogenesis.

3.1.2 Antiviral signalling and immune evasion

The collaborative role of mitochondria and peroxisomes extends beyond lipid metabolism to include crucial antiviral defence mechanisms. These organelles can function as signalling nodes for the initiation and regulation of cellular immune response[170,171].

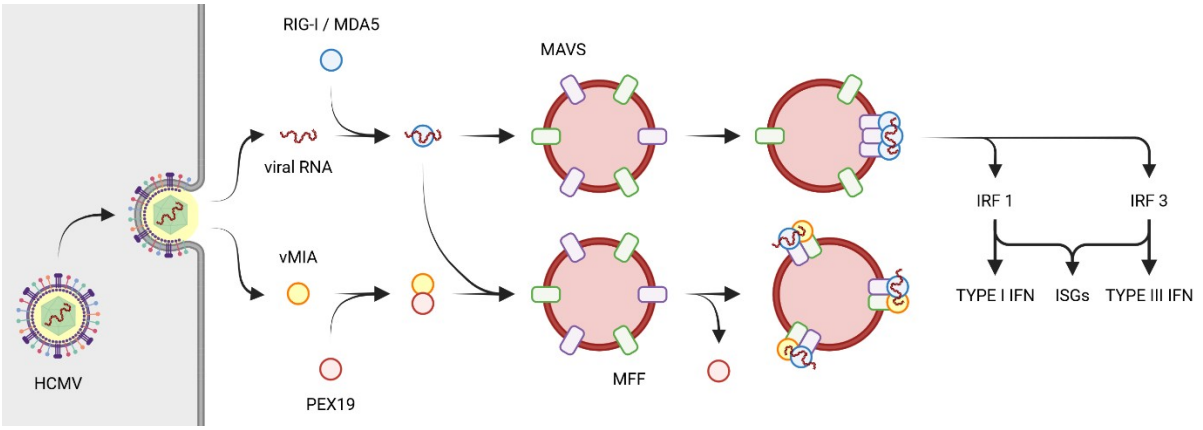

Figure 3.2 Schematic illustration of peroxisomal MAVS mediated antiviral signalling and its disruption by HCMV through vMIA (pUL37x1). Cytosolic detection of viral RNA by the retinoic acid Inducible Gene I like receptors RIG-I and MDA5 triggers oligomerization of mitochondrial antiviral signalling proteins (MAVS) amplifying interferon (IFN) production and facilitating induction of IFN-stimulated genes (ISGs). After exploiting PEX19 for insertion into the peroxisomal membrane, the viral mitochondria-localized inhibitor of apoptosis (vMIA) is able to disrupt MAVS-mediated antiviral signalling by preventing MAVS from undergoing oligomerization. Figure was created using BioRender.

Detection of viral entry

Following viral entry, the presence of viral nucleic acids in the cytosol of the host cell triggers a signalling cascade resulting in the suppression of viral replication and dissemination as well as activation of inflammatory responses[172]. To detect distinct components of viruses and other intracellular pathogens, collectively known as Pathogen Associated Molecular Patterns (PAMPs), host cells utilize specialized Pattern Recognition Receptors (PRRs)[172,173]. Mammalian cells employ cytoplasmic Retinoic acid Inducible Gene I like receptors such as RIG-I and Melanoma Differentiation-Associated protein 5 (MDA5) as complementary PRRs to recognize viral RNA in the cytoplasm[174].

Upon binding to viral RNA, RIG-I and MDA5 stimulate innate immune responses by triggering a cascade of antiviral signalling. This response is subsequently amplified through the interaction of these PRRs with Mitochondrial Antiviral Signalling proteins (MAVSs).

Binding of viral RNA leads to the oligomerization of MAVS in different subcellular compartments through interaction with the Caspase Activation and Recruitment Domain (CARD) of corresponding PRRs. Activation of the MAVS signalling pathway leads to the production of interferons (IFNs) and proinflammatory cytokines. Mammalian cells rely on IFNs and their downstream induction of IFN-stimulated genes (ISGs) to establish an antiviral state (Figure 3.2). ISGs encode numerous effector proteins crucial for disrupting viral replication and enhancing innate immune responses.

The essential role of peroxisomes and mitochondria in mounting an effective defence against viral infections is linked to MAVS being localized to their membranes. Peroxisome associated MAVS contribute to this host defence mechanism by triggering immediate but transient type-I-IFN-independent induction of ISGs upon detection of PAMPs. Complementary to the rapid initiation of antiviral signalling through peroxisomal MAVS, mitochondria associated MAVS mediate delayed stabilization and amplification of the immune response. This process relies on sustained type-I-IFN-dependent expression of ISGs[170,175,176]. This separation of the MAVS driven antiviral response into two separate pathways exhibiting different kinetics allows for precise and dynamic regulation of the corresponding immune signalling.

Antiviral defence mechanisms

Peroxisomes are involved in several other crucial aspects of innate immunity beyond their critical role in antiviral signalling. One of these key aspects is the synthesis of eicosapentaenoic acid (EPA) and docosapentaenoic acid (DPA), which is facilitated by the peroxisomal fatty acid metabolism.

These lipids are indispensable for the production of anti-inflammatory and immunomodulatory lipids and thus further contribute to the ability of mammalian cells to effectively combat viral infections. For instance, EPA serves as precursor for the synthesis of resolvins and protectins, which disrupt pro-inflammatory pathways by interfering with NF-κB and MAPK signaling[177,178].

The ability of peroxisomes to regulate ROS homeostasis represents another critical component of the host cell immune response as ROS is integral to the elimination of pathogens through phagocytosis[179]. Peroxisomal ROS production enhances phagocytic efficiency by modulating actin polymerization at phagosome membranes. Furthermore, ROS production enables pathogen clearance by creating a toxic oxidative microenvironment that disrupts viral integrity. While ROS are used in these defence mechanisms, peroxisomal antioxidant enzymes prevent host cell damage[180].

Viral immune evasion

Through their diverse contribution to host-pathogen interactions and antiviral defence mechanisms, peroxisomes have emerged as critical organelles in mounting an effective host defence against viruses. The significance of peroxisomes in cellular immune response is further emphasized by the fact that viruses including HCMV have evolved intricate strategies specifically aimed at evading and disrupting peroxisomal antiviral signalling. The mechanism HCMV employs to prevent peroxisomes from provoking an immune response is enabled by the IE gene encoding the predominant UL37 exon 1 protein (pUL37x1)[181,182,183].

This viral protein, which is also known as viral Mitochondrial-localized Inhibitor of Apoptosis (vMIA) inserts itself into peroxisomal membranes by interacting with PEX19, the cytosolic chaperone of the PMP import machinery. There, vMIA interferes with MAVS signalling and induces fragmentation of the organelle. In mitochondria, HCMV relies on triggering fragmentation of the organelle to inhibit the corresponding MAVS signaling[184,185]. However, the ability of vMIA to induce fission and to disrupt MAVS-mediated antiviral response in peroxisomes has been discovered to be governed by two independent mechanisms.

vMIA prevents peroxisomes from propagating the antiviral signalling cascade originating from RIG-1 and MDA5 by inhibiting oligomerization of peroxisomal MAVS (Figure 3.2). This process has been found to require MFF[186]. The increase in peroxisomal division observed during HCMV infection is contingent on a functional membrane fission machinery. In the absence of MFF or DRP1, peroxisomal division is disrupted, which was found to result in the inability of vMIA to promote peroxisome proliferation[167]. Recently, a model for the role of the DRP1-dependent fission machinery in HCMV-induced peroxisomal fragmentation has been suggested by the group of Ileana Cristea according to which vMIA promotes recruitment of MFF to peroxisomes by activating PEX11β. This highlights another key difference between the antiviral responses emanating from peroxisomes and mitochondria as peroxisomal MAVS signalling apparently functions independently of changes in organelle morphology through fusion or fission[187,183,186].

Given the critical role of peroxisomes in antiviral signalling through MAVS oligomerization and their susceptibility to vMIA-induced fragmentation, the structural characterization of these organelles in their native cellular context becomes paramount for advancing our understanding of innate immune mechanisms and how HCMV eludes these[188,180].

3.1.3 Cryo correlative light and electron microscopy

Correlative light and electron microscopy (CLEM) is a technique that integrates the labeling specificity obtainable through fluorescence light microscopy (FM) with the high-resolution structural information provided by electron microscopy (EM)[189,190]. The principle of CLEM is to localize molecules of interest using a fluorescence signal, making use, for example, of fluorescent genetic tags, and then image using high-resolution EM. This way the structure and identity of any molecule is available. The technique that employs this correlative approach to study vitrified samples is called cryo-CLEM and offers significant advantage for targeted structural biology research, as it allows biological specimens to be examined in a near-native state. However, cryo-CLEM introduces a considerable number of additional difficulties and limitations compared to its room temperature counterpart[191,192].

A major source of the challenges associated with cryo-CLEM is the need to maintain the samples at liquid nitrogen temperatures. For this purpose, vitrified samples generally remain submerged in liquid nitrogen while being stored or handled. However, as a consequence of their direct contact with liquid nitrogen, the samples are at risk of being contaminated with crystalline ice. When exposed to air, ice crystals can form in the liquid nitrogen through condensation of ambient humidity and adhere to the submerged specimen. Ice contamination can cause significant problems during cryo-ET data acquisition. Smaller crystals reduce the signal to noise ratio of acquired data, while larger crystals can completely obscure the region interest[108,193,194,195]. In some instances, the contamination risk can be mitigated by keeping the sample in the vapour phase, which refers to the layer of cold nitrogen gas that forms above liquid nitrogen due to evaporation. For example, this method is used in the STELLARIS 8 cryo confocal fluorescence microscope (Leica Microsystems) to cool the sample.

Cooling through direct contact with liquid nitrogen or its vapour phase stands in contrast to how temperature control is achieved in cryo-EM. In cryo-EM instruments, such as Aquilos, Arctis (see chapter 1.4) and Krios (see chapter 1.3), the sample is introduced into the vacuum of the electron column, which precludes the use of liquid nitrogen as coolant. Instead, the metal stage holding the sample is passively cooled, allowing thermal energy from the EM-grid to dissipate into the stage through conduction. As a result, ice contamination of a sample on the stage is virtually impossible[196].

In cryo-FM, the need to maintain the sample at liquid nitrogen temperatures also limits the radiant exposure that can be used to excite the fluorophores in vitrified biological specimens[197]. In this case, radiant exposure indicates the amount of energy that is delivered by the light source to the surface of the sample. If the rate at which this energy is absorbed by the specimen exceeds the rate at which it can dissipate through the cooling system, the temperature of the sample rises.

At temperatures exceeding approximately -135 °C the amorphous phase of the vitreous ice transitions into a crystalline phase. This process is called devitrification and causes irreversible structural damage in cryogenically preserved biological specimens. Since radiant exposure is defined as the product of light intensity per surface area and the exposure time, a safe range for the corresponding imaging parameters has to be determined and maintained to prevent devitrification. Conversely, the objective in cryo-FM instruments has to be kept at room temperature to maintain its structural integrity[108,195,198].

Several considerations have to be taken into account when determining a strategy for fluorescent labeling that is suitable for cryo-CLEM. The fact that cryogenic fixation is used to preserve live cells in a near-native state greatly reduces the number of applicable labeling approaches. For example, immunolabeling is generally considered to be incompatible with cellular cryo-CLEM as immunolabeling of intracellular targets typically requires prior chemical or physical permeabilization of the cell membrane. Because these treatments compromise the native structure of the sample, they would defeat the purpose of vitrification[109,110]. The most common compatible approach relies on the recombinant expression of fluorescently labelled proteins or the use of live cell staining.

Another challenge in cryo-CLEM is correlating data from two fundamentally different imaging modalities. Precise image registration is essential to achieve accurate spatial correlation between the fluorescent signals observed in cryo-FM and the structural data obtained through cryo-EM. In CLEM, image registration typically relies on the presence of multiple features that are clearly visible in both microscopes to serve as fiducial markers. If the position of these fiducial markers can be pinpointed with both cryo-EM and cryo-FM, their coordinates can be mapped onto each other to align the corresponding images. For this purpose, gold nanoparticles or polystyrene microspheres stained with fluorescent dyes can be added to the sample just before vitrification to create artificial fiducial markers[190].

The limitations of cryo-CLEM are exacerbated when investigating structures inside vitrified cells. To gain access to the intracellular space, site-specific thinning of the sample in a cryo-FIB-SEM instrument is employed to produce electron-transparent lamellae[199,200].

However, every examination or processing of the vitrified cells in a microscope entails exposure of the sample to liquid nitrogen during loading and unloading. Consequently, incorporating FIB-milling with cryo-CLEM further increases the risk of ice contamination. If the sample was contaminated prior to being loaded into the cryo-FIB-SEM instrument, the crystalline ice on its surface can also impede the milling process[201,112]. Integrating FIB-milling with cryo-CLEM also leads to most of the cell and consequently the majority of fluorophores in the ROI being removed during the milling process. As a result, the fluorescent signal emitted from a lamella represents only a fraction of the initially observed fluorescence[202].

Due to the platinum layer that is applied to the sample during lamella preparation, the area of the grid that has not been thinned by FIB-milling appears opaque in cryo-ET. As a result, the requirements for a fiducial marker suitable for precise image registration are further restricted, as anything outside the lamella sites, like fluorescent beads on the sample surface, would be rendered invisible. For this reason, exploring alternative approaches to overcome this issue and the various other challenges encountered in cryo-CLEM is of great importance.

Our collaborative efforts with the group of Ileana Cristea (Princeton University, NJ, USA) inspired us to elucidate the effects of HCMV-induced organelle remodeling on peroxisomes in the infected cells. For this purpose, we first sought to explore peroxisomes under physiological conditions using *in situ* cryo-ET. However, our current understanding of the morphology of mammalian peroxisomes in vitrified cells is very limited. To address this, I set out to characterize the morphology of mammalian peroxisomes by integrating cryo-CLEM with the conventional *in situ* cryo-ET workflow.

3.2 Results

3.2.1 Integrating cryo-FM with *in-situ* cryo-ET

Before employing cryo-CLEM to identify and characterize mammalian peroxisomes in a near-native state using cryo-ET, a suitable target for fluorescent labelling had to be identified. The exclusive peroxisomal localization of most PEX proteins would make them obvious candidates as specific peroxisome markers. However, each of these proteins typically performs multiple critical functions in peroxisomes. Consequently, recombinant expression of a fluorescently labelled PEX protein poses the inherent risk of interfering with peroxisome biogenesis and function[203,134]. Instead, we employed a construct fusing peroxisomal targeting sequence 1 (PTS1) with the fluorescent protein mCherry, which was kindly provided by the group of Ileana Cristea in the framework of our collaboration. PTS1 is a signalling peptide that labels proteins for peroxisomal matrix import (see chapter 3.1.1). This allows PTS1-mCherry to accumulate inside peroxisomes, which makes it a highly specific peroxisomal marker. The recombinant expression of PTS1-mCherry was found to have no effect on the native morphology and function of peroxisomes visible in FM. Since PTS1 solely facilitates PEX5-mediated translocation of the fluorophore inside peroxisomes, PTS1-mCherry labelling was also assumed to have negligible or no impact on the native structure and HCMV-induced remodeling of peroxisomes.

Our approach to investigate viral remodeling of peroxisomes involved combining PTS1-mCherry with a genetically engineered variant of HCMV, in which vMIA is labelled with GFP. The viral protein vMIA enables HCMV to suppress antiviral responses of the host cell by disrupting peroxisomal and mitochondrial MAVS signalling. Research conducted by in the group of Ileana Cristea (Princeton University, NJ, USA) indicates that the localization of vMIA shifts as infection progresses. During the first 72h of infection, vMIA localizes to both peroxisomal and outer mitochondrial membrane. As the infection progresses further, vMIA transitions to predominant mitochondrial association.

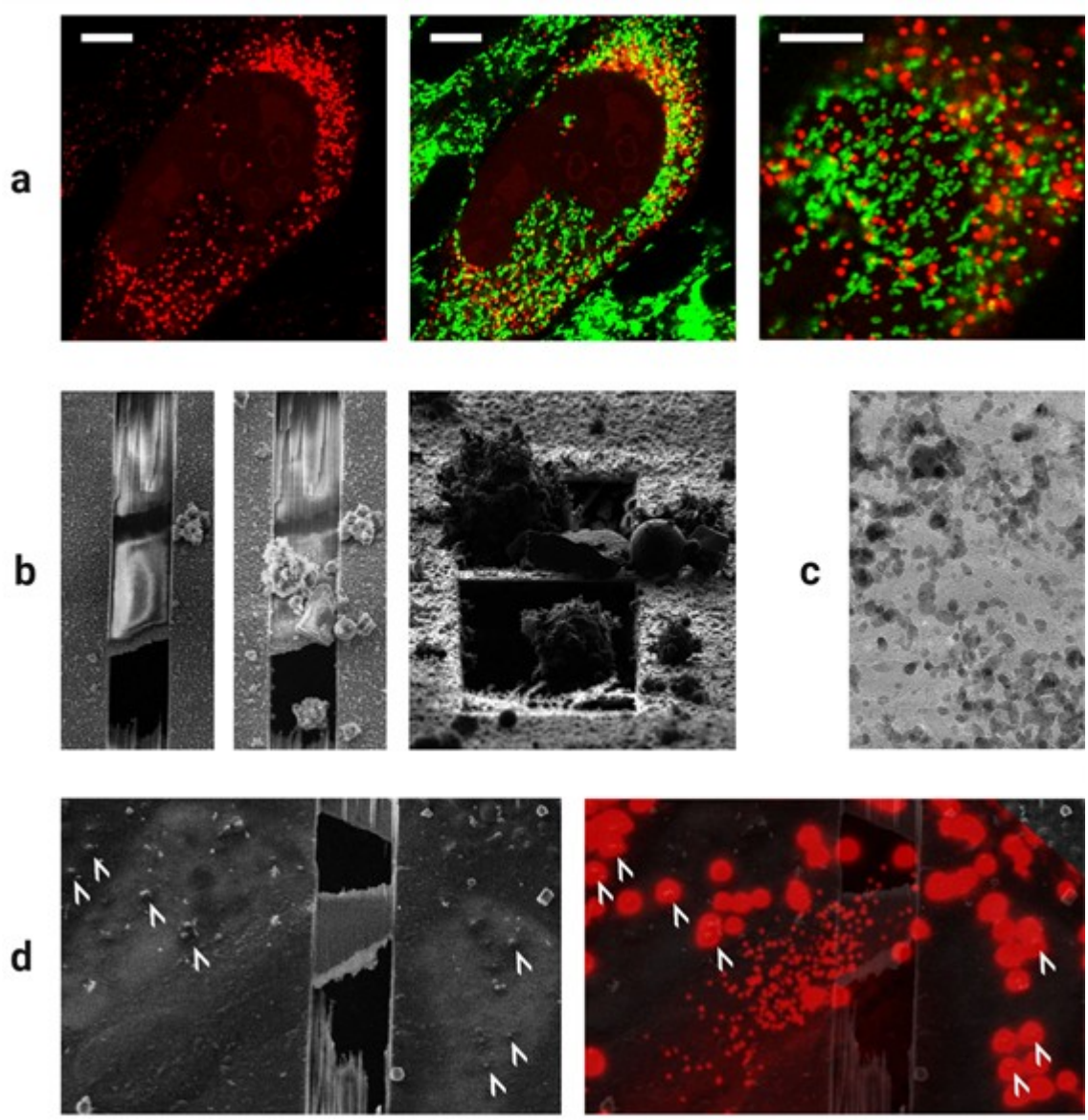

Figure 3.3 Representative examples illustrating different challenges in cryo-CLEM targeting mammalian peroxisomes. (a) Human fibroblast cells were transfected with PTS1-mCherry and subsequently infected with HCMV expressing vMIA-GFP. The sample was fixed with paraformaldehyde at 120 hours post-infection (hpi) and imaged using confocal fluorescence microscopy. All three panels depict the same cell imaged at different z-stack layers, with the left and middle panels representing the same slice and the right panel a different and slightly magnified one (scale bar 10 µm). (b) Lamella observed in cryo-FIB-SEM before (left) and after (middle, right) cryo-FM imaging. (c) Cryo-TEM micrograph recorded at 26000x magnification showing a polished lamella covered with ice contamination originating from cryo-FM imaging. (d) Fluorescent TetraSpeck microspheres used for image registration as seen in cryo-FIB-SEM (left) and in the cryo-CLEM data integrating cryo-FIB-SEM with cryo-FM of PTS1-mCherry (right). White arrows indicate beads, which were visible in cryo-SEM and thus, could be used for image registration. In (b) and (d), lamella serves as a scale bar (width 10 µm).

To be able to use PTS1-mCherry and vMIA-GFP as fluorescent markers, protocols for the corresponding transfection and infections had to be integrated with the conventional cryo-ET sample preparation workflow. First, we implemented a protocol for the transient transfection of PTS1-mCherry into primary human fibroblasts and optimized the transfection efficiency and cytotoxicity. For this purpose, we screened different combinations of parameters including, the incubation time, number of cells to be transfected and the amount of plasmid DNA and transfection reagent used, which were subsequently evaluated by FM. The protocol was then tested for its compatibility with HCMV infection and vMIA-GFP expression. Peroxisomes were labelled in primary MRC-5 cells through transient overexpression of PTS1-mCherry and subsequently infected with HCMV expressing vMIA-GFP. The cells were then chemically fixed with PFA and examined using confocal fluorescence microscopy. The PTS1-mCherry fluorescence observed during these preliminary experiments match the expected morphology cellular distribution of peroxisomes (Figure 3.3 a). HCMV infection also seemed to promote localized clustering of peroxisomes in close proximity to the nucleus. Furthermore, HCMV is known to induce mitochondrial fragmentation, which is consistent with the morphology of the mitochondria visualized by vMIA-GFP in the sample.

The next step was to integrate the protocol for transfection and subsequent infection with cryo-ET sample preparation. For this purpose, primary human fibroblast cells were cultured to confluency and seeded onto cryo-EM grids. After the cells were allowed to adhere to the grids overnight, they were subjected to transfection and, depending on experimental setup, subsequent infection with HCMV. Additionally, fluorescent beads were added to the grids immediately before plunge-freezing to serve as fiducial markers for image registration between the different imaging modalities.

The standard workflow for *in-situ* cryo-ET experiments involves stepwise progression through specimen preparation, vitrification, FIB-milling, and cryo-ET. Two points at which cryo-FM can be incorporated into this workflow were considered viable, specifically, before and after lamella preparation.

Initial testing of these two approaches quickly revealed that performing cryo-FM imaging after FIB-milling is not feasible due to substantial ice contamination present on the polished lamellae. The ice contamination was suspected to originate from two distinct sources, each manifesting in different forms. We attributed the large crystals (Figure 3.3 b) to steps involving transfer of specimens in nitrogen liquid or vapour, while the smaller (Figure 3.3 c) crystals were assumed to originate from the incubation on the cryo-stage during cryo-FM imaging.

In contrast, performing cryo-FM imaging prior to FIB-milling was found to be a promising approach. Through this workflow, any ice contamination compromising ROIs would be removed during FIB-milling (see Chapter 3.2.2). Additionally, the fluorescence data allows for a targeted approach when selecting potential lamella sites. Selecting ROIs based on cryo-FM data improves the yield of lamellae containing the fluorescently labelled target.

The fact that most of the sample material at the ROI is ablated during lamella preparation presented a considerable disadvantage. This makes it inherently difficult to reliably determine whether the source of the original fluorescent signal will be preserved in the polished lamella or removed during FIB-milling. Our strategy to tackle this issue involved the use of fluorescent beads as fiducial markers. In theory, these would facilitate three dimension image registration between cryo-FM and cryo-FIB-SEM. Through this correlative approach, the location of the fluorescent target within the sample volume could be determined and the lamella placed accordingly.

That said, the use of fluorescent beads as fiducial markers was not without its own challenges. One limitation was the compromised visibility of the beads in the cryo-FIB-SEM instrument due to their tendency to be covered by the ice contamination acquired during cryo-FM imaging (Figure 3.3 d). The intense brightness and broad emission spectrum of the fluorescent beads also posed the risk of overwhelming the detection of PTS1-mCherry and vMIA-GFP.

Still, fluorescent beads may serve as effective fiducial markers to enable image registration between cryo-FM and cryo-FIB-SEM. They are however incompatible with correlative approaches integrating cryo-FM with *in-situ* cryo-ET here. This is because the platinum deposition during FIB-milling renders the sample opaque in cryo-EM, except in the areas that have been thinned by FIB-milling.

3.2.2 Implementing novel cryo-CLEM workflow

To leverage cryo-CLEM for the identification and characterization of peroxisomes through in-situ cryo-ET, the problems outlined in the previous paragraph had to be addressed. For this purpose, we devised an innovative workflow, drawing inspiration from an idea of my dear colleague Dr. Ulrike Laugks. The basic concept of this approach centres on introducing a strategic interruption of the FIB-milling process. The lamella preparation workflow was divided into two distinct stages, namely rough milling followed by polishing, so that cryo-FM imaging could be carried out between these steps.

After the initial rough milling, lamellae of approximately 500 nm in thickness are produced and the FIB-milling process was halted. The grids were then transferred to the cryo-FM instrument to visualize fluorescently labelled structures in the thinned areas of the vitrified cells., The grids were then transferred back to the cryo-FIB-SEM instrument to polish the lamellae containing the structure of interest to a final thickness of 150 – 200 nm (Figure 3.4). To facilitate the implementation of this specific workflow, we used a specialized sample holder that is compatible with both the cryo-FIB-SEM and the cryo-FM instrument. Mounting the grids in this so-called CLEM-shuttle eliminated the need to directly handle them during each transfer between the two microscopes and the associated increased risk of physically damaging the sample.

Accordingly, the optimized workflow starts with the grids being mounted into the CLEM-shuttle, which is then loaded into the cryo-FM instrument. Here, wide-field fluorescence imaging was employed to acquire an overview map of the whole grid (Figure 3.4 b).

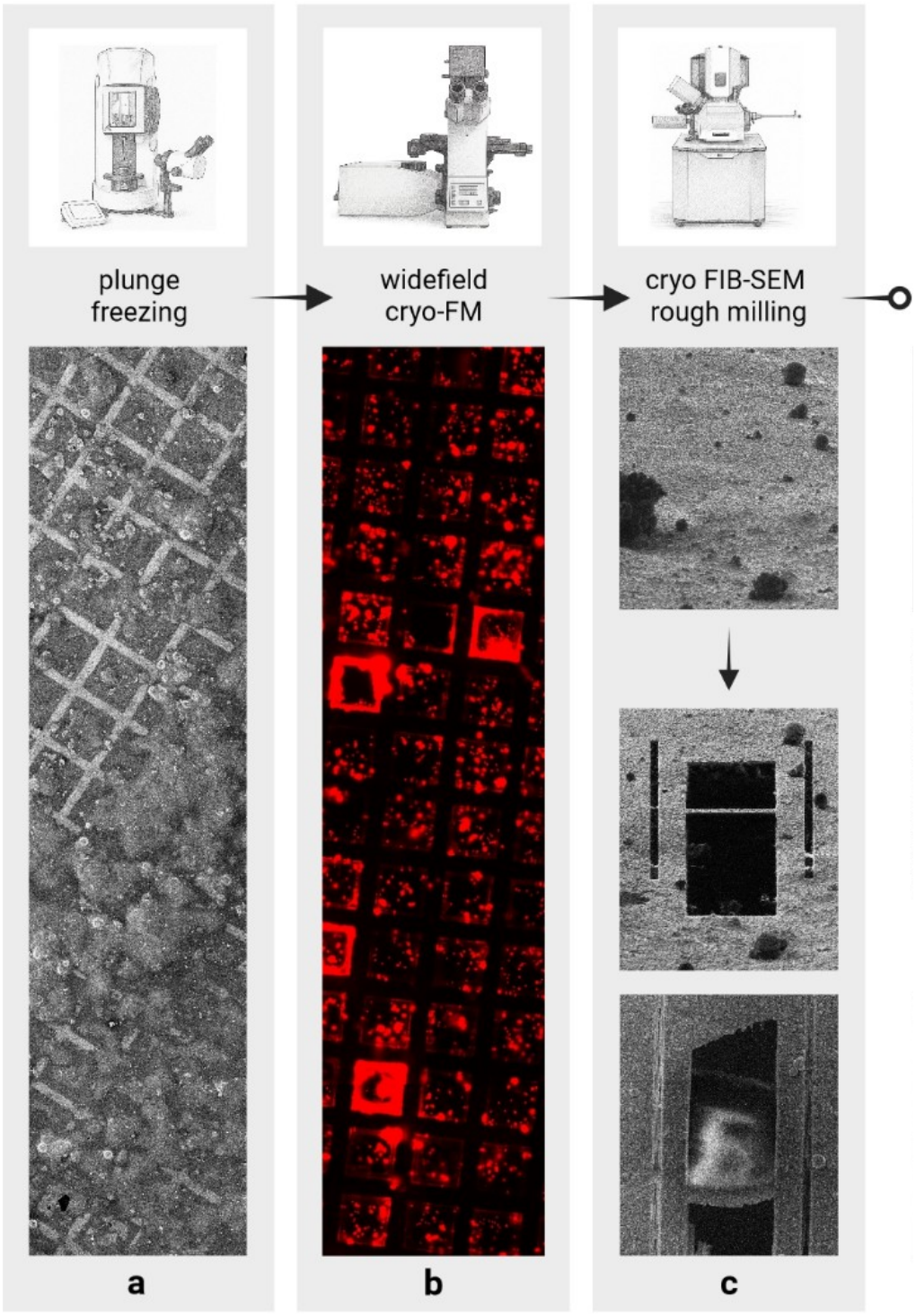

Figure 3.4 Schematic overview of cryo-CLEM workflow integrating cryo-FM and two-step FIB-milling with cryo-ET. Part one. Grids are vitrified by plunge freezing and subsequently mapped using wide-field cryo-FM. Next, cryo-FIB-SEM guided by the fluorescence map produces rough milled lamellae. Part two of the workflow is illustrated in Figure 3.5. (a) SEM overview image of vitrified human fibroblast cells on EM-grid. (b) Wide-field cryo-FM overview image of the same grid showing PTS1-mCherry fluorescence. (c) Shown is the same area of the vitrified sample imaged at milling angle, before (top) and after (middle) rough milling. The bottom panel is a top view SEM image of the lamella in the middle panel.

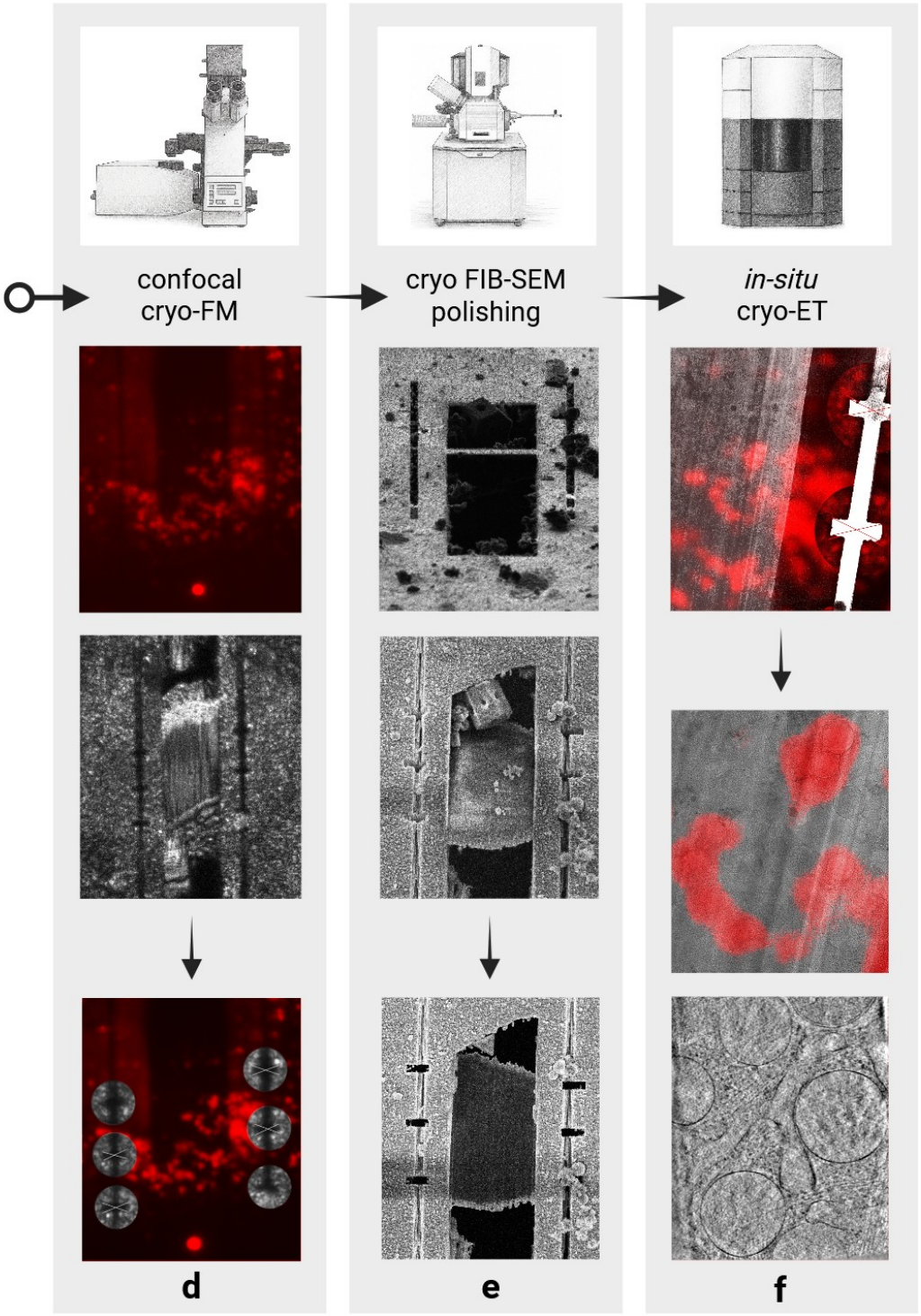

Figure 3.5 Schematic overview of cryo-CLEM workflow integrating cryo-FM and two-step FIB-milling with cryo-ET. Part two. After rough milling, fluorescently labelled structures in the lamellae are visualized by confocal cryo-FM. Next, FIB-milling is used to remove ice contamination from and subsequently polish lamellae exhibiting discernible fluorescence. Correlation of confocal cryo-FM images with cryo-TEM micrographs enables targeted cryo-ET data acquisition. (d) Confocal cryo-FM top view images of the same lamella visualizing PTS1-mCherry fluorescence (top) and reflected light (middle). The bottom panel shows the superposition of the two previous panels created for cryo-CLEM. (e) Shown is the same lamella imaged at milling angle (top) and from the top (middle) after transfer from cryo-FM to the cryo-FIB-SEM instrument. The bottom panel shows a top view of the same lamella after polishing. (f) Image registration correlating cryo-FM image with cryo-TEM micrograph of the lamella (top) enables targeted cryo-ET data acquisition and provides cryo-CLEM composite visualizing colocalization of membrane-bound structures with fluorescent signal. The bottom panel shows a slice through a reconstructed tomogram containing multiple peroxisomes.

After transferring the shuttle to the cryo-FIB-SEM instrument, viable lamella sites were selected using the fluorescent map to identify ROIs. The sample was then thinned at these locations using FIB-milling to approximately 500 nm in thickness (Figure 3.4 c). Following this, up to six rectangular perforations were milled perpendicularly to the sample surface next to each lamella. These perforations served as fiducial markers that are discernible in both cryo-FM and cryo-ET, thereby facilitating precise image registration between these two imaging modalities. Subsequently, the shuttle was reloaded into the cryo-FM instrument, where confocal fluorescence imaging was used to investigate the presence of fluorescently labelled structures in the rough milled lamellae (Figure 3.4 d). After transferring the shuttle back to the cryo-FIB-SEM instrument, the FIB-milling process of lamellae exhibiting discernible fluorescence of the labelled structure was continued. Successful completion of the FIB-milling process yielded a lamella polished to a final thickness of 150 - 200 nm.

Here, the key advantage of this workflow is evident. Any ice contamination present on the rough milled lamellae, can now be eradicated by FIB-milling before starting the polishing process (Figure 3.4 e). In doing so, we are able to examine the rough milled lamellae by cryo-FM while virtually eliminating the negative impact on the associated ice contamination on the cryo-ET data acquisition. This represents a significant improvement over the conventional cryo-CLEM workflow involving cryo-FM imaging prior to FIB-milling. During polishing, rough milled lamellae, exhibiting a thickness of approximately 500 nm, are thinned to 150 - 200 nm. Given that membrane-bound organelles in eukaryotic cells generally exceed 100 nm in diameter, fluorescently labelled structures in rough milled lamella that produce a pronounced signal are likely to persist after polishing.

The workflow was named Pia's protocol.

3.2.3 Identifying and characterizing peroxisomes

We leveraged Pia's protocol to identify and characterize peroxisomes in vitrified human fibroblasts using *in-situ* cryo-ET. For this, primary MRC-5 cells were seeded onto gold grids overlaid with holey silicon dioxide film (from Quantifoil) and transfected with PTS1-mCherry. A subset of grids was plunge-frozen 24h after the transfection was initiated to serve as uninfected "mock" samples. At this point, the remaining grids were infected with HCMV expressing vMIA fused to GFP and subsequently incubated for a period of 3 - 5 days before plunge-freezing. The lamellae, produced by applying Pia's protocol to these samples, were examined in a cryo-TEM microscope operated at 300 kV. The results illustrated in Figure 3.5 were obtained by applying Pia's protocol to MRC-5 cells expressing PTS1-mCherry, which were vitrified 72 hours post infection (hpi) with HCMV carrying vMIA-GFP.

First, micrographs were acquired at 3600x magnification (low-mag) to create an overview map for each lamella. Here, micrograph refers to a single two-dimensional image captured by cryo-TEM. These were then correlated to the corresponding confocal cryo-FM images. To achieve this, the rectangular holes next to each lamella, which were created during rough milling, were used as fiducial markers for image registration (Figure 3.5 a). Based on the generated cryo-CLEM composite, structures in the overview maps that coincide with fluorescent spots were selected for subsequent cryo-ET data acquisition. Tilt-series of these structures were then recorded at 26000x magnification (high-mag).

In the low-mag micrograph of the lamella (Figure 3.5 b), a population of spherical membrane-bound structures lacking any conspicuous luminal structures were visible (examples indicated with red stars). These vesicles had relatively uniform dimensions. The majority of mitochondria (examples indicated with green hexagons) had a similarly small and spherical morphology, contrasting the large, tubular mitochondria typically observed in uninfected cells (Figure 3.7 c). The difference in ultrastructure is consistent with existing evidence of HCMV infection inducing mitochondrial fragmentation in the host cell[95,87].

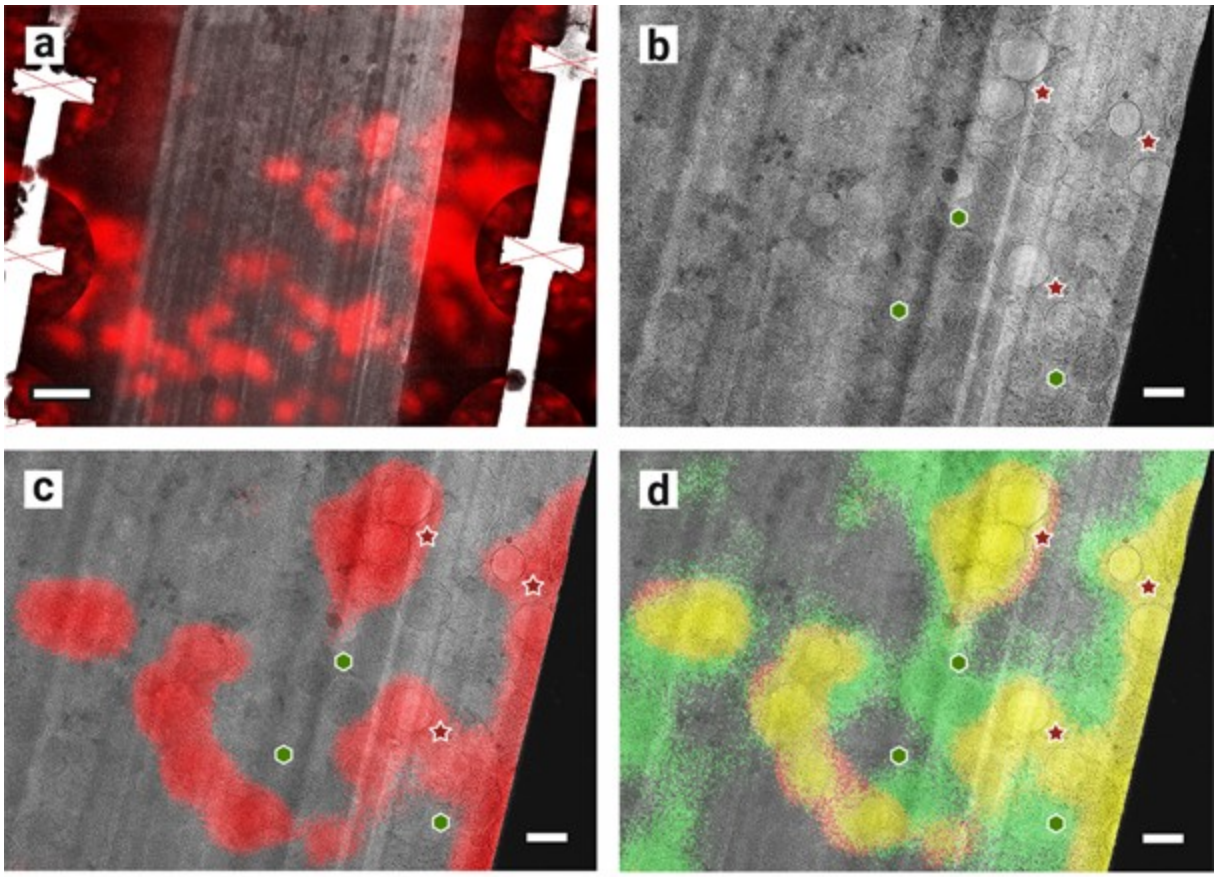

Figure 3.6 Identification and characterization of mammalian peroxisomes through cryo-CLEM and in-situ cryo-ET. Results illustrated in this figure were obtained from primary MRC-5 cells transfected with PTS1-mCherry and infected with HCMV vMIA-GFP, which were vitrified 72 hpi. (a) Coarse cryo-CLEM image created on-the-fly at the beginning of cryo-ET session to enable targeted data acquisition. An overview of the lamella was stitched together from multiple low-mag cryo-TEM micrographs and correlated with the corresponding confocal cryo-FM image of PTS1-mCherry fluorescence. The centre of the milled fiducial markers (rectangles perpendicular to the stress relieve cuts) were approximated (red crosses) and used for image registration (scale bar 2 µm).(b-d) shows a single low-mag cryo-TEM micrograph of the sample (scale bar 500 nm). Putative peroxisomes were marked with red stars. Green hexagons denote examples of mitochondria. (c) cryo-CLEM image visualizing PTS1-mCherry fluorescence in lamella. (d) cryo-CLEM image visualizing superposition of PTS1-mCherry and vMIA-GFP fluorescence in lamella.

Correlation of the low-mag micrograph with the corresponding cryo-FM data revealed that the inconspicuous vesicles coincided with the red fluorescence signal (Figure 3.5 c). Given that PTS1-mCherry can be assumed to specifically label the peroxisome matrix, this observation suggests that these vesicles are in fact peroxisomes. The vMIA-GFP signal in the cryo-CLEM data provides further evidence to substantiate this conclusion (Figure 3.5 d).

The fluorescent signal of vMIA-GFP appears to colocalize with both the putative peroxisomes and the mitochondria. This aligns with previous research showing that vMIA localizes to both organelles in host infected cells 72 hpi[78,186]. However, the micrograph also shows signs indicating that the lamella is not fully vitreous. The black and white spots visible in the upper left quadrant of the micrograph are called Bragg reflections and occur due to the presence of crystalline ice. While this indicates that Pia's protocol requires further methodological refinement, it also suggests that conclusions from these high-mag tomograms should be approached with care, as some features may arise from crystallization artefacts rather than representing native cellular structures

3.2.4 Integrating plasma-FIB milling and iFLM with cryo-CLEM

As mentioned above, the utilization of a cryo-FIB-SEM instrument outfitted with an iFLM module offers substantial benefits for workflows integrating cryo-CLEM with *in-situ* cryo-ET. For this reason, we sought to reproduce the findings achieved with Pia's protocol by employing a plasma cryo-FIB-SEM instrument (Arctis, Thermo Fisher Scientific). The significant advantage of this approach is that the objective of the iFLM module is directly integrated with the cryo-FIB-SEM vacuum chamber, therefore fluorescence and FIB-SEM can be achieved without transfer between instruments. This dramatically reduces the risk of ice contamination, devitrification and mechanical damage compared to cryo-CLEM workflows such as Pia's protocol where the sample must be shuttled multiple times between microscopes. To bridge the gap between low-mag micrographs and high-mag tomograms, we also implemented a script that would allow us to acquire a tilt-series of the lamella at low-mag (see chapter 4.1). The tomograms reconstructed from these tilt-series (here referred to as overview tomograms) (Figure 3.6 e) were used to add spatial context to the high-mag tomograms. The images displayed in Figure 3.6 represent the outcome of employing Arctis to examine uninfected MRC-5 cells expressing PTS1-mCherry.

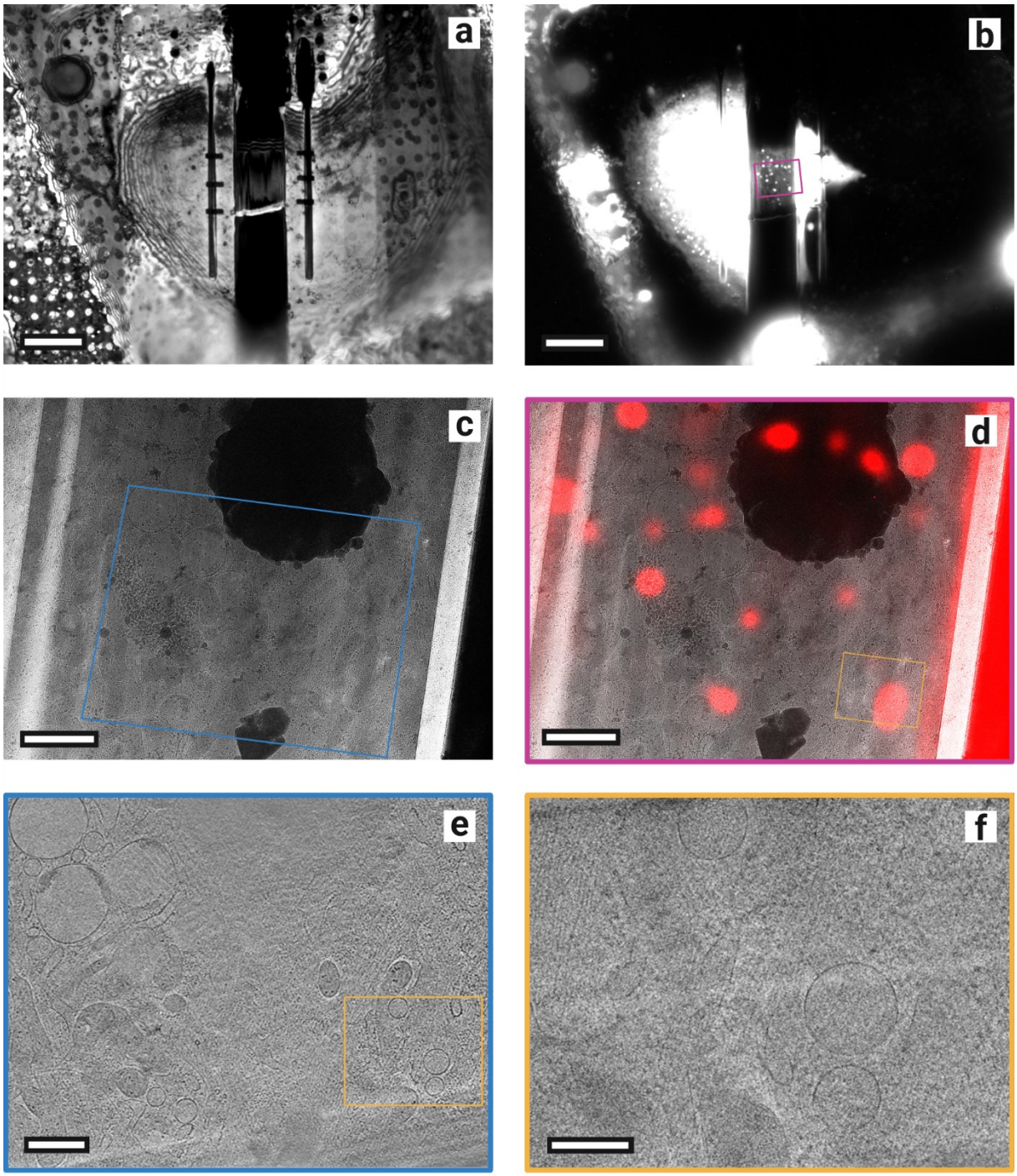

Figure 3.7 Cryo-CLEM analysis of mammalian peroxisomes in uninfected cells using plasma cryo-FIB-SEM and iFLM. Wide-field cryo-FM imaged of lamella after rough milling showing (a) reflected light and (b) fluorescence at 550 nm excitation indicating PTS1-mCherry localization (scale bar 10 µm). (c) Low-mag cryo-TEM micrograph of polished lamella (scale bar 1 µm). (d) Cryo-CLEM correlating cryo-TEM with cryo-FM at 550 nm excitation (scale bar 1 µm). (e) Slice through overview tomogram of lamella reconstructed from low-mag tilt-series (scale bar 500 nm). (f) Slice through tomogram of peroxisomes reconstructed from high-mag tilt-series (scale bar 200 nm).

After the samples were loaded into Arctis, they were processed following the same procedure outlined in Pia's protocol. The only deviation resulted from the fact that, unlike the STELLARIS 8 microscope used for Pia's protocol, the iFLM module of Arctis is limited to wide-field cryo-FM. Therefore, the procedure for cryo-FM imaging of lamellae in Arctis had to be modified. After rough milling, each lamella was examined using a channel for reflected light (Figure 3.6 a) and a channel for fluorescence at 550 nm excitation (Figure 3.6 b).

Despite the anticipated reduction in ice contamination when using a cryo-FIB-SEM instrument equipped with iFLM hardware, substantial ice build-up in the lamellae was still common. Ice crystals, such as those visible in the low-mag cryo-TEM micrograph of the lamella (Figure 3.6 c). Contrary to the common assumption that storage is a primary cause of ice contamination, we concluded that the ice build-up was most likely the result of the transfer to the cryo-TEM instrument.

The micrograph reveals the presence of roughly spherical vesicles lacking any large luminal structures, similar to those observed in our experiment employing Pia's protocol (Figure 3.5 b). The cryo-CLEM data correlating the cryo-TEM image with the fluorescence at 550 nm (Figure 3.6 d) shows that these structures colocalize with spots of discernible PTS1-mCherry fluorescence. Consistent with our previous results, these findings further substantiate our identification of these vesicles as peroxisomes.

Given that the lamella examined here was prepared from an uninfected cell, the mitochondrial morphology warrants particular attention. Here, mitochondria appear larger and more tubular compared to those previously observed in infected cells (Figure 3.7 c), which is consistent with HCMV-induced organelle remodeling.

Two peroxisomes are visible in the lower half of the high-mag tomogram (Figure 3.6 f) and exhibit close correlation with strong PTS1-mCherry fluorescence. While the lowermost and the uppermost peroxisome in the tomogram appear similar in diameter, the intensity of the fluorescence emitted by the peroxisome in the upper half of the tomogram is faint compared to the peroxisomes in the lower half.

There are two possible explanations to this. Either there is a difference in the concentration of PTS1-mCherry, or this could be a geometrical consequence of slight differences in sectioning through spheres. Small changes in the distance from the vesicle equator can result in relatively large changes in fluorescence. The poor contrast in the reconstructed overview tomogram (Figure 3.6 e) and high-mag tomogram (Figure 3.6 f) can be explained by the thickness of the lamella being close to 300 nm impeding alignment during reconstruction. Poor alignment of the ion beam, caused by technical issues we were unaware of at the time, resulted in lamellae being damaged or destroyed during polishing before the intended final thickness of 150 – 200 nm could be achieved. As a result, the thickness of successfully polished lamellae was typically at the borderline of cryo-TEM compatibility.

3.3 Discussion

Our research was focused on identifying and characterizing mammalian peroxisomes in their native cellular environment as well as their remodeling during HCMV infection. For this purpose, we developed Pia's protocol – a cryo-CLEM workflow integrating cryo-FM and cryo-FIB-SEM with cryo-ET.

One of the most significant findings from our experiments is that peroxisomes in human fibroblasts seem to lack distinctive morphological features that would make them readily distinguishable from other membrane-bound subcellular structures such as vesicles in cryo-TEM. This observation suggests that a striking contrast exists between them and peroxisomes found in other organisms, particularly fungi and plants. In these organisms, peroxisomes often contain prominent paracrystalline core structures formed from catalytically active matrix proteins[204,205,206]. These crystalline inclusions can be so pronounced that they influence the overall shape of the peroxisome[207].

The composition of these protein crystals is not always fixed and can vary depending on both the organism and environmental conditions. For instance, in yeast, the identity of the crystallized protein depends largely on the carbon source provided for growth[208]. These crystalline structures are thought to serve important regulatory functions within peroxisomes. By compartmentalizing enzymes, they may facilitate metabolic channelling or regulate enzyme activity through controlled solubilization[209].

The presence of these distinctive crystalline inclusions has historically made peroxisomes in yeast and plant cells relatively easy to identify in electron microscopy studies. Our initial strategy for identifying mammalian peroxisomes in cryo-ET was based on the assumption that similar distinctive features would be present. Once confirmed using Pia's protocol, this would allow us to recognize peroxisomes by their morphological characteristics. Contrary to our expectations, our findings revealed that mammalian peroxisomes do not have any characteristic features and would be impossible to identify without a correlative approach.

Several factors may explain the absence of crystals in mammalian peroxisomes. Most microscopic data on peroxisomes in plants and yeast was acquired using fixation methods such as chemical fixation and freeze substitution[207]. Therefore, it is conceivable that the formation of crystalline inclusions might be an artefact of sample preparation, which would not be present in the near-native state preserved by vitrification. The absence of crystals may also be specific to the human fibroblast cell line we examined. This suspicion is substantiated by reports of crystalline inclusions in peroxisomes of certain human cell types, like hepatocytes[210]. Different cell types may exhibit varying degrees of peroxisome specialization, reflecting their specific metabolic requirements. The crystallization of peroxisomal matrix proteins may also be a response to specific metabolic conditions, particularly starvation. Since our cell cultures were maintained under optimal growth conditions with abundant nutrients, they may not have experienced the metabolic stress that induces crystal formation. Whatever the case may be, the absence of distinctive features in peroxisomes of vitrified human fibroblasts presents a challenge for their identification through in-situ cryo-ET.

Furthermore, the relevance of our initial findings was limited by problems during FIB-milling, particularly polishing. The resulting excessive thickness of the polished lamellae in combination with generally poor vitrification prevented useful analysis of the high-resolution information obtained from the high-mag tomograms.

These aspects highlight the fact that our work only represents the first step in the identification and characterization of peroxisomes through *in-situ* cryo-ET. Given the challenges in identifying peroxisomes based on morphological criteria alone, alternative and complementary labeling approaches will be essential for future studies.

HCMV infection induces profound structural and functional alterations in host cell organelles. Research conducted by the group of Ileana Cristea (Princeton University, NJ, USA) using room temperature fluorescence microscopy suggested that HCMV gives rise to a subpopulation of peroxisomes exhibiting an enlarged and flattened morphology during late stages of infection. This phenotype is believed to facilitate enhanced metabolic output. particularly for plasmalogen synthesis, due its increased surface area to volume ratio. This would align with the understanding that plasmalogens are precursors for integral structural components of HCMV virions, making them indispensable for viral replication[88].

The aim of our research was to investigate these morphological changes in greater detail using *in-situ* cryo-ET. To study alterations in peroxisome structure during HCMV infection, we first needed to identify and characterize peroxisomes in uninfected cells to establish a baseline. For this purpose, we developed Pia's protocol. Using this bespoke cryo-CLEM workflow, we combined PTS1-mCherry and vMIA-GFP to examine peroxisome morphology in cells infected with HCMV. Initially, vMIA-GFP served mainly as a fluorescent label allowing us to determine which cells are infected.

However, we were unable to confirm the existence of enlarged and flattened peroxisomes in HCMV-infected cells. There are several possible explanations for this discrepancy that should be considered.

Given that *in-situ* cryo-ET allows us to examine only a tiny fraction of the intracellular volume, and considering that the altered morphology is thought to occur in just a subpopulation of peroxisomes, the simplest explanation is that we did not capture them in our samples. The use of PTS1-mCherry as a peroxisome marker may have exacerbated this issue. PTS1-mCherry requires a fully operational peroxisomal matrix protein import machinery to accumulate in peroxisomes. Should this mechanism somehow be compromised in the peroxisomes subpopulation affected by HCMV-induced remodeling, these structures would be invisible to PTS1-mCherry labelling, biasing our targeting toward unaffected peroxisomes. As a result, our analysis could have been skewed towards unaffected peroxisomes, leading to a biased representation.

An alternative explanation for the previously reported morphological changes is that they might represent peroxisomes at different stages of the proliferation process rather than distinct subpopulations. During peroxisome proliferation, peroxisomes undergo elongation before division, forming tubular protrusions that eventually separate to form new peroxisomes. During this process, the distribution of peroxisomal membrane and matrix proteins is polarized. The mature spherical part of the peroxisome retains most membrane components of the peroxisomal matrix protein import machinery. Only after division do premature peroxisomes acquire the necessary components to facilitate matrix protein import[211,90]. Consequently, PTS1-mCherry would not accumulate in the elongated tubular part of elongated peroxisomes and would only visualize spherical mature peroxisomes.

The group of Ileana Cristea (Princeton University, NJ, USA) initially discovered the remodeling of peroxisomes during HCMV infection by room temperature fluorescence microscopy in fixed human fibroblast cells using immunolabeling of PEX14. However, there is strong evidence suggesting that during peroxisome proliferation, PEX14 almost exclusively localizes to the tubular membrane protrusion of the elongated peroxisome[211,164]. In addition to visualizing mature peroxisomes, fluorescently labelled antibodies targeting PEX14 would therefore be limited to detecting the tubular extension of elongated peroxisomes.

Consequently, the enlarged and flattened peroxisome morphology observed in HCMV-infected cells might actually be the tubular membrane protrusion of peroxisomes undergoing proliferation. The fact that this labeling artefact was only apparent in infected cells could be explained by the organelle remodeling during HCMV infection. As HCMV drives peroxisome biogenesis, the proportion of peroxisomes undergoing proliferation at any given time in infected cells would increase proportionally. The significant difference between uninfected and infected cells may be attributed to HCMV further amplifying this effect through its impact on the expression of host cell proteins that play a crucial role in peroxisomal fission, such as PEX11β, MFF and DRP1. By causing erratic changes in the expression of these proteins, HCMV could create an imbalance in the abundance of components of the peroxisomal fission machinery. Through this process, HCMV could cause peroxisomes undergoing proliferation to become trapped in an elongated intermediate state. This would lead to an accumulation of tubular protrusions of peroxisomal membrane that would be detectable by PEX14-based labeling. A simple approach to ascertain the limitation of PTS1 and PEX14 based peroxisome markers is to explore alternative and complementary labeling strategies. This would also facilitate further investigation of morphological changes in peroxisomes during HCMV infection.

Despite our efforts, the existence of peroxisome populations exhibiting altered morphology in HCMV-infected cells remains a mystery to be solved. However, HCMV-induced remodeling of peroxisomes is recognized for its dual role in surpassing peroxisomal MAVS-mediated antiviral signalling and promoting peroxisomal proliferation. The viral protein vMIA, encoded by the UL37 gene, plays a crucial role in these processes. vMIA has been shown to localize to peroxisomes and interact with components of the peroxisomal membrane fission machinery, such as PEX11β and MFF to drive peroxisomal proliferation[78,93]. Beyond its previous use as a simple indicator for infection, utilization of vMIA-GPF would therefore allow us to study these host-pathogen interactions in greater detail.

To study these interactions in a feasible manner, we devised an approach that involves trapping peroxisomes in different intermediate states of the proliferation process. For instance, in the absence of DRP1, peroxisome proliferation has been shown to stop immediately before fission, causing the peroxisomes to become trapped in an intermediate morphology resembling beads on a string[212,213]. Furthermore, recombinant expression of a specific PEX11β-YFP mutant has been shown to terminate peroxisomal proliferation after formation of the tubular membrane protrusion[166]. Utilization of these and similar mutations should be considered a promising approach to study the role of vMIA in the upregulation of peroxisome proliferation during HCMV infection.

Our research has led to the development of a novel cryo-CLEM workflow named Pia's protocol, that integrates cryo-FM and cryo-FIB-SEM with cryo-ET. We demonstrated that this integrated approach enables *in-situ* identification and characterization of subcellular organelles in a near-native state. Even though we were unable to definitively identify peroxisomes in human fibroblast cells, our research still provides proof of concept for Pia's protocol. Despite its potential, our cryo-CLEM workflow faced several technical challenges that limited its effectiveness. One significant issue was ice contamination during wide-field cryo-FM imaging, which had a substantial negative impact on FIB-milling. Fine-grained ice settled onto the sample surface, forming a layer that compromised the adherence and homogeneity of the platinum coating applied during sample preparation for FIB-milling. This resulted in uneven surface topography and spatial variations in milling rates, manifesting as parallel streaks on the polished lamella. Because these artefacts reflect irregular sample thickness, they impede the ability to polish lamellae to a final thickness of 150 - 200 nm without damaging or destroying them. Several approaches could be considered to mitigate this issue.

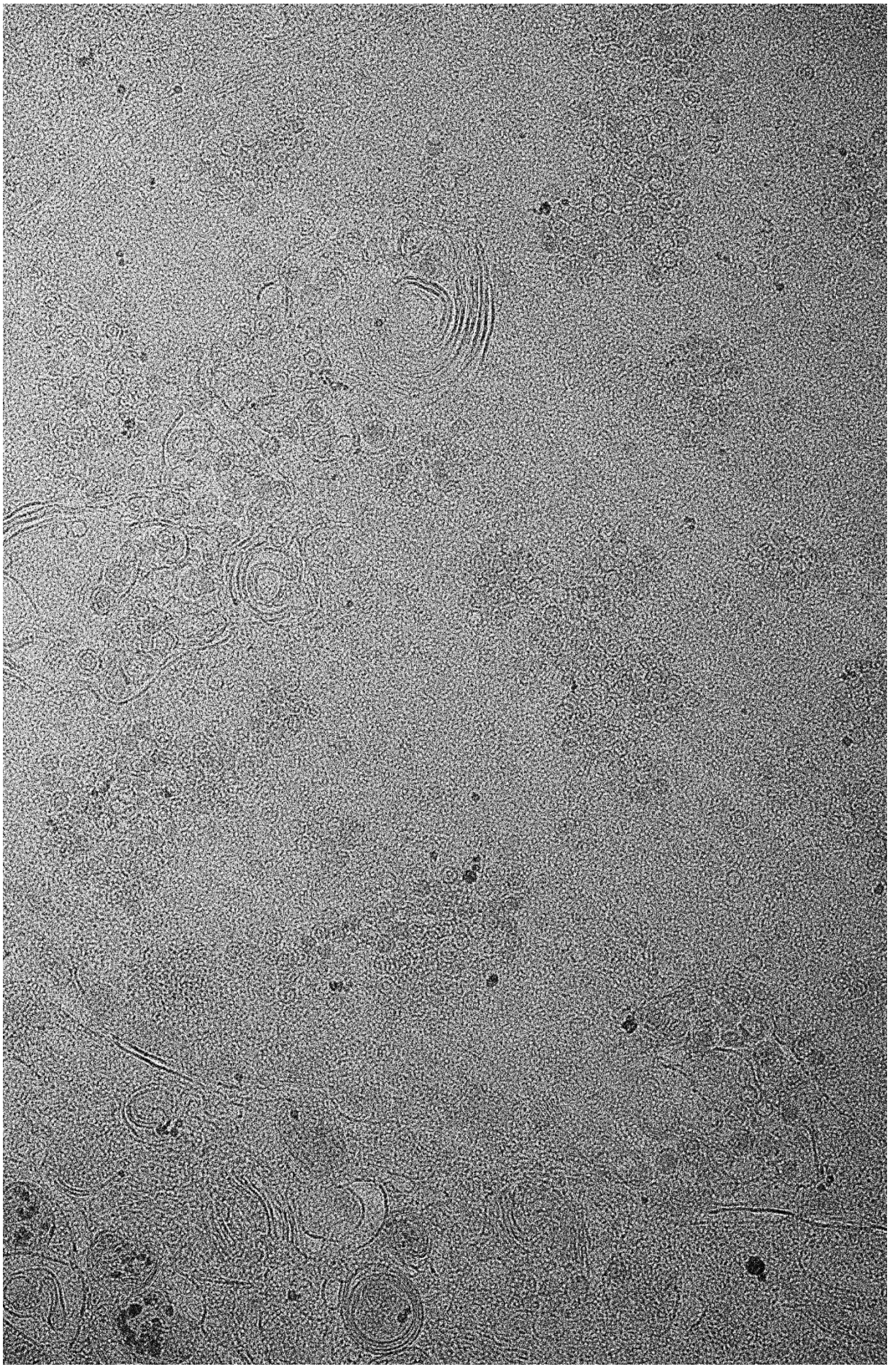

4 Secondary envelopment

4.1 Overview tomograms

Cryo-ET has emerged as an indispensable technique in structural biology to study proteins and macromolecular complexes in a near-native state at nanometre resolution. When combined with FIB-milling to produce electron-transparent lamellae from vitrified cells, cryo-ET allows for an analysis of intracellular ultrastructure in its native environment. The high-mag tomograms obtained through this *in-situ* cryo-ET approach provide exceptional details, enabling the visualization of protein complexes, membrane structures and subcellular organelles. However, high-mag data acquisition inherently constrains the field of view to a small fraction of the available lamella surface. In conventional cryo-ET data acquisition, target areas must be spaced far enough to avoid radiation damage due to double exposure. Additionally, each tilt-series acquisition requires a similarly sized sacrificial area to be used for focusing. Collectively, this can result in large areas of the lamella remaining unexplored. This limitation becomes particularly problematic when attempting to investigate how local molecular interactions contribute to large scale cellular processes or affect cellular organization.

To address this limitation, I created a SerialEM script called tomoov that allows for automated batch acquisition of low-mag tilt-series at view magnification, which for the experiments presented in this work, was typically 3600x. By collecting and reconstructing these overview tomograms, it becomes possible to visualize most of the lamella volume while still achieving sufficient resolution and contrast to identify and localize relatively small structures such as viral capsids. This view of a lamella provides spatial, morphological and contextual information that could otherwise remain inaccessible and may offer novel insights that transform the interpretation of the corresponding high-mag tomograms. Overview tomograms also have the potential to significantly improve workflow efficiency by providing a comprehensive 3D map of the lamella, that can be used to identify optimal targets for subsequent high-mag data acquisition based on cellular features, organelle distribution, or the presence of specific structures of interest.

Typically, the selection of areas for high-mag data acquisition is based on preliminary low-dose low-mag micrographs that may not represent the full diversity of structures present within the lamella, which can lead to systematic sampling bias. Integrating overview tomograms with cryo-CLEM approaches has the potential to improve correlation precision by bridging the gap between molecular localization of fluorescent markers and the broader cellular ultrastructure. This enhanced correlation capability is valuable for studying dynamic processes such as organelle biogenesis, protein transport, or stress responses, where understanding the spatial relationships between different cellular components is essential.

For these reasons, overview tomograms represent a particularly powerful tool for investigating viral assembly and the associated organelle remodeling during HCMV infection. Elucidating the interaction and spatial relationship between different cellular and viral compartments within the vAC is crucial for comprehending the complex processes governing tegumentation and secondary envelopment of viral capsids. The spatial coverage of overview tomograms has the potential to reveal how different regions of the vAC are organized and whether there are distinct functional domains within the compartment.

4.2 Results

The research presented in this chapter employed cryo-FM and *in-situ* cryo-ET to investigate the morphology and function of the vAC in human fibroblast cells infected with HCMV. The vAC is a complex perinuclear structure formed during HCMV infection through extensive viral remodeling of the host secretory and endocytic pathways. It serves as the principal site for tegumentation and secondary envelopment during HCMV assembly.

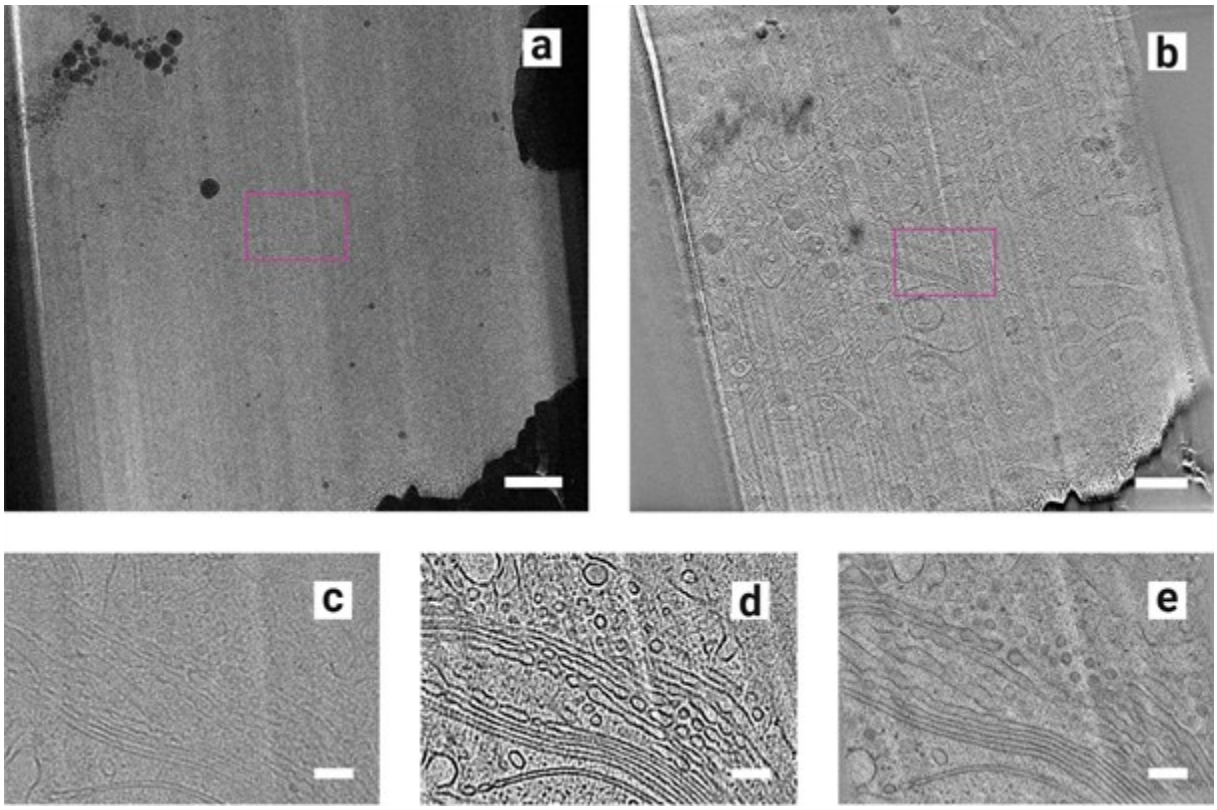

Figure 4.1 Overview tomograms. Results illustrated here were obtained through FIB-milling of vitrified human foreskin fibroblast (HFF) cells, which have been infected with HCMV and plunge-frozen 120 hours post infection. (a) cryo-TEM micrograph recorded at 3600x magnification (scale bar 1 µm). (b) Slice through overview tomogram reconstructed from cryo-TEM tilt-series acquired at 3600x magnification (scale bar 1 µm). (c) magnification of the area in panel (a) indicated by the pink rectangle (scale bar 200 nm). (d) magnification of the area in panel (b) indicated by the pink rectangle (scale bar 200 nm). (e) Slice through tomogram reconstructed from cryo-TEM tilt-series acquired at 26000x magnification (scale bar 200 nm).

To investigate the morphology of the vAC during HCMV infection, human foreskin fibroblast (HFF) cells were grown on EM-grids, infected with HCMV expressing gM fused to mScarlet and incubated for five days. Because gM is the most abundant protein in the viral envelope of HCMV, it provides a reliable marker for secondary envelopment and consequently for the vAC[73,214]. The samples were vitrified by plunge-freezing at 120 hpi. By preserving cellular ultrastructure in a near-native state, vitrification differs from with chemical fixation and plastic embedding, which can introduce significant distortions in membrane structure and organelle morphology. Following plunge-freezing, lamellae were prepared from vitrified cells by FIB-milling using an Aquilos cryo-FIB-SEM outfitted with an iFLM module (Thermo Fisher Scientific).

Due to the substantial size of the vAC, occupying a considerable portion of the intracellular volume, the 20x objective (NA 0.7) of the iFLM module was sufficient to target the vAC during lamella placement based on gM-mScarlet fluorescence. After completing the FIB-milling process, the polished lamellae were imaged using a cryo-TEM instrument operating at 300 kV. Each lamella was first examined by recording a tilt-series at 3600x magnification (low-mag), which was then reconstructed to create an overview tomogram, providing comprehensive coverage of the cellular ultrastructure within the thinned section of the sample. This was followed by the acquisition of tilt-series at 26000x magnification (high-mag) targeting intracellular structures that matched prior descriptions of vAC characteristics.

In the overview tomograms (Figure 4.2, 4.4 and 4.5), the vAC appears as a dense collection of membrane compartments and numerous vesicular structures of varying sizes and morphologies. This organization is consistent with previous reports describing the vAC as an accumulation of membrane-bound structures from different cellular origins, formed through viral remodeling of the host secretory and endocytic pathways. Membranes derived from the TGN appear fragmented and were prominently visible as flattened stacks of tubular and vesicular structures (Figure 4.4 a, Figure 4.5 a). Multivesicular bodies (MVBs) are abundant throughout only one of the vACs examined here, appearing as large vesicular structures containing multiple intraluminal vesicles (Figure 4.4 b).

Our data provides ultrastructural insight into the membrane dynamics governing secondary envelopment during HCMV assembly. Budding events facilitating secondary envelopment were captured at various stages, showing capsids in the process of acquiring their final envelope through interaction with membrane compartments derived from different host cell organelles, such as the Golgi-Apparatus and the ER (Figure 4.3). The identification of capsids at various stages of secondary envelopment supports the model of coordinated membrane wrapping driven by interaction between partially tegumented capsids and tegument proteins associated with the viral envelope. The tegument layer appeared as an electron-dense region between the capsid and the developing envelope. The traditional model of HCMV secondary envelopment involves capsids individually budding into small vesicles.

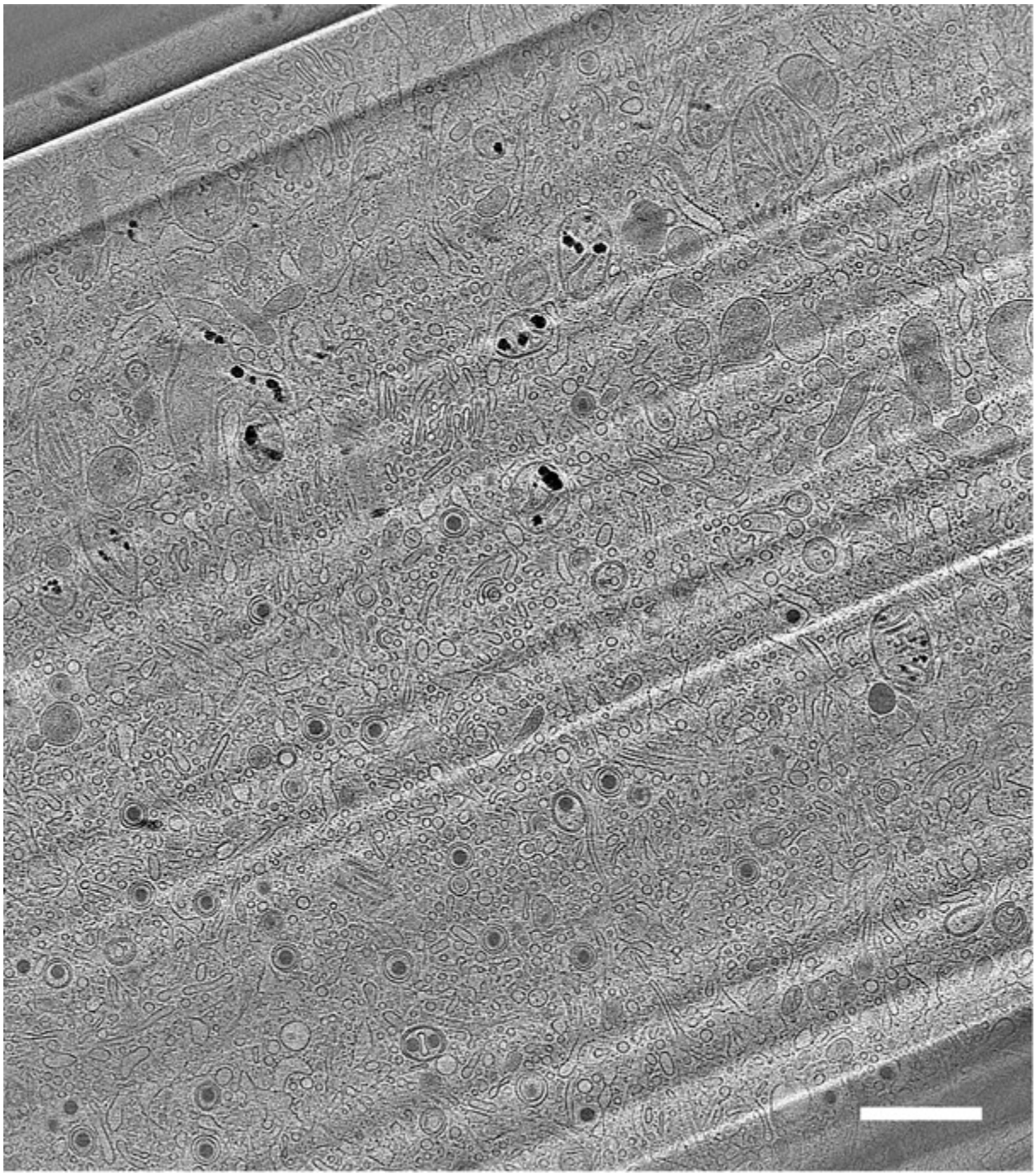

Figure 4.2 *In-situ* cryo-ET analysis of HCMV secondary envelopment in the viral assembly compartment (vAC). Slice through overview tomogram of lamella reconstructed form cryo-TEM tilt-series acquired at 3600x magnification (scale bar 1 µm). Lamella was produced from vitrified human foreskin fibroblast (HFF) cells, plunge-frozen 120 hours post infection with HCMV.

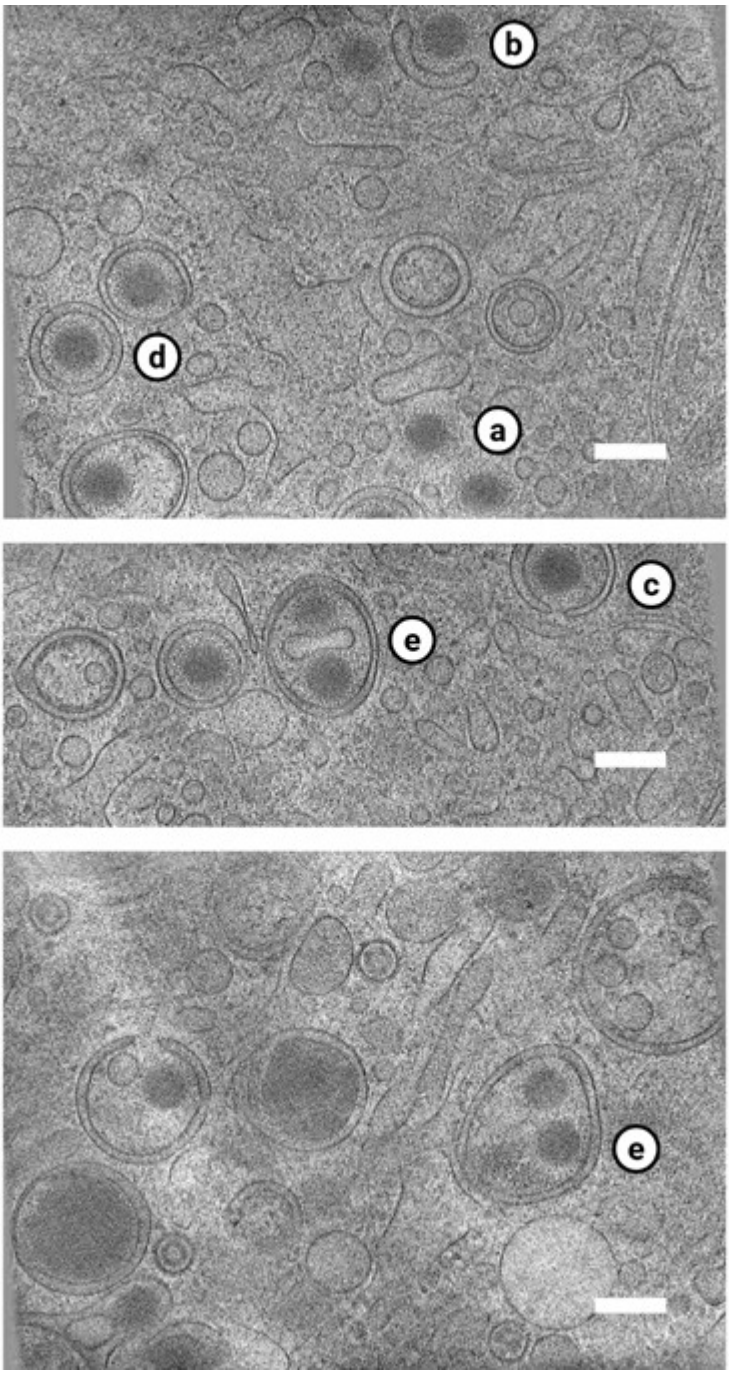

Figure 4.3 Different stages of HCMV secondary envelopment observed through In-situ cryo-ET. Each panel shows a slice through a tomogram reconstructed from cryo-TEM tilt-series acquired at 26000x magnification (scale bar 200 nm). Results shown here were obtained from vitrified human foreskin fibroblast (HFF) cells plunge-frozen 120 hours post infection with HCMV. (a) Naked capsids containing viral DNA (C-capsids). (b) Beginning of secondary envelopment facilitated by membrane wrapping around C-capsid. (c) Secondary envelopment near completion evident from the small opening still present in the envelope. (d) Successful completion of the secondary envelopment process concludes assembly of HCMV virions. (e) Errors occurring during secondary envelopment can produce aberrant membrane-bound structures containing multiple capsids and other cellular components.

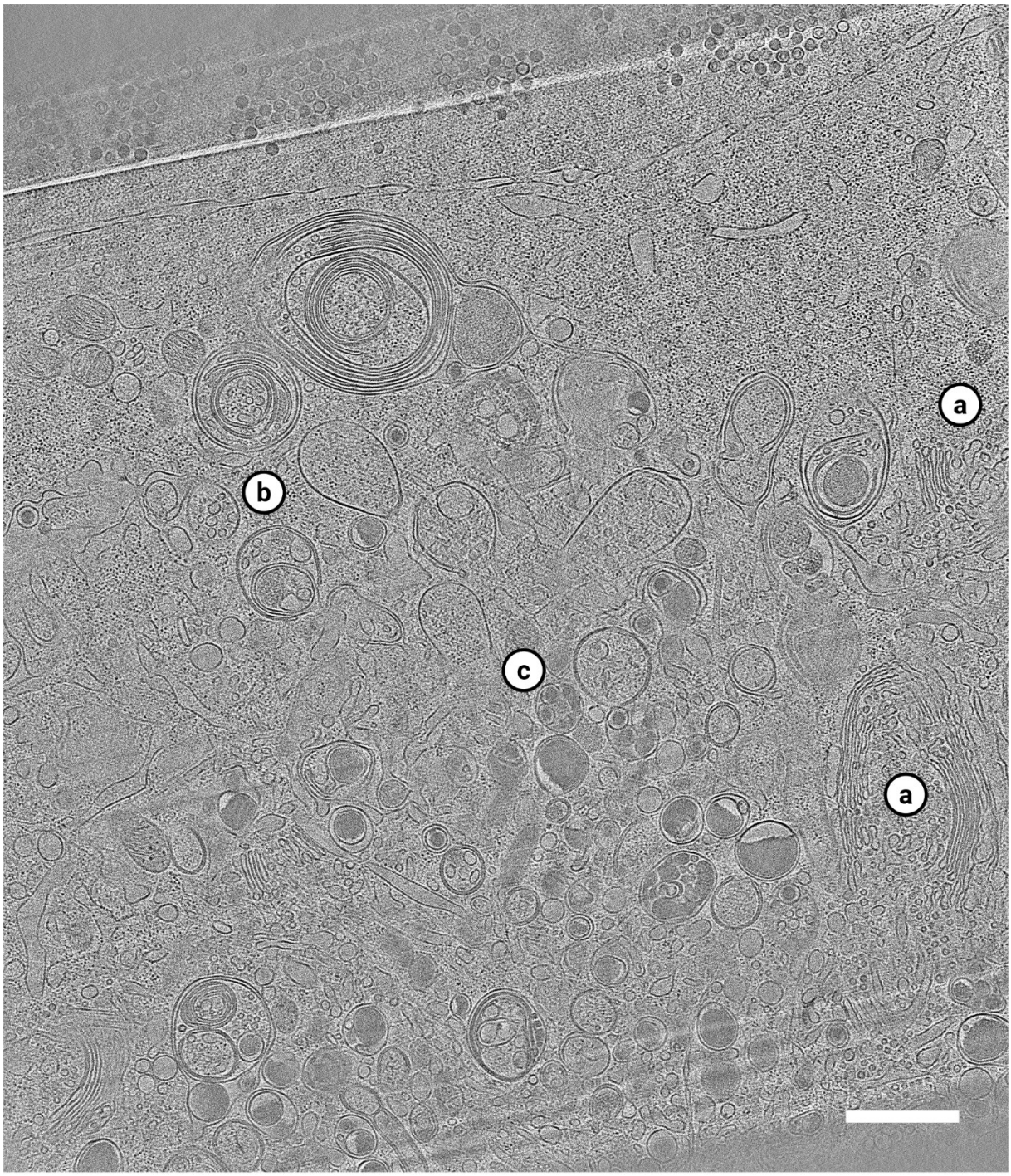

Figure 4.4 Structural characterization of the HCMV viral assembly compartment (vAC) using In-situ cryo-ET. Slice through overview tomogram of lamella reconstructed form cryo-TEM tilt-series acquired at 3600x magnification (scale bar 1 µm). Lamella was produced from vitrified human foreskin fibroblast (HFF) cells, plunge-frozen 120 hours post infection with HCMV. (a) Flattened stacks of fragmented Golgi-Apparatus. (b) Multivesicular body (MVB). (c) MVB containing cellular components and virions, also known as multiviral bodies (MViBs).

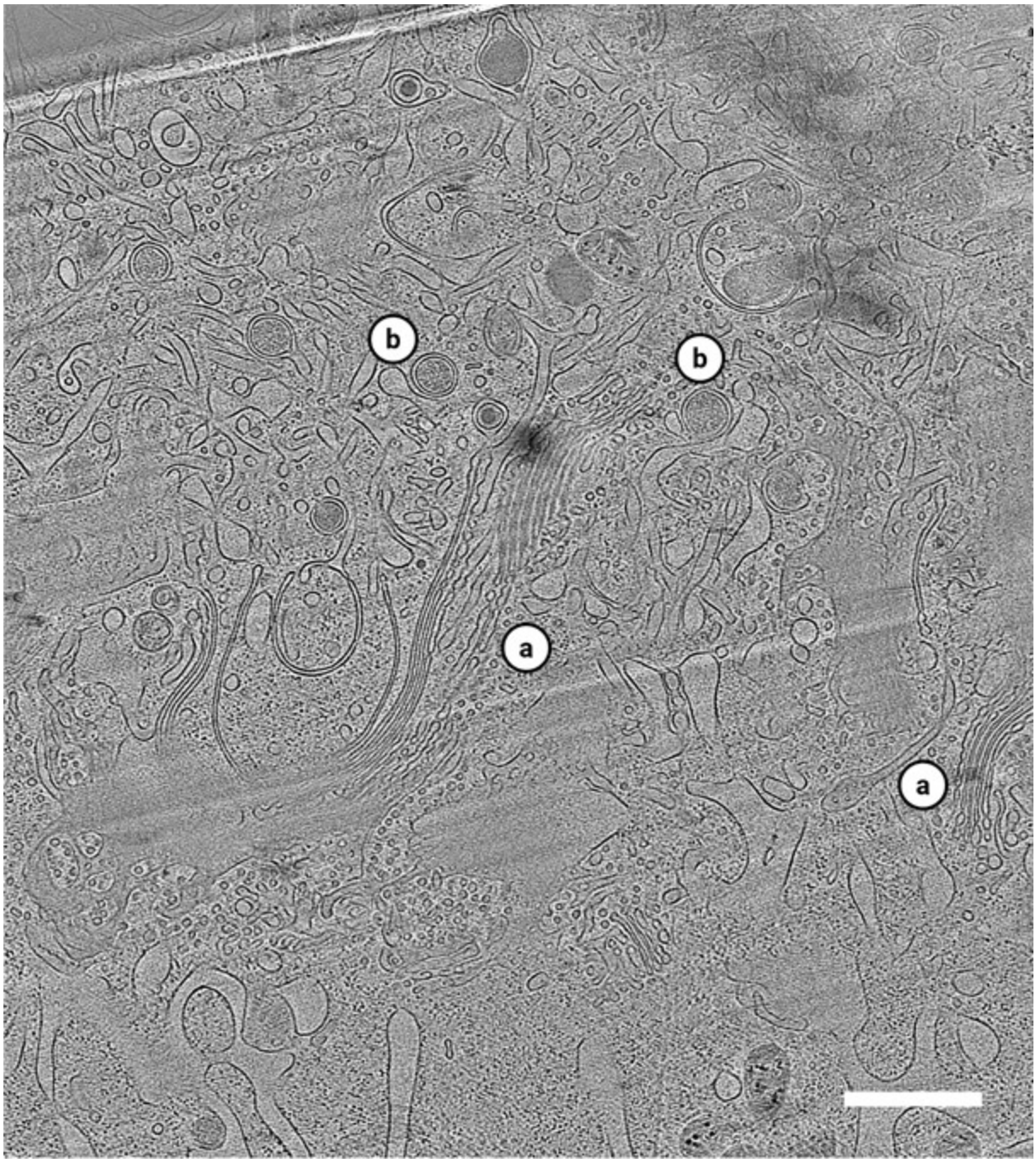

Figure 4.5 Structural characterization of the HCMV viral assembly compartment (vAC) using In-situ cryo-ET. Slice through overview tomogram of lamella reconstructed form cryo-TEM tilt-series acquired at 3600x magnification (scale bar 1 µm). Lamella was produced from vitrified human foreskin fibroblast (HFF) cells, plunge-frozen 120 hours post infection with HCMV. (a) Flattened stacks of fragmented Golgi-Apparatus. (b) Viral envelopes that contain tegument but lack a capsid, also known as dense bodies.

Our cryo-ET analysis provides structural validation for this pathway, showing numerous examples of single enveloped virions inside a vesicle. We also found that capsids devoid of viral genomes, containing only residual scaffold proteins, were able to undergo secondary envelopment, suggesting that the molecular machinery involved in this process exhibits a degree of non-selectivity (Figure 4.2). Furthermore, putative non-infectious dense bodies were found throughout the vAC, appearing as spherical enveloped particles containing electron-dense tegument but lacking a capsid (Figure 4.5 b). The presence of dense bodies in different stages of envelopment suggests that they utilize the same assembly machinery as infectious virions. A particularly striking observation was the presence of multiviral bodies (MViBs) within the vAC. These structures represented a distinct population from conventional transport vesicles, often containing multiple enveloped viral particles (Figure 4.4 c). The identification of MViBs represents a significant finding that supports emerging models of alternative pathways for HCMV secondary envelopment, involving the budding of capsid into the limiting endosomal membrane of MVBs.

4.3 Discussion

Viral assembly compartment

The present work contributes to our understanding of HCMV assembly by providing structural insight into the complex architecture of the vAC and the processes that govern tegumentation and secondary envelopment of viral capsids in infected human fibroblasts. Unlike previous electron microscopy studies that relied on chemical fixation and freeze substitution, our in-situ cryo-ET approach allowed us to preserve the cellular ultrastructure, including the membrane structures composing the vAC, in a near-native state. Chemical fixatives and heavy metal stains are well known to introduce significant distortions in membrane architecture, particularly affecting complex structure, such as MVBs and membrane contact sites[215].

Thus, maintaining the structural integrity of the sample by using cryo-EM to examine the vitrified specimen is imperative when attempting to study the membrane dynamics and vesicular morphologies in the vAC. The vAC appears as a dense accumulation of membrane compartments and numerous vesicular structures of varying sizes and morphologies. Our findings confirm the presence of multiple populations of membrane-bound structures derived from different cellular origins, including endosomes, MVBs and stacks of TGN within the vAC. The complexity of membrane identity within the vAC reflects the substantial viral remodeling of the host secretory and endocytic pathways that enables vAC formation during HCMV infection[77]. This observation substantiates the concept of HCMV utilizing multiple distinct membrane sources and corresponding pathways to facilitate secondary envelopment, since the vAC serves as principal site, where tegumented capsids acquire their viral envelope by budding into host-derived membranes[62].

Secondary envelopment

The traditional model of HCMV secondary envelopment involves tegumented capsids individually budding into small vesicles[216]. Our cryo-ET data provides structural evidence for this pathway, capturing capsids at various stages of secondary envelopment and showing numerous examples of single enveloped virions inside vesicles, thereby elucidating the membrane dynamics governing this process. The finding that HCMV exploits multiple host-derived membrane sources for secondary envelopment has significant implications for understanding viral tropism. Different membrane compartments exhibit distinct composition of glycoprotein, host cell protein and lipid, which can be incorporated into the viral envelope, potentially facilitating specific host-pathogen interactions[217,218,219]. Notably, we observed capsids devoid of viral genome undergoing secondary envelopment as well. This phenomenon suggests that the molecular mechanisms governing secondary envelopment exhibit a certain degree of non-selectivity regarding capsid content and may represent an inherent inefficiency of HCMV assembly or contribute to other aspects of HCMV infection, like immune modulation[220].

Secretory pathway

Viral remodeling of the secretory pathway, particularly the TGN and associated Golgi-derived membranes, serves as a major source of envelopment membranes for HCMV secondary envelopment. The utilization of secretory pathway membranes for envelopment is evidenced by the colocalization of viral glycoproteins with TGN markers[221]. Viral glycoproteins are transported through the secretory pathway and accumulate in TGN-derived membranes within the vAC, where they become available for incorporation into budding virions. Our observation of fragmented Golgi-derived membranes appearing as stacks of tubular and vesicular structures aligns with extensive previous research on the impact of HCMV-induced organelle remodeling on the Golgi-apparatus. The fragmentation of the Golgi ribbon during HCMV infection has been shown to depend on phosphorylation of the Grasp65 protein, which regulates Golgi membrane integrity[222].

Endocytic pathway

Recent research revealed that the endocytic pathway represents an equally important membrane source for secondary envelopment during HCMV assembly[72]. This is corroborated by our findings showing the presence of vesicular structures consistent with MVBs within the vAC. The presence of MVBs throughout the vAC, appearing as large vesicular structures containing multiple intraluminal vesicles, represents a critical observation for investigating alternative pathways for HCVM secondary envelopment. The incorporation of MVB markers, particularly CD63, into the viral envelope supports the notion that HCMV utilizes endocytic membranes for secondary envelopment. CD63-positive vesicles containing HCMV virions have been observed in both fibroblasts and endothelial cells[223]. Previous studies have found evidence pointing towards a crucial role of MVBs in HCMV assembly, with some research suggesting that these structures may serve as platforms for multiviral body (MViB) formation[216,72,73].

Multiviral bodies

One of the most striking findings from our cryo-ET experiments is the visualization of MViBs within vACs. MViBs appear as large multivesicular structures containing multiple enveloped virions, dense bodies and other vesicular material. The identification of MViBs within the vAC represents a significant finding that supports emerging models of alternative HCMV egress pathways, such as the intermittent bulk release described by Flomm *et al.*[73]. Live-cell imaging studies demonstrated the transport of MViBs from the vAC to the plasma membrane where they undergo fusion. This process results in the intermittent bulk release of large numbers of virions, creating extracellular viral accumulations (EVAs) at the cell surface. The intermittent nature of this egress pathway may have implications for viral pathogenesis and spread. Rather than continuous low-level virus release, this mechanism allows for the synchronized release of large numbers of viral particles, potentially overwhelming local immune responses or facilitating more efficient infection of neighbouring cells[224,73]. The differential abundance of MViBs observed between different vACs in this study may reflect the dynamic nature of membrane remodeling during HCMV infection.

Conclusion

The vAC emerges as a complex non-classical organelle that concentrates all the necessary components for efficient HCMV assembly while maintaining spatial organization that facilitates the sequential steps of tegumentation and secondary envelopment. The existence of multiple viral egress pathways facilitating HCMV replication, including individual virion release and bulk release through MViBs, raises important questions about the factors that determine which pathway is utilized in different circumstances. The strategy of leveraging multiple pathways may provide multiple advantages, including ensuring sustained virion production even when individual egress mechanisms are compromised and enabling the production of virions with diverse membrane compositions and other functional properties. This remarkable complexity likely reflects the evolutionary pressure on HCMV to maximize its reproductive success in the face of sophisticated host defences.

5 Conclusion and Perspective

This thesis has significantly advanced our understanding of HCMV pathogenesis by providing high-resolution structural characterization of virus-induced organelle remodeling in human cells. The development of Pia's protocol represents a significant methodological advancement, enabling the structural characterization of mammalian peroxisomes in their near-native state and revealing their morphology in human fibroblast cells using *in-situ* cryo-ET. However, future research must expand beyond the PTS1-mCherry labeling to employ alternative live-cell peroxisome markers, such as fluorescent fatty acid probes[229]. The investigation of peroxisome morphology and dynamics should also extend to diverse cell types. Cell type-specific investigations are paramount, as peroxisome abundance, morphology, and protein composition vary dramatically across different tissues, from the crystalline core containing peroxisomes in hepatocytes to the metabolically distinct populations in muscle cells and neurons. Furthermore, the study of herpesvirus-induced peroxisome remodeling should encompass more members of the human herpesvirus group, as emerging evidence suggests that peroxisome manipulation is a conserved viral strategy for metabolic reprogramming and immune evasion[88,187]. These investigations will provide crucial insights into the fundamental principles governing peroxisome biology and their role in virus-host interactions. The comprehensive analysis of the vAC through overview tomograms has represented a first step towards elucidating the complex membrane dynamics governing secondary envelopment and provided structural evidence for MViB formation during HCMV infection. Looking forward, these methodological innovations open new avenues for investigating host-pathogen interactions at the structural level, while the fundamental insights into organelle remodeling may inform therapeutic strategies targeting viral manipulation of cellular architecture. Future research should focus on expanding these correlative approaches to investigate how other viruses exploit their host for production and dissemination of infectious progeny.

6 Material and methods

6.1 Cell culture

Primary MRC-5 human fibroblast cells (ATCC CCL-171) at passage 19 (p19) were retrieved from vapour phase storage and immediately resuspended in 5 mL of warm (heated to ~37 °C) Dulbecco's Modified Eagle Medium (DMEM). In order to separate the cells from the DMSO present in the solution they were stored in, the cell suspension was centrifuged for 3 min at 300 rcf and then, the supernatant was carefully aspirated. After resuspending the cell pellet in 5 mL of warm DMEM containing 10% FBS and 1x GlutaMAX, the cell suspension was transferred into a T25 cell culture flask and incubated overnight at 37 °C in a 5% CO2 environment. Upon confluency of the cells reaching 70–80%, the cell culture medium was aspirated and the cells washed once with warm Phosphate-buffered saline (PBS) before dissociating the cells by incubating them for 3-5 in 1 mL TrypLE. After adding 1 mL DMEM containing 10% FBS and 1x GlutaMAX and carefully resuspending the cells, the cell suspension was centrifuged for 3 min at 300 rcf. The supernatant was aspirated to remove the trypsin-containing media and the cell pellet resuspended in 12 mL of warm DMEM containing 10% FBS and 1x GlutaMAX. Finally, the cell suspension was transferred into a T75 cell culture flask and incubated at 37 °C in a 5% CO2 environment until confluency of the cells again reached 70-80%.

6.2 Grid preparation

Initially, 300 mesh holey gold film on R 1.2/1.3 gold grids (Quantifoil) were used. Following reassessment of grid types for best cell seeding and grid handling, 200 mesh holey SiO2 film on R 2/2 gold grids were selected as the most robust for experiments involving FIB-milling and cryo-CLEM. Grids were typically glow discharged in a GloQube (Quorum) for 60 s at negative electrode polarity and 25 mA plasma current. Grids were transferred into µ-slide 2 well co-culture chambered coverslips (ibidi), hereinafter simply referred to as ibidi dish.

To allow for cell adhesion, grids were coated with fibronectin by applying 50 µL of solution (50 µg/mL fibronectin in 20 mM HEPES) on top of each grid and incubating those in the corresponding ibidi slide for 2h at 37 °C. Before proceeding with cell seeding, grids were washed with 50 µL PBS at 37 °C.

6.3 Cell seeding

Seeding of cells on EM grids was performed by dissociating cultured cells once a confluency of 70-80% was reached. Briefly, the cells were washed in PBS, dissociated with TrypLE for 5 min at 37 °C, carefully resuspended in DMEM containing 10% FBS and 1x GlutaMAX, and centrifuged for 3 min at 300 rcf. In the end, the cell pellet was resuspended in DMEM containing 10% FBS and 1x GlutaMAX and the cell count determined through manual counting using a Neubauer chamber. For grids designed as negative control, also referred to as mock grids, 6000 cells were seeded per grid. Grids intended for subsequent transfection and/or infection were seeded with a higher density of 8000 – 10000 cells per grid to compensate for attrition resulting from these procedures. Seeding density was examined using a DM IL LED (Leica) microscope and additional cells added if necessary to achieve the desired density on the grid. Afterwards, ibidi dishes were incubated overnight at 37 °C in a 5% CO2 environment to allow the cells to adhere to the grids.

6.4 Transfection

Transient transfection of primary MRC-5 or HFF cells was typically performed following cell seeding and subsequent adherence overnight, with the grids remaining in the ibidi dish throughout the process. The transfection mix was prepared in serum-free OptiMEM using Lipofectamine 3000 Transfection Reagent (Thermo Fisher Scientific) according to the manufacturer's instructions. The transfection reaction was optimized to deliver 5 ng of plasmid DNA, in 20 nL Lipofectamine 3000 and 10 nL P3000 per 1000 cells, with the final volume administered to each grid not exceeding 50 µL.

After washing the grids with 50 µL 37 °C PBS each and subsequently adding the transfection mix, the reaction was incubated for 24h at 37 °C in a 5% CO2 environment after which the grids were washed twice with 50 µL PBS at 37 °C and then maintained in FluoroBrite medium containing 10% FBS and 1x GlutaMAX at 37 °C in a 5% CO2 environment.

6.5 Infection

Primary MRC-5 or HFF cells were infected with HCMV AD169-pUL37x1-GFP or TB40E gM-mScarlet respectively, directly after cell seeding or transfection, with the grids remaining in the ibidi dish for the entire duration of the procedure. The infection was performed at a Multiplicity Of Infection (MOI) of 5 for transfected cells and an MOI of 3 for untransfected cells. The virus was diluted in serum-free DMEM and applied to the grids, ensuring that no more than 50 µL was added to each grid. After incubating the infection reaction for 1h at 37 °C in a 5% CO2 environment, the grids were washed twice with 50 µL 37 °C PBS each. Finally, the grids were incubated in FluoroBrite medium containing 10% FBS and 1x GlutaMAX until desired time point after infection was reached.

6.6 Plunge-freezing

Cells cultured on gold EM grids were vitrified by plunge-freezing in a mixture of liquid ethane and propane at -180 °C using an EM GP2 Automatic Plunge Freezer (Leica Microsystems). Immediately prior to plunge-freezing, grids were washed with 50 µL serum-free FluoroBrite at 37 °C. Each grid was transferred individually from the ibidi dish to an 8 µL drop of serum-free FluoroBrite medium on Parafilm to facilitate grid handling. After using the GP2 tweezers to pick up the grid, 4 µL of serum-free FluoroBrite medium containing 1 µm TetraSpeck Microspheres were pipetted onto the grid before loading the tweezer into the device. Plunge-freezing was performed with the environmental chamber set to 37 °C and 80% humidity using a blotting time of 7-8 s. Following plunge-freezing, the vitrified grids were stored in liquid nitrogen until further examination.

6.7 FIB-milling

Precise thinning of vitrified cellular specimens through gallium FIB-milling to create electron-transparent lamellae at the region of interest was performed using an Aquilos 2 Cryo-FIB-SEM instrument (Thermo Fisher Scientific). MAPS Software 3.2 (Thermo Fisher Scientific) was used to identify and prepare potential lamella sites. After mapping the grids, a combination of sputter and GIS coating was employed as follows to apply a thin layer of platinum to the sample surface: (1) sputter coating for 10 s at 0.1 mbar and 30 mA, (2) GIS coating for 70 s and (3) sputter coating for 5 s at 0.1 mbar and 7 mA. Potential lamella sites were selected manually and eucentric height for each determined individually using the corresponding feature in the MAPS software. Using serialFIB, the following milling procedure was automated, employing a fixed milling angle of 8 degrees and the stepwise protocol detailed in the table below[225].

In cases where FIB-milling was performed as part of a correlative pipeline, holes made with a rectangular shape and serving as fiducial markers for image registration were milled next to every suitable lamella at a milling angle of 90 degree. Typically, six rectangular holes (three on each side), each measuring 3 µm by 1 µm and intersecting with the stress relief cuts, were milled using an ion beam current of 0.1 nA.

Finally, thinning of the rough milled lamellae to a final thickness of 150 – 250 nm, a process commonly referred to as “polishing”, was performed manually at ion beam currents of 50 – 10 pA using beam shift to precisely control the ablation of material from the lamellae. Finally, sputter coating of the sample for 5 s at 0.1 mbar and 7 mA was performed to mitigate charging of the polished lamellae during TEM data acquisition.

Step	Ion beam current	Duration	Lamella thickness	Pattern thickness
1	0.5 nA	600s	3.0 µm	6.0 µm
2	0.5 nA	300s	2.0 µm	3.0 µm
3	0.3 nA	300s	1.5 µm	1.5 µm
4	0.1 nA	180s	0.8 µm	1.0 µm
5	0.1 nA	180s	0.8 µm	1.0 µm

When using the Arctis Cryo Plasma-FIB (Thermo Fisher Scientific) to produce lamellae, the same workflow established for the Aquilos was attempted to follow. While this plasma FIB instrument shows great potential to significantly increase throughput, sample preparation proved very challenging due to the inadequate state of the proprietary WebUI software at the time.

6.8 Cryo fluorescence microscopy

Cryo fluorescence microscopy of vitrified cells on grids was employed for two distinct purposes, both of which were accomplished using a STELLARIS 8 confocal microscope (Leica). Samples loaded prior to FIB-milling were imaged using the wide field mode to map the fluorescence across the grid to facilitate a targeted approach for subsequent FIB-milling. While signals from a GFP and an mCherry channel were recorded to visualize vMIA-GFP and PTS1-mCherry, respectively, imaging using transmitted light (bright field) enabled correlation of observed fluorescence with the position of cells on the grid. In order to survey the whole grid, a tile set consisting of eight rows and eight columns, covering an area of 1772 µm by 1777 µm was acquired. Prior to recording a tile set, a corresponding focus map was created to compensate for deformation of the grid.

Typically, wide field imaging of grids was performed as part of a cryo-CLEM workflow (Figure 3.4) involving subsequent preparation of rough milled lamellae (300 - 500 nm thick) at the identified regions of interest using an Aquilos 2 cryo-FIB-SEM instrument (see 5.7).

In order to enable direct transfer of samples between the STELLARIS and the Aquilos, the grids were loaded into a custom shuttle designed for compatibility between both instruments. By employing this bespoke sample holder referred to as CLEM-shuttle, the risk of damaging the sample was greatly reduced, as manual handling of the individual grids during transfer was no longer necessary. In addition, utilization of the CLEM-shuttle secured the grids against rotation inside the shuttle when transferring the sample between STELLARIS and Aquilos, thereby maintaining grid orientation. To verify the presence of fluorescently labelled features within the rough milled lamellae, the STELLARIS 8 was operated in confocal mode.

For every good lamella (based on visual inspection after milling), a set of sequential images was recorded at 50x magnification over a distance of 5-6 µm along the z-axis, with the gap between two images being set to 300 nm. The purpose of these so-called z-stacks is to overcome the limited depth of field by capturing a series of images at different focal planes, providing a composite of a sample volume with greater depth of field. Each z-stacks was acquired in three channels: GFP and mCherry channel were recorded to visualize vMIA-GFP and PTS1-mCherry, respectively, and a channel capturing reflected light provided complementary information about the surface topography of the sample. The raw image data was subsequently analysed and processed using Fiji[226]. It should be emphasized that the practice of filtering the liquid nitrogen through a Kimwipe (Kimtech Science) before using it to cool down the transfer station minimized both the likelihood and the extent of ice contamination.

6.9 Electron cryo-tomography - data collection

Tilt series were collected on the polished lamellae using a Titan Krios G3 (Thermo Fisher Scientific) operated at 300 kV and equipped with a BioQuantum energy filter (Gatan) as well as a K3 direct electron detector (Gatan). SerialEM was used to operate the microscope, manage data acquisition and align frames of collected tilt series.

Microscope settings and acquisition parameters of the low-dose mode used for record were optimized to achieve approximately 15 electron per pixel per second on the detector at 26,000x magnification, corresponding to a pixel size of 3.356 Å, with the K3 in counting mode, an energy slit with of 20 eV and an C2 aperture of 70 µm. Tilt series were collected using a dose-symmetric scheme from 68° to -52° and 3° increment steps with a target defocus ranging from -5 µm to -7µm and a total dose of 140 – 180 e-/Å^2 per tilt series. Moreover, for each lamella, a “low mag” tilt series was acquired in low-dose mode view at 4,800x magnification collected bi-directionally from 0° to ±51° using 3° increment steps, an exposure time of 2s per tilt and a defocus offset of -150 µm. The total electron dose per low-mag tilt series was typically below 2 e-/Å^2.

6.10 Electron cryo-tomography - data processing

For tomogram reconstruction, initial marker-free alignment of the tilt series was performed using AreTomo or the patch tracking module of IMOD. Parameters for AreTomo alignment were screened and optimized using a bespoke python script. Given the presence of suitable features like specks of platinum, alignment of selected tomograms was subsequently refined by manually seeding and tracking a corresponding fiducial model using the Beadtracker module of Etomo in IMOD. After applying dose weighting using IMOD mtffilter, tomograms were reconstructed utilizing the tilt module of IMOD Etomo with radial filtering set to SIRT-like filter equivalent to seven iterations for display purposes[227,228]. Volume rendering by segmentation was done manually using IMOD.

6.11 Chemicals

Name	**Supplier**
Dulbecco's Modified Eagle Medium	Gibco
Fetal Bovine Serum (FBS)	Sigma-Aldrich Co.
Fibronectin	Sigma-Aldrich Co.
FluoroBrite medium	Thermo Fisher Scientific
GlutaMAX	Thermo Fisher Scientific
Lipofectamine 3000	Thermo Fisher Scientific
Opti-MEM	Sigma-Aldrich Co.
PBS	Sigma-Aldrich Co.
TrypLE	Thermo Fisher Scientific

6.12 Viral strains

HCMV strain	**Fusion protein**	**Source**
AD169	pUL37x1-GFP	kindly provided to us by Ileana Cristae (Princeton University, NJ, USA)
TB40E	gM-mScarlet	kindly provided to us by Jens Bosse (CSSB Hamburg, Germany)

6.13 Consumables

Name	Supplier
1 µm TetraSpeck Microspheres	Thermo Fisher Scientific
300 mesh holey gold on R 1.2/1.3 gold grids	Quantifoil Micro Tools GmbH
200 mesh holey SiO_2 film on R 2/2 gold grids	Quantifoil Micro Tools GmbH
Flasks for cell culture (T25, T75)	Thermo Fisher Scientific
18 well µ-Slide (chambered coverslip)	ibidi GmbH
Parafilm	Carl Roth
Kimwipes	Kimtech Science

7 References

[1] Woźniakowski, Grzegorz, and Elżbieta Samorek-Salamonowicz. "Animal herpesviruses and their zoonotic potential for cross-species infection." Annals of agricultural and environmental medicine : AAEM vol. 22,2 (2015): 191-4, doi:10.5604/12321966.1152063.

[2] Long, Simon Y et al. "Review of Elephant Endotheliotropic Herpesviruses and Acute Hemorrhagic Disease." ILAR journal vol. 56,3 (2016): 283-96, doi:10.1093/ilar/ilv041.

[3] Boonprasert, Khajohnpat et al. "Survival analysis of confirmed elephant endotheliotropic herpes virus cases in Thailand from 2006 - 2018." PloS one vol. 14,7 (2019): e0219288, doi:10.1371/journal.pone.0219288.

[4] Gibson, W. "Structure and formation of the cytomegalovirus virion." Current topics in microbiology and immunology vol. 325 (2008): 187-204, doi:10.1007/978-3-540-77349-8_11.

[5] DaPalma, T et al. "A systematic approach to virus-virus interactions." Virus research vol. 149,1 (2010): 1-9, doi:10.1016/j.virusres.2010.01.002.

[6] Hartley, J W et al. "Serial propagation of the guinea pig salivary gland virus in tissue culture." Proceedings of the Society for Experimental Biology and Medicine. Society for Experimental Biology and Medicine (New York, N.Y.) vol. 96,2 (1957): 281-5, doi:10.3181/00379727-96-23455.

[7] Wertheim, Joel O et al. "Evolutionary origins of human herpes simplex viruses 1 and 2." Molecular biology and evolution vol. 31,9 (2014): 2356-64, doi:10.1093/molbev/msu185.

[8] Zuhair, Mohamed et al. "Estimation of the worldwide seroprevalence of cytomegalovirus: A systematic review and meta-analysis." Reviews in medical virology vol. 29,3 (2019): e2034, doi:10.1002/rmv.2034.

[9] Rossini, Giada et al. "Interplay between human cytomegalovirus and intrinsic/innate host responses: a complex bidirectional relationship." Mediators of inflammation vol. 2012 (2012): 607276, doi:10.1155/2012/607276.

[10] Cannon, Michael J et al. “Review of cytomegalovirus seroprevalence and demographic characteristics associated with infection.” Reviews in medical virology vol. 20,4 (2010): 202-13, doi:10.1002/rmv.655.

[11] Loewendorf, A, and C A Benedict. “Modulation of host innate and adaptive immune defenses by cytomegalovirus: timing is everything.” Journal of internal medicine vol. 267,5 (2010): 483-501, doi:10.1111/j.1365-2796.2010.02220.x.

[12] Reeves, Matthew B, and John H Sinclair. “Analysis of latent viral gene expression in natural and experimental latency models of human cytomegalovirus and its correlation with histone modifications at a latent promoter.” The Journal of general virology vol. 91,3 (2010): 599-604, doi:10.1099/vir.0.015602-0.

[13] Knipe, David M et al. “Snapshots: chromatin control of viral infection.” Virology vol. 435,1 (2013): 141-56, doi:10.1016/j.virol.2012.09.023.

[14] Goodrum, Felicia. “Human Cytomegalovirus Latency: Approaching the Gordian Knot.” Annual review of virology vol. 3,1 (2016): 333-357, doi:10.1146/annurev-virology-110615-042422.

[15] Forte, Eleonora et al. “Cytomegalovirus Latency and Reactivation: An Intricate Interplay With the Host Immune Response.” Frontiers in cellular and infection microbiology vol. 10 (2020): 130, doi:10.3389/fcimb.2020.00130.

[16] Kano, Y, and T Shiohara. “Current understanding of cytomegalovirus infection in immunocompetent individuals.” Journal of dermatological science vol. 22,3 (2000): 196-204, doi:10.1016/s0923-1811(99)00085-7.

[17] Plotogea, Mihaela et al. “An Overview of Cytomegalovirus Infection in Pregnancy.” Diagnostics (Basel, Switzerland) vol. 12,10 (2022): 2429, doi:10.3390/diagnostics12102429.

[18] Sakowska, Justyna et al. “Autoimmunity and Cancer-Two Sides of the Same Coin.” Frontiers in immunology vol. 13 (2022): 793234, doi:10.3389/fimmu.2022.793234.

[19] Wargo, Jennifer A et al. “Immune Effects of Chemotherapy, Radiation, and Targeted Therapy and Opportunities for Combination With Immunotherapy.” Seminars in oncology vol. 42,4 (2015): 601-16, doi:10.1053/j.seminoncol.2015.05.007.

[20] Perello, R et al. “Cytomegalovirus infection in HIV-infected patients in the era of combination antiretroviral therapy.” BMC infectious diseases vol. 19,1 (2019): 1030, doi:10.1186/s12879-019-4643-6.

[21] Yu, Xuekui et al. “Atomic structure of the human cytomegalovirus capsid with its securing tegument layer of pp150.” Science (New York, N.Y.) vol. 356,6345 (2017): eaam6892, doi:10.1126/science.aam6892.

[22] Gibson, W et al. “Cytomegalovirus "missing" capsid protein identified as heat-aggregable product of human cytomegalovirus UL46.” Journal of virology vol. 70,11 (1996): 7454-61, doi:10.1128/JVI.70.11.7454-7461.1996.

[23] Li, Zhihai et al. “Structural basis for genome packaging, retention, and ejection in human cytomegalovirus.” Nature communications vol. 12,1 (2021): 4538, doi:10.1038/s41467-021-24820-3.

[24] Brandariz-Nuñez, Alberto et al. “Pressure-driven release of viral genome into a host nucleus is a mechanism leading to herpes infection.” eLife vol. 8 (2019): e47212, doi:10.7554/eLife.47212.

[25] Smith, Rebecca Marie et al. “Role of human cytomegalovirus tegument proteins in virion assembly.” Viruses vol. 6,2 (2014): 582-605, doi:10.3390/v6020582.

[26] Jih, Jonathan et al. “The incredible bulk: Human cytomegalovirus tegument architectures uncovered by AI-empowered cryo-EM.” Science advances vol. 10,8 (2024): eadj1640, doi:10.1126/sciadv.adj1640.

[27] Yu, Xuekui et al. “Biochemical and structural characterization of the capsid-bound tegument proteins of human cytomegalovirus.” Journal of structural biology vol. 174,3 (2011): 451-60, doi:10.1016/j.jsb.2011.03.006.

[28] Cappadona, Ilaria et al. “Human Cytomegalovirus pUL47 Modulates Tegumentation and Capsid Accumulation at the Viral Assembly Complex.” Journal of virology vol. 89,14 (2015): 7314-28, doi:10.1128/JVI.00603-15.

[29] Kalejta, Robert F. “Tegument proteins of human cytomegalovirus.” Microbiology and molecular biology reviews : MMBR vol. 72,2 (2008): 249-65, doi:10.1128/MMBR.00040-07.

[30] Phillips, Stacia L, and Wade A Bresnahan. “The human cytomegalovirus (HCMV) tegument protein UL94 is essential for secondary envelopment of HCMV virions.” Journal of virology vol. 86,5 (2012): 2523-32, doi:10.1128/JVI.06548-11.

[31] Foglierini, Mathilde et al. “HCMV Envelope Glycoprotein Diversity Demystified.” Frontiers in microbiology vol. 10 (2019): 1005, doi:10.3389/fmicb.2019.01005.

[32] Filippov, Alexander E, and Stanislav N Gorb. “Spatial model of the gecko foot hair: functional significance of highly specialized non-uniform geometry.” Interface focus vol. 5,1 (2015): 20140065, doi:10.1098/rsfs.2014.0065.

[33] Gerna, Giuseppe et al. “Human Cytomegalovirus Cell Tropism and Host Cell Receptors.” Vaccines vol. 7,3 (2019): 70, doi:10.3390/vaccines7030070.

[34] Kinzler, Eric R, and Teresa Compton. “Characterization of human cytomegalovirus glycoprotein-induced cell-cell fusion.” Journal of virology vol. 79,12 (2005): 7827-37, doi:10.1128/JVI.79.12.7827-7837.2005.

[35] Wang, Yu-Qing, and Xiang-Yu Zhao. “Human Cytomegalovirus Primary Infection and Reactivation: Insights From Virion-Carried Molecules.” Frontiers in microbiology vol. 11 (2020): 1511, doi:10.3389/fmicb.2020.01511.

[36] Revello, M Grazia, and Giuseppe Gerna. “Human cytomegalovirus tropism for endothelial/epithelial cells: scientific background and clinical implications.” Reviews in medical virology vol. 20,3 (2010): 136-55, doi:10.1002/rmv.645.

[37] Dargan, Derrick J et al. “Sequential mutations associated with adaptation of human cytomegalovirus to growth in cell culture.” The Journal of general virology vol. 91,6 (2010): 1535-46, doi:10.1099/vir.0.018994-0.

[38] Kschonsak, Marc et al. “Structures of HCMV Trimer reveal the basis for receptor recognition and cell entry.” Cell vol. 184,5 (2021): 1232-1244, doi:10.1016/j.cell.2021.01.036.

[39] Wu, Kai et al. “Role of PDGF receptor-α during human cytomegalovirus entry into fibroblasts.” Proceedings of the National Academy of Sciences of the United States of America vol. 115,42 (2018): E9889-E9898, doi:10.1073/pnas.1806305115.

[40] Wille, Paul T et al. “Human cytomegalovirus (HCMV) glycoprotein gB promotes virus entry in trans acting as the viral fusion protein rather than as a receptor-binding protein.” mBio vol. 4,3 (2013): e00332-13, doi:10.1128/mBio.00332-13.

[41] Nguyen, Christopher C, and Jeremy P Kamil. “Pathogen at the Gates: Human Cytomegalovirus Entry and Cell Tropism.” Viruses vol. 10,12 (2018): 704, doi:10.3390/v10120704.

[42] Isaacson, Marisa K, and Teresa Compton. “Human cytomegalovirus glycoprotein B is required for virus entry and cell-to-cell spread but not for virion attachment, assembly, or egress.” Journal of virology vol. 83,8 (2009): 3891-903, doi:10.1128/JVI.01251-08.

[43] Hetzenecker, Stefanie et al. “HCMV Induces Macropinocytosis for Host Cell Entry in Fibroblasts.” Traffic (Copenhagen, Denmark) vol. 17,4 (2016): 351-68, doi:10.1111/tra.12355.

[44] Kalejta, R F. “Functions of human cytomegalovirus tegument proteins prior to immediate early gene expression.” Current topics in microbiology and immunology vol. 325 (2008): 101-15, doi:10.1007/978-3-540-77349-8_6.

[45] Li, Tuo et al. “Human cytomegalovirus tegument protein pUL83 inhibits IFI16-mediated DNA sensing for immune evasion.” Cell host & microbe vol. 14,5 (2013): 591-9, doi:10.1016/j.chom.2013.10.007.

[46] Cohen, Tobias et al. “The Microtubule Inhibitor Podofilox Inhibits an Early Entry Step of Human Cytomegalovirus.” Viruses vol. 8,10 (2016): 295, doi:10.3390/v8100295.

[47] Fay, Nikta, and Nelly Panté. “Nuclear entry of DNA viruses.” Frontiers in microbiology vol. 6 (2015): 467, doi:10.3389/fmicb.2015.00467.

[48] Shenk, Thomas, and James C Alwine. “Human Cytomegalovirus: Coordinating Cellular Stress, Signaling, and Metabolic Pathways.” Annual review of virology vol. 1,1 (2014): 355-74, doi:10.1146/annurev-virology-031413-085425.

[49] Mason, Rebecca et al. “Repression of the major immediate early promoter of human cytomegalovirus allows transcription from an alternate promoter.” The Journal of general virology vol. 104,9 (2023): doi:10.1099/jgv.0.001894.

[50] Stinski, Mark F, and Hiroki Isomura. “Role of the cytomegalovirus major immediate early enhancer in acute infection and reactivation from latency.” Medical microbiology and immunology vol. 197,2 (2008): 223-31, doi:10.1007/s00430-007-0069-7.

[51] Rozman, Batsheva et al. “Temporal dynamics of HCMV gene expression in lytic and latent infections.” Cell reports vol. 39,2 (2022): 110653, doi:10.1016/j.celrep.2022.110653.

[52] Isomura, Hiroki et al. “The human cytomegalovirus gene products essential for late viral gene expression assemble into prereplication complexes before viral DNA replication.” Journal of virology vol. 85,13 (2011): 6629-44, doi:10.1128/JVI.00384-11.

[53] Caragliano, Enrico et al. “Human cytomegalovirus forms phase-separated compartments at viral genomes to facilitate viral replication.” Cell reports vol. 38,10 (2022): 110469, doi:10.1016/j.celrep.2022.110469.

[54] Wood, L J et al. “Human cytomegalovirus capsid assembly protein precursor (pUL80.5) interacts with itself and with the major capsid protein (pUL86) through two different domains.” Journal of virology vol. 71,1 (1997): 179-90, doi:10.1128/JVI.71.1.179-190.1997.

[55] Borst, Eva Maria et al. “The Essential Human Cytomegalovirus Proteins pUL77 and pUL93 Are Structural Components Necessary for Viral Genome Encapsidation.” Journal of virology vol. 90,13 (2016): 5860-5875, doi:10.1128/JVI.00384-16.

[56] Ligat, Gaetan et al. “Identification of Amino Acids Essential for Viral Replication in the HCMV Helicase-Primase Complex.” Frontiers in microbiology vol. 9 (2018): 2483, doi:10.3389/fmicb.2018.02483.

[57] Wilkie, Adrian R et al. “A Role for Nuclear F-Actin Induction in Human Cytomegalovirus Nuclear Egress.” mBio vol. 7,4 (2016): e01254-16, doi:10.1128/mBio.01254-16.

[58] Sanchez, Veronica, and William Britt. “Human Cytomegalovirus Egress: Overcoming Barriers and Co-Opting Cellular Functions.” Viruses vol. 14,1 (2021): 15, doi:10.3390/v14010015.

[59] Marschall, Manfred et al. “Nuclear Egress Complexes of HCMV and Other Herpesviruses: Solving the Puzzle of Sequence Coevolution, Conserved Structures and Subfamily-Spanning Binding Properties.” Viruses vol. 12,6 (2020): 683, doi:10.3390/v12060683.

[60] Close, William L et al. “Betaherpesvirus Virion Assembly and Egress.” Advances in experimental medicine and biology vol. 1045 (2018): 167-207, doi:10.1007/978-981-10-7230-7_9.

[61] Das, Subhendu, and Philip E Pellett. “Spatial relationships between markers for secretory and endosomal machinery in human cytomegalovirus-infected cells versus those in uninfected cells.” Journal of virology vol. 85,12 (2011): 5864-79, doi:10.1128/JVI.00155-11.

[62] Alwine, James C. “The human cytomegalovirus assembly compartment: a masterpiece of viral manipulation of cellular processes that facilitates assembly and egress.” PLoS pathogens vol. 8,9 (2012): e1002878, doi:10.1371/journal.ppat.1002878.

[63] Sanchez, V et al. “Accumulation of virion tegument and envelope proteins in a stable cytoplasmic compartment during human cytomegalovirus replication: characterization of a potential site of virus assembly.” Journal of virology vol. 74,2 (2000): 975-86, doi:10.1128/jvi.74.2.975-986.2000.

[64] Jean Beltran, Pierre M et al. “A Portrait of the Human Organelle Proteome In Space and Time during Cytomegalovirus Infection.” Cell systems vol. 3,4 (2016): 361-373.e6, doi:10.1016/j.cels.2016.08.012.

[65] Das, Subhendu et al. “Identification of human cytomegalovirus genes important for biogenesis of the cytoplasmic virion assembly complex.” Journal of virology vol. 88,16 (2014): 9086-99, doi:10.1128/JVI.01141-14.

[66] Procter, Dean J et al. “The HCMV Assembly Compartment Is a Dynamic Golgi-Derived MTOC that Controls Nuclear Rotation and Virus Spread.” Developmental cell vol. 45,1 (2018): 83-100.e7, doi:10.1016/j.devcel.2018.03.010.

[67] Procter, Dean J et al. “Cytoplasmic control of intranuclear polarity by human cytomegalovirus.” Nature vol. 587,7832 (2020): 109-114, doi:10.1038/s41586-020-2714-x.

[68] Stevens, Alexander et al. “Structure-guided mutagenesis targeting interactions between pp150 tegument protein and small capsid protein identify five lethal and two live-attenuated HCMV mutants.” Virology vol. 596 (2024): 110115, doi:10.1016/j.virol.2024.110115.

[69] Penkert, Rhiannon R, and Robert F Kalejta. “Nuclear localization of tegument-delivered pp71 in human cytomegalovirus-infected cells is facilitated by one or more factors present in terminally differentiated fibroblasts.” Journal of virology vol. 84,19 (2010): 9853-63, doi:10.1128/JVI.00500-10.

[70] Schmolke, S et al. “Nuclear targeting of the tegument protein pp65 (UL83) of human cytomegalovirus: an unusual bipartite nuclear localization signal functions with other portions of the protein to mediate its efficient nuclear transport.” Journal of virology vol. 69,2 (1995): 1071-8, doi:10.1128/JVI.69.2.1071-1078.1995.

[71] Hensel, G et al. “Nuclear localization of the human cytomegalovirus tegument protein pp150 (ppUL32).” The Journal of general virology vol. 76 (Pt 7) (1995): 1591-601, doi:10.1099/0022-1317-76-7-1591.

[72] Bergner, Tim et al. “Secondary Envelopment of Human Cytomegalovirus Is a Fast Process Utilizing the Endocytic Compartment as a Major Membrane Source.” Biomolecules vol. 14,9 (2024): 1149, doi:10.3390/biom14091149.

[73] Flomm, Felix J et al. “Intermittent bulk release of human cytomegalovirus.” PLoS pathogens vol. 18,8 (2022): e1010575, doi:10.1371/journal.ppat.1010575.

[74] Arii J “ ESCRT-III-dependent and -independent egress of herpesviruses.” Front. Virol. 4 (2024): 1378054, doi:10.3389/fviro.2024.1378054.

[75] Tognarelli, Eduardo I et al. “Modulation of Endosome Function, Vesicle Trafficking and Autophagy by Human Herpesviruses.” Cells vol. 10,3 (2021): 542, doi:10.3390/cells10030542.

[76] Mettenleiter, Thomas C et al. “Herpesvirus assembly: an update.” Virus research vol. 143,2 (2009): 222-34, doi:10.1016/j.virusres.2009.03.018.

[77] Cepeda, Victoria et al. “Human cytomegalovirus final envelopment on membranes containing both trans-Golgi network and endosomal markers.” Cellular microbiology vol. 12,3 (2010): 386-404, doi:10.1111/j.1462-5822.2009.01405.x.

[78] Federspiel, Joel D et al. “Mitochondria and Peroxisome Remodeling across Cytomegalovirus Infection Time Viewed through the Lens of Inter-ViSTA.” Cell reports vol. 32,4 (2020): 107943, doi:10.1016/j.celrep.2020.107943.

[79] Wilkie, Adrian R et al. “A Role for Nuclear F-Actin Induction in Human Cytomegalovirus Nuclear Egress.” mBio vol. 7,4 (2016): e01254-16, doi:10.1128/mBio.01254-16.

[80] Milbradt, Jens et al. “Novel mode of phosphorylation-triggered reorganization of the nuclear lamina during nuclear egress of human cytomegalovirus.” The Journal of biological chemistry vol. 285,18 (2010): 13979-89, doi:10.1074/jbc.M109.063628.

[81] Mosher BS, Kowalik TF and Yurochko AD “Overview of how HCMV manipulation of host cell intracellular trafficking networks can promote productive infection.” Front. Virol. vol. 2 (2022): 1026452, doi:10.3389/fviro.2022.1026452.

[82] Zhang, H. et al., "A cytomegalovirus immunevasin triggers integrated stress response-dependent reorganization of the endoplasmic reticulum, bioRxiv, 10 Aug. 2019, doi:10.1101/641068.

[83] Zhang, Hongbo et al. “The Human Cytomegalovirus Nonstructural Glycoprotein UL148 Reorganizes the Endoplasmic Reticulum.” mBio vol. 10,6 (2019): e02110-19, doi:10.1128/mBio.02110-19.v

[84] Combs, Joseph A et al. “Human Cytomegalovirus Alters Host Cell Mitochondrial Function during Acute Infection.” Journal of virology vol. 94,2 (2020): e01183-19, doi:10.1128/JVI.01183-19.

[85] Goldmacher, Victor S. “vMIA, a viral inhibitor of apoptosis targeting mitochondria.” Biochimie vol. 84,2-3 (2002): 177-85, doi:10.1016/s0300-9084(02)01367-6.

[86] McCormick, A Louise et al. “Disruption of mitochondrial networks by the human cytomegalovirus UL37 gene product viral mitochondrion-localized inhibitor of apoptosis.” Journal of virology vol. 77,1 (2003): 631-41, doi:10.1128/jvi.77.1.631-641.2003.

[87] Betsinger, Cora N et al. “The human cytomegalovirus protein pUL13 targets mitochondrial cristae architecture to increase cellular respiration during infection.” Proceedings of the National Academy of Sciences of the United States of America vol. 118,32 (2021): e2101675118, doi:10.1073/pnas.2101675118.

[88] Jean Beltran, Pierre M et al. “Infection-Induced Peroxisome Biogenesis Is a Metabolic Strategy for Herpesvirus Replication.” Cell host & microbe vol. 24,4 (2018): 526-541.e7, doi:10.1016/j.chom.2018.09.002.

[89] Ferreira, Ana Rita et al. “Emerging roles of peroxisomes in viral infections.” Trends in cell biology vol. 32,2 (2022): 124-139, doi:10.1016/j.tcb.2021.09.010.

[90] Kumar, Rechal et al. “The peroxisome: an update on mysteries 3.0.” Histochemistry and cell biology vol. 161,2 (2024): 99-132, doi:10.1007/s00418-023-02259-5.

[91] Prinz, William A et al. “The functional universe of membrane contact sites.” Nature reviews. Molecular cell biology vol. 21,1 (2020): 7-24, doi:10.1038/s41580-019-0180-9.

[92] Scorrano, Luca et al. “Coming together to define membrane contact sites.” Nature communications vol. 10,1 (2019): 1287, doi:10.1038/s41467-019-09253-3.

[93] Cook, Katelyn C et al. “Restructured membrane contacts rewire organelles for human cytomegalovirus infection.” Nature communications vol. 13,1 (2022): 4720, doi:10.1038/s41467-022-32488-6.

[94] Siddiquey, Mohammed N A et al. “The Human Cytomegalovirus Endoplasmic Reticulum-Resident Glycoprotein UL148 Activates the Unfolded Protein Response.” Journal of virology vol. 92,20 (2018): e00896-18, doi:10.1128/JVI.00896-18.

[95] Hofstadter, William A et al. “Infection-induced peripheral mitochondria fission drives ER encapsulations and inter-mitochondria contacts that rescue bioenergetics.” Nature communications vol. 15,1 (2024): 7352, doi:10.1038/s41467-024-51680-4.

[96] Hofstadter, William A et al. “Viral regulation of organelle membrane contact sites.” PLoS biology vol. 22,3 (2024): e3002529, doi:10.1371/journal.pbio.3002529.

[97] Abbe, E. “Beiträge zur Theorie des Mikroskops und der mikroskopischen Wahrnehmung.” Archiv f. mikrosk. Anatomie 9 (1873): 413–468, doi:10.1007/BF02956173.

[98] Abbe , "The Relation of Aperture and Power in the Microscope (continued)" Journal of the Royal Microscopical Society, vol. 2, no. 4 (1882): 460-473, doi:10.1111/j.1365-2818.1882.tb04805.x

[99] De Broglie, L. “Waves and Quanta.” Nature 112 (1923): 540, doi:10.1038/112540a0.

[100] Ondrej L Krivanek “Aberration correction in electron microscopy and spectroscopy.” Microscopy and Microanalysis vol. 27,1 (2021): 3474–3478, doi:10.1017/S1431927621012435.

[101] Kikuchi, J.-i. and Yasuhara, K. (2012). Transmission Electron Microscopy (TEM). In Supramolecular Chemistry (eds P.A. Gale and J.W. Steed), doi:10.1002/9780470661345.smc022.

[102] Ilett M, S'ari M, Freeman H, Aslam Z, Koniuch N, Afzali M, Cattle J, Hooley R, Roncal-Herrero T, Collins SM, Hondow N, Brown A, Brydson R. “Analysis of complex, beam-sensitive materials by transmission electron microscopy and associated techniques.” Philos Trans A Math Phys Eng Sci. vol. 379,2186 (2020): 20190601, doi:10.1098/rsta.2019.0601.

[103] Vernon-Parry, Karen. Scanning electron microscopy: An introduction. III-Vs Review. 13 (2000): 40–44, doi:10.1016/S0961-1290(00)80006-X.

[104] Himes, Benjamin, and Nikolaus Grigorieff. “Cryo-TEM simulations of amorphous radiation-sensitive samples using multislice wave propagation.” IUCrJ vol. 8,6 (2021): 943-953, doi:10.1107/S2052252521008538.

[105] Dickerson, Joshua L et al. “Imaging biological macromolecules in thick specimens: The role of inelastic scattering in cryoEM.” Ultramicroscopy vol. 237 (2022): 113510, doi:10.1016/j.ultramic.2022.113510.

[106] Cosslett, V E. “Radiation damage in the high resolution electron microscopy of biological materials: a review.” Journal of microscopy vol. 113,2 (1978): 113-29, doi:10.1111/j.1365-2818.1978.tb02454.x.

[107] Ray Egerton “Understanding Radiation Damage in Beam-Sensitive TEM Specimens, Microscopy and Microanalysis” vol. 26,2 (2020): 84–86, doi:10.1017/S1431927620013331.

[108] Dubochet, J et al. “Cryo-electron microscopy of vitrified specimens.” Quarterly reviews of biophysics vol. 21,2 (1988): 129-228, doi:10.1017/s0033583500004297.

[109] Thompson, Rebecca F et al. “An introduction to sample preparation and imaging by cryo-electron microscopy for structural biology.” Methods (San Diego, Calif.) vol. 100 (2016): 3-15, doi:10.1016/j.ymeth.2016.02.017.

[110] Tamada, Hiromi et al. “Ultrastructural comparison of dendritic spine morphology preserved with cryo and chemical fixation.” eLife vol. 9 e56384. 4 Dec. 2020, doi:10.7554/eLife.56384.

[111] Küçükoğlu, Berk et al. “Low-dose cryo-electron ptychography of proteins at sub-nanometer resolution.” Nature communications vol. 15,1 (2024): 8062, doi:10.1038/s41467-024-52403-5.

[112] Tacke, Sebastian et al. “A streamlined workflow for automated cryo focused ion beam milling.” Journal of structural biology vol. 213,3 (2021): 107743, doi:10.1016/j.jsb.2021.107743.

[113] Schaffer, Miroslava et al. “Cryo-focused Ion Beam Sample Preparation for Imaging Vitreous Cells by Cryo-electron Tomography.” Bio-protocol vol. 5,17 (2015): e1575, doi:10.21769/bioprotoc.1575.

[114] Prewett, P. D., and Jefferies, D. K., "Characteristics of a gallium liquid metal field emission ion source," Journal of Physics D: Applied Physics, vol. 13,9 (1980): 1747-1755, doi:10.1088/0022-3727/13/9/024.

[115] Zhang, Yu et al. “Large volume tomography using plasma FIB-SEM: A comprehensive case study on black silicon.” Ultramicroscopy vol. 233 (2022): 113458, doi:10.1016/j.ultramic.2021.113458.

[116] Fernandez JJ, Laugks U, Schaffer M, Bäuerlein FJ, Khoshouei M, Baumeister W, Lucic V. “Removing Contamination-Induced Reconstruction Artifacts from Cryo-electron Tomograms.” Biophys J. vol. 110,4 (2016):850-9, doi: 10.1016/j.bpj.2015.10.043.

[117] Lucas, Bronwyn A, and Nikolaus Grigorieff. “Quantification of gallium cryo-FIB milling damage in biological lamellae.” Proceedings of the National Academy of Sciences of the United States of America vol. 120,23 (2023): e2301852120, doi:10.1073/pnas.2301852120.

[118] Lam, Vinson, and Elizabeth Villa. “Practical Approaches for Cryo-FIB Milling and Applications for Cellular Cryo-Electron Tomography.” Methods in molecular biology (Clifton, N.J.) vol. 2215 (2021): 49-82, doi:10.1007/978-1-0716-0966-8_3.

[119] Baumeister, Wolfgang. “Cryo-electron tomography: A long journey to the inner space of cells.” Cell vol. 185,15 (2022): 2649-2652, doi:10.1016/j.cell.2022.06.034.

[120] Fernandez, Jose-Jesus et al. “Cryo-tomography tilt-series alignment with consideration of the beam-induced sample motion.” Journal of structural biology vol. 202,3 (2018): 200-209, doi:10.1016/j.jsb.2018.02.001.

[121] Hong, Ye et al. “Cryo-Electron Tomography: The Resolution Revolution and a Surge of In Situ Virological Discoveries.” Annual review of biophysics vol. 52 (2023): 339-360, doi:10.1146/annurev-biophys-092022-100958.

[122] Kudryashev, Mikhail. “The big chill: Growth of in situ structural biology with cryo-electron tomography.” QRB discovery vol. 5 (2024): e10, doi:10.1017/qrd.2024.10.

[123] Kaarbø, Mari et al. “Human cytomegalovirus infection increases mitochondrial biogenesis.” Mitochondrion vol. 11,6 (2011): 935-45, doi:10.1016/j.mito.2011.08.008.

[124] Hu, Judy Z et al. “Continuity of Mitochondrial Budding: Insights from BS-C-1 Cells by In Situ Cryo-electron Tomography.” Microscopy and microanalysis : the official journal of Microscopy Society of America, Microbeam Analysis Society, Microscopical Society of Canada vol. 31,1 (2025): ozae122, doi:10.1093/mam/ozae122.

[125] Wozny, Michael R et al. “In situ architecture of the ER-mitochondria encounter structure.” Nature vol. 618,7963 (2023): 188-192, doi:10.1038/s41586-023-06050-3.

[126] Phillips, Melissa J, and Gia K Voeltz. “Structure and function of ER membrane contact sites with other organelles.” Nature reviews. Molecular cell biology vol. 17,2 (2016): 69-82, doi:10.1038/nrm.2015.8.

[127] Kors, Suzan et al. “Regulating peroxisome-ER contacts via the ACBD5-VAPB tether by FFAT motif phosphorylation and GSK3β.” The Journal of cell biology vol. 221,3 (2022): e202003143, doi:10.1083/jcb.202003143.

[128] Obara, Christopher J et al. “Motion of VAPB molecules reveals ER-mitochondria contact site subdomains.” Nature vol. 626,7997 (2024): 169-176, doi:10.1038/s41586-023-06956-y.

[129] Yoniles, Joseph et al. “Time-resolved cryogenic electron tomography for the study of transient cellular processes.” Molecular biology of the cell vol. 35,7 (2024): mr4, doi:10.1091/mbc.E24-01-0042.

[130] Giacomello, M, and L Pellegrini. “The coming of age of the mitochondria-ER contact: a matter of thickness.” Cell death and differentiation vol. 23,9 (2016): 1417-27, doi:10.1038/cdd.2016.52.

[131] Gordaliza-Alaguero, Isabel et al. “Metabolic implications of organelle-mitochondria communication.” EMBO reports vol. 20,9 (2019): e47928, doi:10.15252/embr.201947928.

[132] Sassano, Maria Livia et al. “ER-mitochondria contact sites; a multifaceted factory for Ca2+ signaling and lipid transport.” Frontiers in cell and developmental biology vol. 10 (2022): 988014, doi:10.3389/fcell.2022.988014.

[133] Wanders, Ronald J A, and Hans R Waterham. “Biochemistry of mammalian peroxisomes revisited.” Annual review of biochemistry vol. 75 (2006): 295-332, doi:10.1146/annurev.biochem.74.082803.133329.

[134] Fujiki, Yukio et al. “Peroxisome biogenesis in mammalian cells.” Frontiers in physiology vol. 5 (2014): 307, doi:10.3389/fphys.2014.00307.

[135] Pieuchot, Laurent, and Gregory Jedd. “Peroxisome assembly and functional diversity in eukaryotic microorganisms.” Annual review of microbiology vol. 66 (2012): 237-63, doi:10.1146/annurev-micro-092611-150126.

[136] Wanders, R J A. “Peroxisomes, lipid metabolism, and peroxisomal disorders.” Molecular genetics and metabolism vol. 83,1-2 (2004): 16-27, doi:10.1016/j.ymgme.2004.08.016.

[137] Schrader, Michael, and H Dariush Fahimi. “The peroxisome: still a mysterious organelle.” Histochemistry and cell biology vol. 129,4 (2008): 421-40, doi:10.1007/s00418-008-0396-9.

[138] Wanders, Ronald J A. “Metabolic functions of peroxisomes in health and disease.” Biochimie vol. 98 (2014): 36-44, doi:10.1016/j.biochi.2013.08.022

[139] Fransen, Marc & Nordgren, Marcus & Wang, Bo & Apanasets, Oksana. Role of peroxisomes in ROS/RNS-metabolism: Implications for human disease. Biochimica et biophysica acta. vol. 1822 (2011): 1363-73, doi:10.1016/j.bbadis.2011.12.001.

[140] Ferreira, Ana Rita et al. “Peroxisomes and Innate Immunity: Antiviral Response and Beyond.” International journal of molecular sciences vol. 20,15 (2019): 3795, doi:10.3390/ijms20153795.

[141] Silva, Beatriz S C et al. “Maintaining social contacts: The physiological relevance of organelle interactions.” Biochimica et biophysica acta. Molecular cell research vol. 1867,11 (2020): 118800, doi:10.1016/j.bbamcr.2020.118800.

[142] Wanders RJA, Waterham HR and Ferdinandusse S “Metabolic Interplay between Peroxisomes and Other Subcellular Organelles Including Mitochondria and the Endoplasmic Reticulum.” Front. Cell Dev. Biol. vol. 3 (2016): 83, doi:10.3389/fcell.2015.00083.

[143] Schrader, Michael et al. “Proliferation and fission of peroxisomes - An update.” Biochimica et biophysica acta vol. 1863,5 (2016): 971-83, doi:10.1016/j.bbamcr.2015.09.024.

[144] Weller, S., Gould, S. J., and Valle, D., "Peroxisome Biogenesis Disorders," Annual Review of Genomics and Human Genetics, vol. 4,1 (2003): 165-211, doi:10.1146/annurev.genom.4.070802.110424.

[145] Braverman, Nancy E et al. “Peroxisome biogenesis disorders in the Zellweger spectrum: An overview of current diagnosis, clinical manifestations, and treatment guidelines.” Molecular genetics and metabolism vol. 117,3 (2016): 313-21, doi:10.1016/j.ymgme.2015.12.009.

[146] Sugiura, Ayumu et al. “Newly born peroxisomes are a hybrid of mitochondrial and ER-derived pre-peroxisomes.” Nature vol. 542,7640 (2017): 251-254, doi:10.1038/nature21375.

[147] Schrader, M et al. “Fission and proliferation of peroxisomes.” Biochimica et biophysica acta vol. 1822,9 (2012): 1343-57, doi:10.1016/j.bbadis.2011.12.014.

[148] Toro, Andrés A et al. “Pex3p-dependent peroxisomal biogenesis initiates in the endoplasmic reticulum of human fibroblasts.” Journal of cellular biochemistry vol. 107,6 (2009): 1083-96, doi:10.1002/jcb.22210.

[149] Agrawal, Gaurav, and Suresh Subramani. “De novo peroxisome biogenesis: Evolving concepts and conundrums.” Biochimica et biophysica acta vol. 1863,5 (2016): 892-901, doi:10.1016/j.bbamcr.2015.09.014.

[150] Kim, Peter K et al. “The origin and maintenance of mammalian peroxisomes involves a de novo PEX16-dependent pathway from the ER.” The Journal of cell biology vol. 173,4 (2006): 521-32, doi:10.1083/jcb.200601036.

[151] Aranovich, Alexander et al. “PEX16 contributes to peroxisome maintenance by constantly trafficking PEX3 via the ER.” Journal of cell science vol. 127,Pt 17 (2014): 3675-86, doi:10.1242/jcs.146282.

[152] Fujiki, Y et al. “Polypeptide and phospholipid composition of the membrane of rat liver peroxisomes: comparison with endoplasmic reticulum and mitochondrial membranes.” The Journal of cell biology vol. 93,1 (1982): 103-10, doi:10.1083/jcb.93.1.103.

[153] Jones, Jacob M et al. “PEX19 is a predominantly cytosolic chaperone and import receptor for class 1 peroxisomal membrane proteins.” The Journal of cell biology vol. 164,1 (2004): 57-67, doi:10.1083/jcb.200304111.

[154] Erdmann, Ralf, and Wolfgang Schliebs. “Peroxisomal matrix protein import: the transient pore model.” Nature reviews. Molecular cell biology vol. 6,9 (2005): 738-42, doi:10.1038/nrm1710

[155] Leon, Sebastien & Goodman, Joel & Subramani, Suresh. “Uniqueness of the mechanism of protein import into the peroxisome matrix: Transport of folded, co-factor-bound and oligomeric proteins by shuttling receptors.” Biochimica et biophysica acta. vol. 1763 (2007): 1552-64, doi:10.1016/j.bbamcr.2006.08.037.

[156] Hagmann, Vera et al. “Chemically monoubiquitinated PEX5 binds to the components of the peroxisomal docking and export machinery.” Scientific reports vol. 8,1 (2018): 16014, doi:10.1038/s41598-018-34200-5.

[157] N.B. Blok, D. Tan, R.Y. Wang, P.A. Penczek, D. Baker, F. DiMaio, T.A. Rapoport, & T. Walz, “Unique double-ring structure of the peroxisomal Pex1/Pex6 ATPase complex revealed by cryo-electron microscopy.” Proc. Natl. Acad. Sci. U.S.A. vol. 112,30 (2015): E4017-E4025, doi.org/10.1073/pnas.1500257112.

[158] Okumoto, Kanji et al. “Distinct modes of ubiquitination of peroxisome-targeting signal type 1 (PTS1) receptor Pex5p regulate PTS1 protein import.” The Journal of biological chemistry vol. 289,20 (2014): 14089-108, doi:10.1074/jbc.M113.527937.

[159] Farré, Jean-Claude et al. “Peroxisome biogenesis, membrane contact sites, and quality control.” EMBO reports vol. 20,1 (2019): e46864, doi:10.15252/embr.201846864.

[160] Schrader, Michael et al. “Organelle interplay-peroxisome interactions in health and disease.” Journal of inherited metabolic disease vol. 43,1 (2020): 71-89, doi:10.1002/jimd.12083.

[161] Neuman, Sarah D et al. “A novel superfamily of bridge-like lipid transfer proteins.” Trends in cell biology vol. 32,11 (2022): 962-974, doi:10.1016/j.tcb.2022.03.011.

[162] Covill-Cooke, Christian et al. “Peroxisomal fission is modulated by the mitochondrial Rho-GTPases, Miro1 and Miro2.” EMBO reports vol. 21,2 (2020): e49865, doi:10.15252/embr.201949865.

[163] Castro, Inês G et al. “A role for Mitochondrial Rho GTPase 1 (MIRO1) in motility and membrane dynamics of peroxisomes.” Traffic (Copenhagen, Denmark) vol. 19,3 (2018): 229-242, doi:10.1111/tra.12549.

[164] Passmore, Josiah B et al. “Mitochondrial fission factor (MFF) is a critical regulator of peroxisome maturation.” Biochimica et biophysica acta. Molecular cell research vol. 1867,7 (2020): 118709, doi:10.1016/j.bbamcr.2020.118709.

[165] Woudenberg, Jannes et al. “Lipid rafts are essential for peroxisome biogenesis in HepG2 cells.” Hepatology (Baltimore, Md.) vol. 52,2 (2010): 623-33, doi:10.1002/hep.23684.

[166] Delille, Hannah K et al. “Pex11pbeta-mediated growth and division of mammalian peroxisomes follows a maturation pathway.” Journal of cell science vol. 123,16 (2010): 2750-62, doi:10.1242/jcs.062109.

[167] Itoyama, Akinori et al. “Mff functions with Pex11pβ and DLP1 in peroxisomal fission.” Biology open vol. 2,10 (2013): 998-1006, doi:10.1242/bio.20135298.

[168] Williams, Chris et al. “The membrane remodeling protein Pex11p activates the GTPase Dnm1p during peroxisomal fission.” Proceedings of the National Academy of Sciences of the United States of America vol. 112,20 (2015): 6377-82, doi:10.1073/pnas.1418736112.

[169] Covill-Cooke, Christian et al. “Regulation of peroxisomal trafficking and distribution.” Cellular and molecular life sciences : CMLS vol. 78,5 (2021): 1929-1941, doi:10.1007/s00018-020-03687-5.

[170] Dixit, Evelyn et al. “Peroxisomes are signaling platforms for antiviral innate immunity.” Cell vol. 141,4 (2010): 668-81, doi:10.1016/j.cell.2010.04.018.

[171] Di Cara, Francesca. “Peroxisomes in host defense.” PLoS pathogens vol. 16,7 (2020): e1008636, doi:10.1371/journal.ppat.1008636.

[172] Carty, Michael et al. “Detection of Viral Infections by Innate Immunity.” Biochemical pharmacology vol. 183 (2021): 114316, doi:10.1016/j.bcp.2020.114316.

[173] Ferreira, Ana Rita et al. “Peroxisomes and Innate Immunity: Antiviral Response and Beyond.” International journal of molecular sciences vol. 20,15 (2019): 3795, doi:10.3390/ijms20153795.

[174] Saito, Takeshi, and Michael Gale Jr. “Differential recognition of double-stranded RNA by RIG-I-like receptors in antiviral immunity.” The Journal of experimental medicine vol. 205,7 (2008): 1523-7, doi:10.1084/jem.20081210.

[175] Ren, Zhihua et al. “Regulation of MAVS Expression and Signaling Function in the Antiviral Innate Immune Response.” Frontiers in immunology vol. 11 (2020): 1030, doi:10.3389/fimmu.2020.01030.

[176] Hou, Fajian et al. “MAVS forms functional prion-like aggregates to activate and propagate antiviral innate immune response.” Cell vol. 146,3 (2011): 448-61, doi:10.1016/j.cell.2011.06.041.

[177] Nath, Anu S et al. “Modulation of the cell membrane lipid milieu by peroxisomal β-oxidation induces Rho1 signaling to trigger inflammatory responses.” Cell reports vol. 38,9 (2022): 110433, doi:10.1016/j.celrep.2022.110433.

[178] Wanders, Ronald J A et al. “Fatty Acid Oxidation in Peroxisomes: Enzymology, Metabolic Crosstalk with Other Organelles and Peroxisomal Disorders.” Advances in experimental medicine and biology vol. 1299 (2020): 55-70, doi:10.1007/978-3-030-60204-8_5.

[179] Schrader, Michael, and H Dariush Fahimi. “Peroxisomes and oxidative stress.” Biochimica et biophysica acta vol. 1763,12 (2006): 1755-66, doi:10.1016/j.bbamcr.2006.09.006.

[180] Di Cara, Francesca et al. “Peroxisomes in Immune Response and Inflammation.” International journal of molecular sciences vol. 20,16 (2019): 3877, doi:10.3390/ijms20163877.

[181] Ma, Junhe et al. “Structural mechanism of Bax inhibition by cytomegalovirus protein vMIA.” Proceedings of the National Academy of Sciences of the United States of America vol. 109,51 (2012): 20901-6, doi:10.1073/pnas.1217094110.

[182] Goldmacher, V S. “Cell death suppression by cytomegaloviruses.” Apoptosis : an international journal on programmed cell death vol. 10,2 (2005): 251-65, doi:10.1007/s10495-005-0800-z.

[183] Magalhães, Ana Cristina et al. “Peroxisomes are platforms for cytomegalovirus' evasion from the cellular immune response.” Scientific reports vol. 6 (2016): 26028, doi:10.1038/srep26028.

[184] Castanier, Céline et al. “Mitochondrial dynamics regulate the RIG-I-like receptor antiviral pathway.” EMBO reports vol. 11,2 (2010): 133-8, doi:10.1038/embor.2009.258.

[185] Goldmacher, V S et al. “A cytomegalovirus-encoded mitochondria-localized inhibitor of apoptosis structurally unrelated to Bcl-2.” Proceedings of the National Academy of Sciences of the United States of America vol. 96,22 (1999): 12536-41, doi:10.1073/pnas.96.22.12536.

[186] Ferreira, Ana Rita et al. “Human Cytomegalovirus vMIA Inhibits MAVS Oligomerization at Peroxisomes in an MFF-Dependent Manner.” Frontiers in cell and developmental biology vol. 10 (2022): 871977, doi:10.3389/fcell.2022.871977.

[187] Indari, Omkar et al. “Herpesviral interplay with peroxisome: An underexplored viral niche.” Genes & diseases vol. 10,4 (2023): 1133-1135, doi:10.1016/j.gendis.2023.01.033.

[188] Marques, Mariana et al. “The Interplay between Human Cytomegalovirus and Pathogen Recognition Receptor Signaling.” Viruses vol. 10,10 (2018): 514, doi:10.3390/v10100514.

[189] Wolff, Georg et al. “Towards correlative super-resolution fluorescence and electron cryo-microscopy.” Biology of the cell vol. 108,9 (2016): 245-58, doi:10.1111/boc.201600008.

[190] Schellenberger, Pascale et al. “High-precision correlative fluorescence and electron cryo microscopy using two independent alignment markers.” Ultramicroscopy vol. 143,100 (2014): 41-51, doi:10.1016/j.ultramic.2013.10.011.

[191] Sartori, Anna et al. “Correlative microscopy: bridging the gap between fluorescence light microscopy and cryo-electron tomography.” Journal of structural biology vol. 160,2 (2007): 135-45, doi:10.1016/j.jsb.2007.07.011.

[192] Chang, Yi-Wei et al. “Correlated cryogenic photoactivated localization microscopy and cryo-electron tomography.” Nature methods vol. 11,7 (2014): 737-9, doi:10.1038/nmeth.2961.

[193] Dobro, Megan J et al. “Plunge freezing for electron cryomicroscopy.” Methods in enzymology vol. 481 (2010): 63-82, doi:10.1016/S0076-6879(10)81003-1.

[194] Smeets, Marit & Bieber, Anna & Capitanio, Cristina & Schioetz, Oda & Heijden, Thomas & Effting, Andries & Piel, Éric & Lazem, Bassim & Erdmann, Philipp & Plitzko, Juergen. Integrated Cryo-Correlative Microscopy for Targeted Structural Investigation In Situ. Microscopy Today. vol. 29 (2021): 20-25, doi:10.1017/S1551929521001280.

[195] Mojiri, S. et al., "Effects of base temperature, immersion medium, and EM grid material on devitrification thresholds in cryogenic optical super-resolution microscopy." Journal of structural biology vol. 217,3 (2025): 1047-8477, doi:10.1016/j.jsb.2025.108231.

[196] Downing, K., and Chiu, W., "Cold stage design for high resolution electron microscopy of biological materials" Electron Microscopy Reviews, vol. 3,2 (1990): 213-226, doi:10.1016/0892-0354(90)90002-A

[197] Tuijtel, Maarten W et al. “Correlative cryo super-resolution light and electron microscopy on mammalian cells using fluorescent proteins.” Scientific reports vol. 9,1 (2019): 1369, doi:10.1038/s41598-018-37728-8.

[198] Schwartz, Cindi L et al. “Cryo-fluorescence microscopy facilitates correlations between light and cryo-electron microscopy and reduces the rate of photobleaching.” Journal of microscopy vol. 227,2 (2007): 98-109, doi:10.1111/j.1365-2818.2007.01794.x.

[199] Rigort, Alexander et al. “Micromachining tools and correlative approaches for cellular cryo-electron tomography.” Journal of structural biology vol. 172,2 (2010): 169-79, doi:10.1016/j.jsb.2010.02.011.

[200] Hampton, C., Strauss, J., Ke, Z. et al. Correlated fluorescence microscopy and cryo-electron tomography of virus-infected or transfected mammalian cells. Nat Protoc vol. 12 (2017): 150–167, doi:10.1038/nprot.2016.168.

[201] Katherine Lau, Caspar Jonker, Jingyue Liu, Marit Smeets, The Undesirable Effects and Impacts of Ice Contamination Experienced in the Cryo-Electron Tomography Workflow and Available Solutions, Microscopy Today vol. 30,3 (2022): 30–35, doi:10.1017/S1551929522000621.

[202] Alexander Rigort, Robert Kirmse, Volker Doring, Michael Schwertner, Ralf Wolleschensky, Imaging of Vitrified Biological Specimens by Confocal Cryo-Fluorescence Microscopy and Cryo-FIB/SEM Tomography, Microscopy and Microanalysis vol. 21,3 (2015): 1121–1122, doi:10.1017/S143192761500639X.

[203] Mahalingam, Shanmuga S et al. “Balancing the Opposing Principles That Govern Peroxisome Homeostasis.” Trends in biochemical sciences vol. 46,3 (2021): 200-212, doi:10.1016/j.tibs.2020.09.006.

[204] Vonck, J, and E F van Bruggen. “Architecture of peroxisomal alcohol oxidase crystals from the methylotrophic yeast Hansenula polymorpha as deduced by electron microscopy.” Journal of bacteriology vol. 174,16 (1992): 5391-9, doi:10.1128/jb.174.16.5391-5399.1992.

[205] Kleff, S et al. “The predominant protein in peroxisomal cores of sunflower cotyledons is a catalase that differs in primary structure from the catalase in the peroxisomal matrix.” European journal of biochemistry vol. 245,2 (1997): 402-10, doi:10.1111/j.1432-1033.1997.t01-1-00402.x.

[206] David B Carson, Joseph J Cooney, Microbodies in fungi: a review, Journal of Industrial Microbiology, vol.6,1 (1990): 1–18, doi:10.1007/BF01576172.

[207] Schönherr, Robert et al. “Protein crystallization in living cells.” Biological chemistry vol. 399,7 (2018): 751-772, doi:10.1515/hsz-2018-0158.

[208] Veenhuis, Marten et al. “Peroxisome assembly in yeast.” Microscopy research and technique vol. 61,2 (2003): 139-50, doi:10.1002/jemt.10323.

[209] Bäcker, Nils et al. “Peroxisomal core structures segregate diverse metabolic pathways.” Nature communications vol. 16,1 (2025): 1802, doi:10.1038/s41467-025-57053-9.

[210] Biempica, L. “Human hepatic microbodies with crystalloid cores.” The Journal of cell biology vol. 29,2 (1966): 383-6, doi:10.1083/jcb.29.2.383.

[211] Carmichael, Ruth E, and Michael Schrader. “Determinants of Peroxisome Membrane Dynamics.” Frontiers in physiology vol. 13 (2022): 834411, doi:10.3389/fphys.2022.834411.

[212] Koch, Annett et al. “Peroxisome elongation and constriction but not fission can occur independently of dynamin-like protein 1.” Journal of cell science vol. 117,17 (2004): 3995-4006, doi:10.1242/jcs.01268.

[213] Carmichael, Ruth E et al. “Fission Impossible (?)-New Insights into Disorders of Peroxisome Dynamics.” Cells vol. 11,12 (2022): 1922, doi:10.3390/cells11121922.

[214] Varnum, Susan M et al. “Identification of proteins in human cytomegalovirus (HCMV) particles: the HCMV proteome.” Journal of virology vol. 78,20 (2004): 10960-6, doi:10.1128/JVI.78.20.10960-10966.2004.

[215] Tsang, Tin Ki et al. “High-quality ultrastructural preservation using cryofixation for 3D electron microscopy of genetically labeled tissues.” eLife vol. 7 (2018): e35524, doi:10.7554/eLife.35524.

[216] Read, Clarissa et al. “Regulation of Human Cytomegalovirus Secondary Envelopment by a C-Terminal Tetralysine Motif in pUL71.” Journal of virology vol. 93,13 (2019): e02244-18, doi:10.1128/JVI.02244-18.

[217] Bentley, Kirsten et al. “Virion proteomics of genetically intact HCMV reveals a regulator of envelope glycoprotein composition that protects against humoral immunity.” Proceedings of the National Academy of Sciences of the United States of America vol. 122,38 (2025): e2425622122, doi:10.1073/pnas.2425622122.

[218] Cimato, Giorgia et al. “Human cytomegalovirus glycoprotein variants governing viral tropism and syncytium formation in epithelial cells and macrophages.” Journal of virology vol. 98,7 (2024): e0029324, doi:10.1128/jvi.00293-24.

[219] Hernandez-Gonzalez, Miguel et al. “Viral use and subversion of membrane organization and trafficking.” Journal of cell science vol. 134,5 (2021): jcs252676, doi:10.1242/jcs.252676.

[220] Draganova, Elizabeth B et al. “The Ins and Outs of Herpesviral Capsids: Divergent Structures and Assembly Mechanisms across the Three Subfamilies.” Viruses vol. 13,10 (2021): 1913, doi:10.3390/v13101913.

[221] Homman-Loudiyi, M et al. “Envelopment of human cytomegalovirus occurs by budding into Golgi-derived vacuole compartments positive for gB, Rab 3, trans-golgi network 46, and mannosidase II.” Journal of virology vol. 77,5 (2003): 3191-203, doi:10.1128/jvi.77.5.3191-3203.2003.

[222] Rebmann, G Michael et al. “Phosphorylation of Golgi Peripheral Membrane Protein Grasp65 Is an Integral Step in the Formation of the Human Cytomegalovirus Cytoplasmic Assembly Compartment.” mBio vol. 7,5 (2016): e01554-16, doi:10.1128/mBio.01554-16.

[223] Momtaz, Samina et al. “Cell type-specific biogenesis of novel vesicles containing viral products in human cytomegalovirus infection.” Journal of virology vol. 95,11 (2021): e02358-20, doi:10.1128/JVI.02358-20.

[224] Wedemann, Linda et al. “The unconventional way out-Egress of HCMV through multiviral bodies.” Molecular microbiology vol. 117,6 (2022): 1317-1323, doi:10.1111/mmi.14946.

[225] Klumpe, Sven et al. “A modular platform for automated cryo-FIB workflows.” eLife vol. 10 (2021): e70506, doi:10.7554/eLife.70506.

[226] Schindelin, Johannes et al. “Fiji: an open-source platform for biological-image analysis.” Nature methods vol. 9,7 (20212): 676-82, doi:10.1038/nmeth.2019.

[227] Zheng, Shawn et al. “AreTomo: An integrated software package for automated marker-free, motion-corrected cryo-electron tomographic alignment and reconstruction.” Journal of structural biology: X vol. 6 (2022): 100068, doi:10.1016/j.yjsbx.2022.100068.

[228] Kremer, J R et al. “Computer visualization of three-dimensional image data using IMOD.” Journal of structural biology vol. 116,1 (1996): 71-6, doi:10.1006/jsbi.1996.0013.

[229] Korotkova, Daria et al. “Fluorescent fatty acid conjugates for live cell imaging of peroxisomes.” Nature communications vol. 15,1 (2024): 4314, doi:10.1038/s41467-024-48679-2.

8 GHS list of chemicals

Compound	Hazard pictogram	H statement	P statement
2-Propanol	GHS02, GHS07	H225, H319, H336	P210, P233, P305+P351+P338
Ampicillin	GHS08	H317, H334	P261, P280, P302+P352, P342+P311
Bacillol® AF	GHS02, GHS05, GHS07	H226, H318, H336	P102, P210, P261, P280, P305+P351+P338+P310, P501
Ethanol	GHS02, GHS07	H225, H319	P210, P233, P305+P351+P338
Nitrogen (liquid)	GHS04	H281	P282, P336+P315, P403
OPTISEPT®	GHS05, GHS07, GHS08, GHS09	H302+H332, H314, H317, H334, H335, H341, H350, H410	P202, P260, P280, P303+P361+P353, P304+P340, P305+P351+P338, P308+P313, P405, P501
Paraformaldehyde	GHS02, GHS05, GHS07, GHS08	H228, H302+H332, H315, H317, H318, H335, H341, H350	P202, 210, P270, P280, P305+P351+P338, P308+P313
X-tremeGENE™ HP DNA transfection reagent	GHS02, GHS07	H225, H319	P210, P233, P280, P303+P361+P353, P337+P313, P370+P378

9 Acknowledgements

First and foremost, I want to express my profound gratitude to my family. In particular, I am deeply grateful to Nico, Mona, Elias and Nicole Folesky, together with their relatives and loved ones. Being welcomed into your family with such warmth and generosity has been a privilege and the foundation of this journey. Without your relentless support and encouragement, none of this would have been possible. The same heartfelt appreciation is owed to Clemens, Frédérique and Valérie Gottschling, whose kindness and support have been invaluable and helped me through numerous challenging times. This thesis stands as a testament not only to my own efforts, but equally to your dedication, as it is as much a product of your unwavering support, as it is of my hard work. I am truly fortunate to have such remarkable individuals in my life.

I extend my sincere gratitude to Kay for offering me my dream job and welcoming me into his group. Your insightful guidance and enduring encouragement throughout my doctoral journey have been the cornerstone of my PhD. I appreciated the positive and constructive working environment you created. I would also like to thank Maya for providing constructive feedback and advice. Your time and effort are deeply appreciated.

I owe a tremendous debt of gratitude to Emmanuelle, Emily and Vojta, my incredible supervisor squad, for their exceptional mentorship, immense patience and the countless hours they invested in helping me reach this goal. Thank you for not only putting up with my brand of chaos and crazy, but expertly navigating and enabling me to thrive in spite of it. I am truly fortunate to have been mentored by such an inspiring and dedicated supervisor squad.

Big thanks to all members of the SCBV group. Simon, mon chéri, having you as my science and climbing buddy has been one of the highlights of my PhD. Your cheerfulness and optimism combined with MOTIVATION were absolutely key to me making it through this PhD in one piece. I can't wait to be colleagues again in Okinawa. Märit, thanks for all the great conversations, car rescue missions, Swedish candy runs, and just making this whole thing way more fun. Finding someone who matches my kind of crazy and taste in music is rare. I owe you big time. Henriette, thank you for saving me from my complete lack of organization again and again. Tim, thanks for geeking out about 3D printing with me. Simone, thanks for taking such good care of my lemon tree whenever I left town.

I want to thank everyone at the cryo-EM facility for their exceptional dedication and the extraordinary support they provide. I am particularly grateful to Uli, Cornelia and Michael, whose expertise and patience proved invaluable on numerous occasions throughout this journey. Their unwavering commitment and willingness to go above and beyond made this work possible.

Special thanks go to Nastiia, whose time as my intern represents another highlight of my PhD. Training you was a great experience, and your contribution to this project really mattered. Seeing you now successfully pursuing your own research in the field of neurodegenerative disease stands among my proudest achievements.

I want to thank the group of Ileana Cristea (Princeton University, NJ, USA) for their outstanding support and collaboration. Their contribution of essential resources and expertise greatly expedited my research. The insights and inspiration drawn from their innovative work has been fundamental to the development of this thesis.

10 Declaration

Hiermit versichere ich an Eides statt, die vorliegende Dissertationsschrift selbst verfasst und keine anderen als die angegebenen Quellen und Hilfsmittel benutzt zu haben. Sofern im Zuge der Erstellung der vorliegenden Dissertationsschrift generative Künstliche Intelligenz (gKI) basierte elektronische Hilfsmittel verwendet wurden, versichere ich, dass meine eigene Leistung im Vordergrund stand und dass eine vollständige Dokumentation aller verwendeten Hilfsmittel gemäß der Guten wissenschaftlichen Praxis vorliegt. Ich trage die Verantwortung für eventuell durch die gKI generierte fehlerhafte oder verzerrte Inhalte, fehlerhafte Referenzen, Verstöße gegen das Datenschutz- und Urheberrecht oder Plagiate.

15.07.2025 _____

Datum Unterschrift